Permanent Magnet Fault Current Limiters for Electrical Power Protection Systems

Asmaiel G. M. Ramadan

A thesis submitted in partial fulfilment of the requirements of Sheffield Hallam University for the degree of Doctor of Philosophy

June 2018

Abstract

The main aim of this work is to design and test a permanent magnet fault current limiter (PMFCL) to limit the fault current in electrical power system network. The (fit and forget) device presented in this thesis is based on two important aspects; the best selection of the state of the art soft and hard magnetic materials and the design topology of PMFCL. Rare earth material is used as a permanent magnet, which is the main source of excitation to keep the non-oriented silicon steel iron core in magnetic saturation state. During the normal operation of the device the saturated core offers low impedance to the grid and during the fault state the core inherently rushed to high impedance state that limits the high short circuit current. A commercial Finite Element software (FEM) was used in the device modelling techniques from the commencement till the end of the final design. The work commenced with the verifications and investigations of a recently reported model in 2D (FEM).

Then, a prototype of small scale, in two design configurations of the same PMFCL specifications, was built and tested at the electrical laboratory of Sheffield Hallam University to verify the simulation results and to access the design of the PMFCL device. After that, the 11-kV PMFCL for substation distribution transformer was designed. Finally, the low voltage toroidal core PMFCL was proposed for the existing renewable energy and future wind-photovoltaic (wind-PV) step-up transformer. The dry type PMFCL current-inductance profiles were obtained by 3D (FEM) magneto static solver to predict the behaviour of the devices in the abnormal condition. The calculated RMS current, using 3D (FEM) time saving inductance-current approach, agreed with the peak transient currents obtained by the lengthy computation process time-step solver. The current limitation capability has been calculated in comparison with the air-cored of similar specifications as the PMFCL device and a useful reduction in the fault current has been achieved. The simulation results proved that the proposed PMFCL topologies (toroidal and square-shaped) can protect the renewable energy generator-transformer and real power grids from the fault current. Both the toroidal and full scale PMFCL devices initial and energy cost over an expected service of life have been evaluated.

The merit of the PMFCL device is that it reduces downtime during power system's outages by mitigating the severe fault current in the first half cycle.

Acknowledgements

I would like to express my sincere thanks and greatest gratitude to my thesis supervisor Dr Faris Alnaem for all his help, advice, comments and guidance in the completion of this thesis.

In addition, I would like to give my thanks to my second supervisor, Dr Walid Issa for his help, suggestions and advice.

My thanks to the Electrical and Electronic Engineering Department's staff members for their assistance in obtaining the different parts I needed for the experimental work of the PMFCL.

My thanks to my friends.

My special thanks to my family especially my sons (Mahmud and Yousef) for their support.

Contents

Tables of figures

Table of tables

List of nomenclature

A	Magnetic vector potential	Tesla.meter (T.m)
B	Magnetic flux density	Tesla (T)
SDR	Saturation depth ratio	……
u	core	……
FEM	Finite Element Method	……
H	Magnetic field intensity	Amber/meter (A/M)
H_c	Coercivity	Amber/meter (A/M)
H_c^-	Intrinsic coercivity	Amber/meter (A/M)
H_m	permanent magnet magnetic field intensity	Amber/meter (A/M)
kV	System voltage	Kilovolt
J	Current density	Amber/square meter (A/m^2)
L	Inductance	Henry
l	Length	meter (m)
M	Magnetization vector	Amber/meter (A/M)
m	Magnet	- - -
W	Stored magnetic energy	Watt-second (W.s)
ω	Angular frequency	Rad/sec
f	System frequency	Hertz (Hz)
π	Pi	……
r_{si}	saturated core reluctance	Ampere/weber ($A\ Wb^{-1}$)
PMFCL	Permanent magnet fault current limiter	……
∀	Curl (the differential operator)	m^{-1}
r	Resistance	Ohm (Ω)
S	Cross sectional area	square meter (m^2)
Ø	Magnetic flux	Weber (Wb)

R	Magnetic Reluctance	Ampere/weber (A Wb^{-1})
F_m	Magnetomotive force	Ampere turns (A)
ms	Mild steel 1010	……
N	Number of turns	……
μ_1	Core unsaturated permeability	Wb/ (A m)
μ_m	Permanent magnet permeability	Wb/ (A m)
μ_2	Core saturated permeability	Wb/ (A m)
IF_{max}	Maximum fault current	Amber (A)
B_r	Remanence	Tesla (T)
μ_r	material relative permeability	……
h	Depth	Meter (m)
μ_0	Permeability of free space	$4\pi\times10^{-7}$ H/m
r_{ui}	Core unsaturated reluctance	Ampere/weber (A Wb^{-1})

Chapter 1: - Introduction

1.1 General background

Power systems have been changing and growing significantly over the last decades and will keep changing in the future. Global demand for electrical energy is estimated to double by 2050 [1.1]. This growth will be caused by an ever-increasing population [1.2], enhanced availability of electricity in developing countries [1.1], and the increasing electrification of loads such as domestic heating and electric vehicles [1.3]. The importance of using sustainable sources of energy will have a critical impact on future power systems [1.4] and is already leading to an increased presence of distributed generation (DG), microgrids, DC systems, and power electronic devices. These developments add further diversity to electrical sources and loads, and thereby complicate the system protection and control. The power system has to manage the future load growth; however, the fault current levels will increase. Fault currents are usually momentary and initiate from a variety of sources such as: equipment failures, lightning stroke, growing of tree branches, or in some cases animals, shorting out the power circuits. In all cases the resulting transient current surges can easily damage transmission power lines, power plant and substation components. Under certain conditions faults can affect a part of the power grid producing blackouts extending over several countries or states [1.5]. When a fault takes place, the short circuit current is over eight times that of the circuit breaker normal load current. The high short circuit current rapidly increases the mechanical and thermal stress on the equipment [1.6]. Power systems undergoing rapid extension may encounter that existing switchgear will no longer be adequate to meet the increased short circuit currents. In contrast, countries which do not have a rapid growing demand can nonetheless also suffer from increased short circuit currents level [1.7]. The reduction of the fault current is one of the oldest problems of power systems engineering. Fault current reduction permits the interconnection of large networks without replacing the infrastructure, improves transient system stability, and reduces the cost of apparatus [1.8]. In electrical power system, the increase in system fault current levels due to the increase in demand and consumption of electrical power requires to change the whole infrastructure with higher ratings, which is not possible. The cost of a circuit breaker, a transformer and other devices such as generators and large-sized motors are very expensive and replacing them affects the

reliability of the power system, enlarges the value of the fault current and hence may permanently cause severe damage. Moreover, it is a time and labour consuming process [1.9]- [1.11]. Several means to limiting fault currents have been suggested in the past including upgrading fast circuit breakers, system reconfiguration, installing transformers with higher impedance, current limiting fuses, air-core reactors, etc. [1.9], [1.11]- [1.14]. However, those methods were not satisfactory due to high estimated costs, lack of system security and reliability.

A fault current limiter (FCL) is a changeable impedance device connected in series with a circuit breaker and has insignificant influence in a power system under normal conditions but can limit the current during a transient condition. Fault current limiters not only mitigate fault currents but also provide several other benefits to power system operation, such as serving for transient state stability, protection relays, circuit breakers operation and power quality, etc. There are up to date approaches to limit the fault current such as the introduction of superconductors fault current limiters and solid-state fault current limiters, but they still fall behind in addressing some concerns such as the running cost, installation cost, maintenance cost and reliability. Thus, it is very necessary to develop a preferable current limiting device to reduce the rating of each element required, to lower the capital cost and as a result to improve protection coordination [1.15]. Therefore, there is essential to have the magnetic fault current limiter (MFCL) [1.5], [1.16]- [1.19]. With the development of magnetic materials as well as topology design research, Fault current limiter based on permanent magnet biased saturation has recently attracted a lot of interests of researchers and scientists [1.13], [1.14]. According to the results of previous research, a serious problem of applying the PMFCL into large capacity practice is its insufficient biasing capability of the permanent magnet [1.14]. This new approach is based on two important aspects, the best selection of the state of the art soft and hard magnetic materials and the magnetic current limiter geometry design. With better selection of required materials and design geometry specifications, this project is relied on two main approaches; an analytical and a numerical approach. An analytical approach is used to show the analysis regarding the magnetic flux and magnetic motive force to deduce the equivalent static magnetic circuit model.

A numerical approach is performed by MagNet Finite Element software to model the permanent magnets, the iron cores and the limiter coils under both normal and faulty conditions. In this work, MagNet (FEM) is used to study the transient of the MFCL responses,

taking into consideration the flux leakage to improve the accuracy of the field circuit modelling methodology [1.13]- [1.14].

A numerical approach was used in the simulation and analysis of the PMFCL. This is performed by a commercial Finite Element Method, (FEM) package "MagNet" by Infolytica company. MagNet Finite Element is one of the most developed packages currently accessible for modelling electromagnetic devices on a personal computer [1.20]. The finite element method is a computational technique used to obtain approximate solutions of boundary value problems in engineering. Boundary value problems are also called field problems. The field is the domain of interest and most often represents a physical structure. 2D and 3D (FEM) simulation tools were used taking into considerations many of the parameters that would be otherwise overlooked by the analytical approach, like the flux leakage, core saturation, and the flux density distributions to improve the accuracy of the field circuit modelling [1.9], [1.21].

The work presented in this thesis is designed for power distribution transformers for the sake of economy, current capacity, efficiency, reliability and safety of the power systems. Distribution Transformers (DTs) are an essential part of the power network and their operation determines with a great deal the efficiency of the power system.

1.2 Research motivation

The short-circuit current of the power grids is reaching a critical level, which threatens the security, stability and reliability of the power grids. Hence, how to limit the short-circuit current has become an unavoidable issue in the development of modern power grids [1.22]-[1.24].

If the fault current can be limited, system reliability, safety and cost effectiveness will be improved.

The research motivation has the following attributes:

1- To limit the prospective fault current (peak and RMS) in the first half cycle to a desired and safe value. The safe value is typically higher than the nominal current value but less than the maximum operating value of protection devices such as circuit breakers (CB).

2- To access the design of PMFCL, gain learning knowledge and prove that the PMFCL device is easy to construct and install.

3- To provide power grid with a (fit and forget) cost-effective device that has an automatic system recovery, safe operation and fail save.
4- To solve the problem of equipment underrated, voltage drop, power losses, voltage dips and reduce power system outages.
5- To increase safety, reliability, and power quality of the power system.
6- To protect, extend the service life of transformers and associated utility equipment and reduce the maintenance cost.
7- To expand substation capacity without significantly expanding the required real estate footprint, need for new lines, or creating additional critical assets with expanded security perimeter
8- To reduce capital for redundancy and use cheap load circuit breakers (CBs) instead of expensive high current rating CBs in power distribution system.

1.3 Thesis objectives

Considering the above issues, this work was oriented to achieve the following objectives:

1. To design a low voltage up to 1 kV PMFCL for the renewable energy and 11 kV PMFCL for substation voltage level based on the state of the art soft and hard magnetic materials using 2D and 3D (FEM).
2. To verify the concept of PMFCL through experimental work and ensure the device is performed exactly as we expected it to.
3. To develop (FEM) models for prediction of non-linear behaviour of the PMFCL cores in response to a fault current

1.4 Thesis overview

This thesis is divided into seven chapters. Chapter two highlights the soft and hard magnetic materials characteristics and applications. Chapter three overviews the previous related work and identifies the gap for the research. Chapter four outlines the verifications and validations of a recent published PMFCL model. Chapter five presents the design of a PMFCL prototype. Chapter six commenced with the modelling of the full-scale dry type 11 kV PMFCL. In addition, it covers the design of the low voltage PMFCL for renewable energy generator-step-up transformer. Finally, chapter seven gives the conclusion and future work.

1.5 Published papers

"Design and modelling techniques of permanent magnet fault current limiter." *Energy Procedia* 134 (2017): 616-625.

1.6 Submitted Papers

“Design and modelling of permanent magnet fault current limiter for electrical power applications", accepted paper in 53rd international universities power engineering conference.

References

[1.1] World Energy Council. Deciding the Future: Energy Policy Scenarios to 2050. Technical report, 2007

[1.2] United Nations. World Population Prospects - The 2008 Revision, Technical report, 2009.

[1.3] J. Lassila, et al. (2012). Electric cars as part of electricity distribution - who pays, who benefits? *IET electrical systems in transportation,* 2 (4), 186-194

[1.4] D. MacKay. Sustainable Energy - without the hot air. 2008

[1.5] LEUNG, E. M., et al. (1997). High temperature superconducting fault current limiter development. Applied superconductivity, IEEE transactions on, 7 (2), 985-988.

[1.6] GANG, C., et al. (2003). Simulation study of bridge type solid state fault current limiter. Power Engineering Society General Meeting, 2003, IEEE, 2526 Vol. 4.

[1.7] RENZ, K., THUMM, G. and WEISS, S. (1995). Thyristor control for fault current limitation. Fault Current Limiters - A Look at Tomorrow, IEE Colloquium on, 3/1-3/4.

[1.8] KARADY, G. G. (1992). Principles of fault current limitation by a resonant LC circuit. Generation, transmission and distribution, IEE proceedings C, 139 (1), 1-6.

[1.9] FARHOODNEA, M., MOHAMED, A. and SHAREEF, H. (2014). A comparative study on the performance of custom power devices for power quality improvement. Innovative Smart Grid Technologies - Asia (ISGT Asia), 2014 IEEE, 153-157.

[1.10] HALL, J. and CHEER, A. (2013). Fault current limiter surge protection device for the power grid based upon zero power consumption ceramic ferrite permanent magnets. Electricity Distribution (CIRED 2013), 22nd International Conference and Exhibition, 1-4.

[1.11] SANTRA, T., et al. (2009). Analysis of passive magnetic fault current limiter using wavelet transforms. Power Systems, 2009. ICPS '09 international.

[1.12] Hongshun Liu, et al. (2009). An equivalent magnetic circuit coupled model of PMFCL for transient simulation. Universities Power Engineering Conference (UPEC), 2009 Proceedings of the 44th International, 1-5.

[1.13] Liang Zou, et al. (2009). Study on the feasibility of developing high voltage and large capacity permanent-magnet-biased fault current limiter. Universities Power Engineering Conference (UPEC), 2009 Proceedings of the 44th International, 1-5.

[1.14] Mukhopadhyay SC, Dawson FP, Iwahara M, et al. Analysis, design and experimental results for a passive current limiting device. IEE Proc Electric Power Applications 1999; 146(3):309–16.

[1.15] MORICONI, F., et al. (2010). Modelling and test validation of a 15kV 24MVA superconducting fault current limiter. Transmission and Distribution Conference and Exposition, 2010 IEEE PES, 1-6.

[1.16] POWER, AJ (1995). An overview of transmission fault current limiters. Fault Current Limiters - A Look at Tomorrow, IEE Colloquium on, 1/1-1/5.

[1.17] WROE, F. C. R. (1995). High temperature superconductors for fault current limitation on local power distribution networks. Fault Current Limiters - A Look at Tomorrow, IEE Colloquium on, 2/1-2/4.

[1.18] USUI, K., et al. (2001). A single DC reactor type fault current limiting interrupter for three-phase power system. Applied superconductivity, IEEE transactions, 11 (1), 2126-2129.

[1.19] PUTRUS, G. A., JENKINS, N. and COOPER, C. B. (1995). A static fault current limiting and interrupting device. Fault Current Limiters - A Look at Tomorrow, IEE Colloquium, 5/1-5/6.

[1.20] Magnet user manual by Infolytica, www.infolytica.com.

[1.21] Liang Zou, et al. (2008). Impact of saturation depth ratio of iron-core on the PMFCL. Electrical Machines and Systems, 2008. ICEMS 2008.International Conference, 4338-4343

[1.22] KNOTT, J. C. and MOSCROP, J. W. (2013). Increasing energy efficiency of saturated-core fault current limiters with permanent magnets. Magnetics, IEEE transactions, 49 (7), 4132-4136.

[1.23] KNOTT, J. C. and MOSCROP, J. W. (2013). Increasing energy efficiency of saturated-core fault current limiters with permanent magnets. Magnetics, IEEE transactions on, 49 (7), 4132-4136.

[1.24] Y. Chai, et al. (2016). Safe operation improvement of an electrical power system by superconducting fault current limiters. *2016 Chinese control and decision conference (CCDC),* 1310-1314.

Chapter 2: - State of the art fault current limiting devices (FCLD)

2.1 Introduction

In accordance with the restriction of the flow of excessively large value of current in power system during sudden load switching, overload, fault and any other abnormal operating conditions, different techniques were used in the past [2.1]- [2.16]. One alternative solution to overcome the fault level problems is to upgrade or replace existing switchgear [2.2], [2.6]. However, this option is not acceptable due the following reasons: -

1) High estimated costs as the breakers are very expensive, and swapping them, even if possible, is a labour-intensive process.
2) Lack of system reliability during long period of modifications, shutdowns and construction.
3) Breakers available today for replacement would soon become inadequate [2.14], [2.15].

Another suggestion which was put forward is to go for increased use of distributed generation (DG) which involves placing smaller generation sources closer to the loads. However, even with DG-based system, the possibility of fault occurrence does exist [2.6].

Common measures to limit the fault current are inserting reactors between busbar sections or in series connection to feeders has been considered as another possible solution to limit short circuit currents. These, however, substantially influence the network under normal conditions as they are in the system all the time [2.3]- [2.6].

Conventional fuses and triggered fuses are also used, but they must be replaced after every fault event [2.17]. High speed (less than 1/4 cycle) bus ground switches could be used to divert the fault current before it reaches its highest value. This means that any fault in the vicinity or near a station would cause the ground switch to close and put a solid fault on a bus. This is undesirable because it results in more severe fault and longer fault duration [2.15].

Splitting the grid and/or introducing higher voltage connections, AC or perhaps DC was considered another solution to limit the fault current. Nevertheless, splitting the grid decreases flexibility and lower the system security. Simply this happens because certain parts of the network are duplicated and operated in parallel, if one component fails, it isolated, and the supply remains on. Splitting the network will cut these parallel elements, increase system

impedance and lower the fault infeed. Though, if the elements are no longer in parallel and one element fails, a large power disruption occurs [2.6].

The introduction of higher voltage connection would be expensive and, in any case, may not be possible due to problems obtaining consent for tower raising, wayleaves, etc. [2.6].

Consequently, there is a need for a fault current limiting device, which offers low impedance to the load and a high impedance to the fault current [2.2], [2.6], [2.15].

The need for Fault Current Limiting Devices (FCLD) has long been recognized and a recent study showed that the need for a new fast acting multi-operation fault current limiting device (FCLD) for distribution networks had been identified by most of the USA electric utilities [2.18].

2.2 Requirements of a fault current limiter (FCL)

A typical representation of an electric network is shown in Figure 2-1. If any unforeseen accident happens which leads to a fault, a lot of current will flow [2.16].

The location of FCL is carefully selected so that the fault current can be restricted within an optimum value.

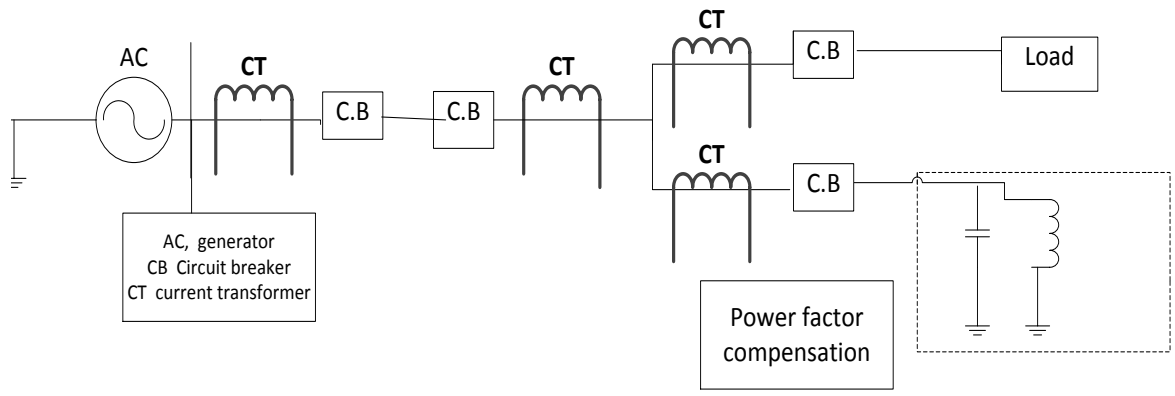

Figure 2- 1 A typical electric power network

The FCL will limit the fault current which will allow the lower rating CBs to be used in the system. Now as the FCL is always there in the system, under normal condition the system should ideally not observe the presence of the FCL. At the same time the FCL should respond almost instantaneously to a fault [2.16].

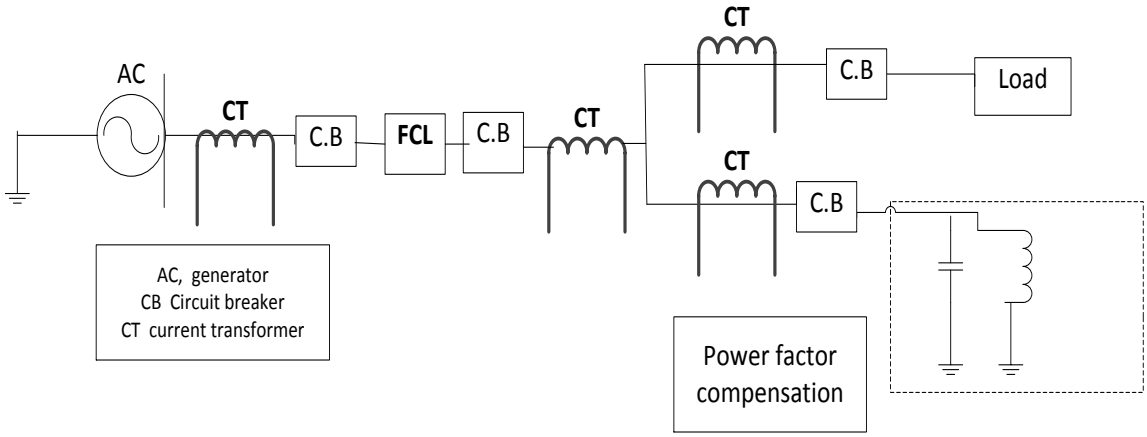

Figure 2- 2 The electric power network with FCL in use

The amount of current is restricted by the internal impedance of the generator and the line between the generator and fault. Usually the internal impedance is very low, so the magnitude of the fault current is very large. The large fault current will initiate the operation of the circuit breaker (CB) and the CB will break the circuit. Usually the CB breaks the circuit at the zero crossing of the current wave [2.16].

In general, any fault current limiter (FCL) should meet the following requirements: -

1. Has low or negligible influence on the network under normal operating conditions.
2. Easy to install, has repetitive operation without any replacement and has short recovery time.
3. Fast response limits all types of fault current in the first cycle and provides self-regulation in the event of any fault.
4. Provides high reliability and improves operational flexibility.
5. Provides safe operation and fails safe.
6. Compatible with existing protection system.
7. Exhibits low impedance to the load current and a high impedance to the fault current with low energy losses.
8. Permits the interconnection of large networks without replacing the circuit breaker, transformer, etc. with oversized equipment, thus increases equipment life and allows transformers parallel operation during normal and contingency periods.
9. Has limited volume and weight [2.1], [2.5], [2.6], [2.23], [2.26].

2.3 Fault current limiters design approaches: -

To overcome the high fault current, many kinds of fault current limiting devices have been used in the last decades. Current-limiting fuses, series reactors, and high-impedance transformers were used. However, these alternatives may cause other problems, such as loss of power system stability, high cost, and increase in power losses, which may ultimately lead to decreased operational flexibility and lower reliability [2.12].

2.3.1 Re-healing fuse.

Current limiting fuses have been used for the protection of electrical systems and equipment for many years. Their capability to control the energy let-through and the peak available fault current, coupled with their cost effectiveness, accounts for their popularity. They are used for the protection of motors, transformers, cables, capacitors and electrical distribution systems. Today, a Smart Fuse, which is based on the recent advanced technology in material science, provides a lower cost protection scheme [2.17]. The Smart Fuse is defined as the fuse which not only operates as per its time current characteristics, but also operates on demand from other protective devices outside the fuse body itself. At present 65 A to 175 A, 26 kV Smart Fuses have been developed. The Smart Fuses can be applied as a low-cost alternative to circuit breakers recognizing the fact that this new device does not duplicate all the operating functions of a circuit breaker [2.17].

The Smart Fuse has been designed to meet the following criteria:

1. Interrupt all currents from its maximum rated interrupting current to its minimum interrupting current. This minimum interrupting current is less than rated current
2. Successfully interrupt if the element opens at any single location.
3. Any damage to the element due to lightning or current surge will not affect fuse operation.
4. Any mechanical damage (such as the fuse being dropped during installation) to the element which lowers the rating of the fuse and causes it to melt while carrying its rated current will not affect fuse operation.
5. Current limiting fuses operating on 1% are not damaged by di/dt. The smart fuse operates on a different principle and is sensitive to di/dt. This normal current rate

of rise in a distribution system is below $30KA/\mu_{sec}$. The fuse has been successfully tested for current surge withstand of $20KA/\mu_{sec}$

In the Smart Fuse, chemical charges placed at strategic points, along the element length produce the multiple breaks required for low current interruption. The components of the smart fuse are as shown in Figure 2-3. The fuse element has an over current sensor (O.C.) located in the centre which produces the time current characteristic. Several chemical charges are placed along the element length at various strategic points. Under normal conditions, the trigger circuit is isolated by a spark gap (A1). When the main element opens at any one point for any reason, the fuse arc voltage operates the spark gap and causes the current to flow through the trigger circuit. The current fires the chemical charges creating the required number of series arcs for the interruption of low currents. At high currents, the multiple notch design operates like any other current limiting fuse. The magnetic choke coil (Ml), the air core inductance L1 and L2 and the air gap A2 are provided for lightning surge immunity. During the current surge, the fuse's inductance L produces a voltage L*di/dt across the fuse. This voltage if high enough, fires the air gap A1 which allows the current to flow through the trigger circuit [2.17]. The entire voltage drops across the magnetic coil M1 which fires the air gap A2. The air core inductances, L1 and L2, limit the current during the initial dv/dt and the coil M1 limits the current after A2 opens. TheI^2tin the trigger circuit is kept far below the firing I^2t of the chemical charges/ignitron system.

Application of the Smart Fuse represents a marked divergence from the standard functional performance as provided by conventional power fuses in the protection of transformers. The innovative communication technology employed in the Smart Fuse construction allows for interfacing between fuses in a multi-phase circuit and with external protective devices and other remote signals. This provides the protective functional capability requirement to a transformer primary circuit breaker. Moreover, it eliminates the transformer secondary main breaker through the application of secondary overcurrent protective relays, Devices 51and 51G (51N) (Generator/Transformer Neutral Ground protection), to signal and initiate a three-phase primary circuit interruption. The Smart Fuse with the use of a resistance grounding system to reduce the fault current is compatible with the application of additional protective devices.

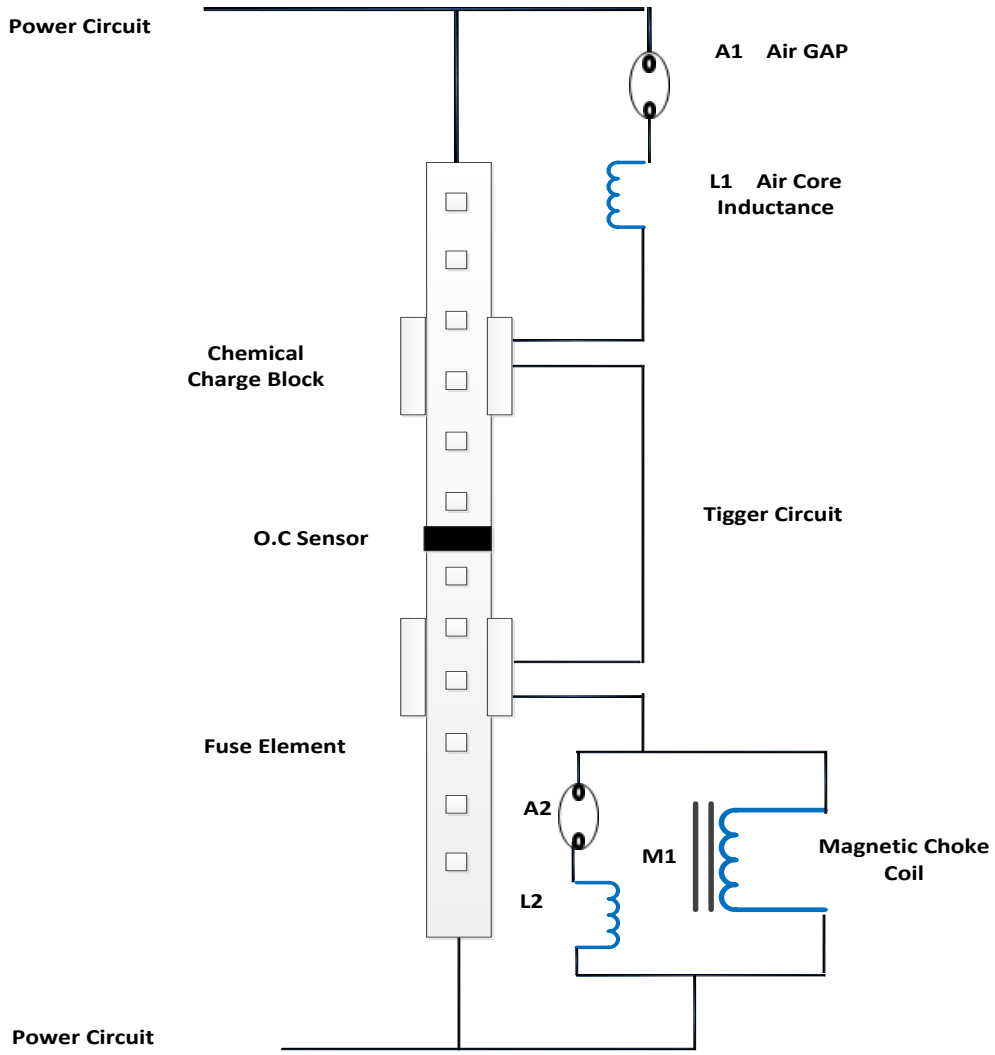

Figure 2- 3 Principle of smart fuse operation

During any abnormal conditions such as high temperature (49 relay) or tank pressure (63 relay), etc. [2.17], the decision comes from Protection Control Centre (PCC) through Control Module (CM), which is an interface between the fuse and the PCC. The Control Module can be an isolation transformer or Opto-Electronics; it isolates the PCC from high voltage power system. In case of a fault, the lookout relay (86) or any other protection command is received by the PCC, which decides and sends an electrical pulse to CM to fire the fuse. A Processing Centre or the PCC is the main information. This protection scheme also alarms an operator and then fires the fuse if no action is taken to protect the transformer, but for severe faults, the fuses are fired immediately to isolate the unit. Elimination of transformer secondary main breaker as shown in Figure 2-4 could provide a significant savings. The Smart Fuse provides an

economical alternative and a solution to any miscoordination problems while meeting the other design criteria objective of keeping ground fault levels to the minimum [2.17].

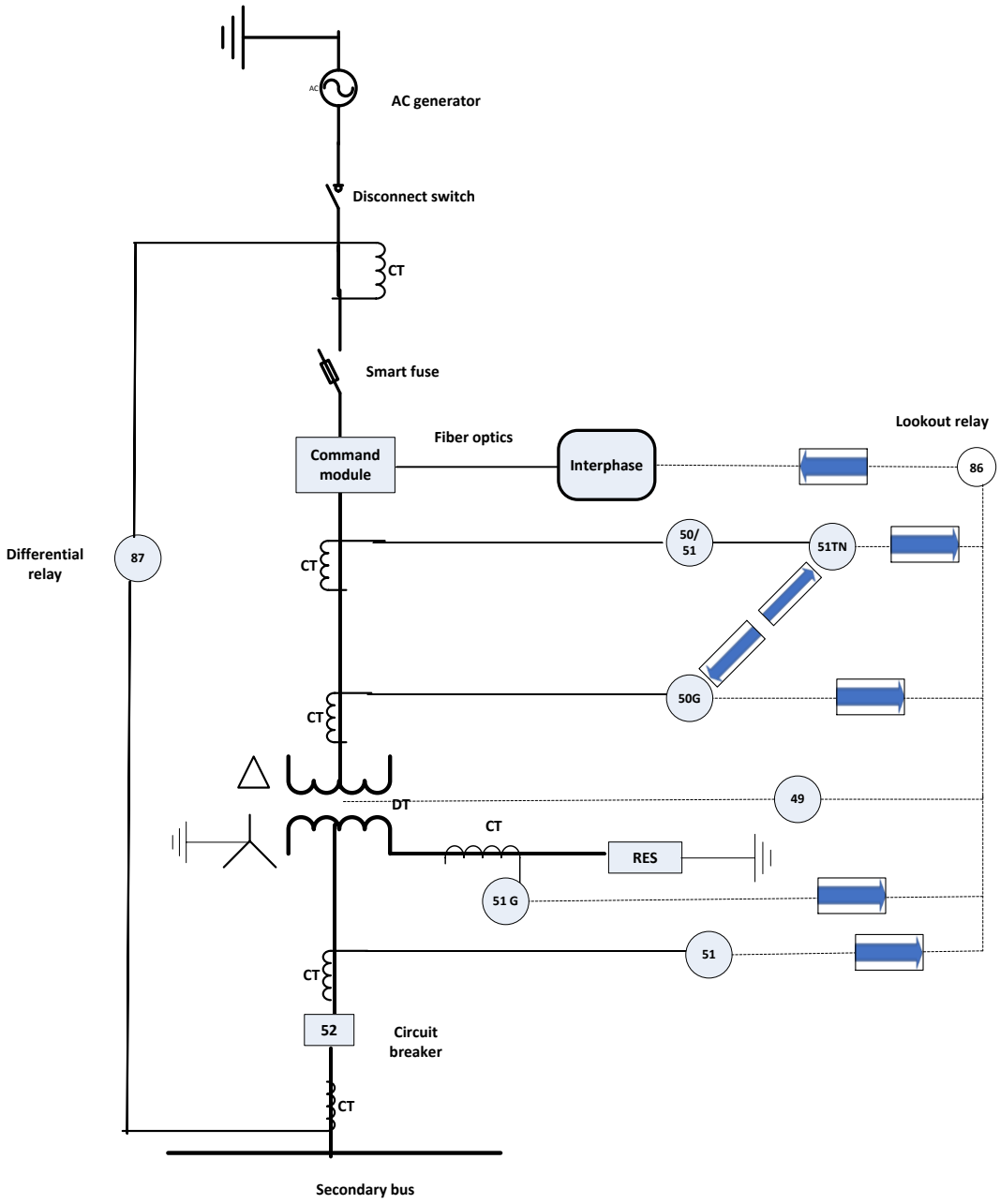

Figure 2- 4 Transformer secondary over current protection with smart fuse

The Smart Fuse retains several of the advantages in transformer protection provided by conventional fuses. Such advantages as initial economy, current limiting action and fast clearing of high current faults are also inherent with the Smart Fuse. Conversely, the Smart

Fuse, through its unique functional capability, overcomes the major disadvantages associated with conventional fuses such as single phasing, the problems of selecting the fuse time current characteristics, the difficulties of coordination with other protective devices, and the inability to provide sensitive secondary overcurrent protection.

However, this kind of fault current limiter has limited number of operations; it produces losses and a voltage drop during fault current periods due to the grounding resistance and the inductances inside the fuse itself. The main disadvantage of Smart Fuse is the limited number of operations [2.17].

2.3.2 Superconducting fault current limiters (SFCLs)

Superconducting fault current limiters (SFCLs) have emerged as an alternative to limit prospective short-circuit currents to lower levels and improve power system reliability and stability by reducing the fault current [2.12]. SFCLs have near zero impedance under the normal condition and large impedance under fault condition [2.1], [2.6], [2.12].

2.3.2.1 Classes of superconductors: -

There are two classes of superconductors; the low and high temperature superconductors. The class of metallic superconductors, which have been available for many years, having critical temperatures $T_c \leq 25K$, are called low temperature superconductors (LTS) and operate typically in a liquid helium bath at 4.2K. These LTSs have been used to make current limiting demonstration devices for the protection of D.C. and A.C. systems for utility applications [2.1], [2.4].

In 1986 a new class of superconductors, referred to as high temperature superconductors (HTS), was discovered. These superconductors were made from compounds of ceramic oxides, which exhibit critical temperatures up to 12OK and raised the possibility of SCFCLs being operated at much higher temperatures. Specifically, Liquid nitrogen, with a boiling point about 77K results in a refrigeration operating cost lower by a factor of 25 to 100 and refrigeration capital cost lower by a factor of about 10 than liquid helium, would be useful for an HTS current limiter. Liquid nitrogen cooling systems are also less complex than liquid helium systems [2.1], [2.4]. These extra benefits, and the fact that at 77K these ceramic oxide superconductors are intrinsically much more stable against thermal perturbations than superconductors operating at 4.2K [2.1], [2.4].

2.3.2.2 Types of superconducting fault current limiters (SFCLs)

- **Resistive limiter**

In this concept the superconductor (SC) is connected directly in the line, which must be protected. When, due to a fault, the critical current of the SC is surpassed, and its resistance increases as it returns to normal resistive state. This is called a superconducting to normal transition (S-N). The advent of low-loss alternating-current superconducting wires and the newly discovered materials which exhibit moderately sharp transition behaviour enable this technique to be employed. Resistive type SCFCLs operating at 4.2K are being considered for application by some utilities, despite being harnessed with the technology and operating costs associated with using liquid helium, the relatively low weight and volume makes it attractive in some applications [2.1].

However, there are some disadvantages associated with this type. Heat generated when a part of the superconductor begins to go normal must be dissipated before the material is damaged. This requires adequate thermal diffusion times, and in the new HTS materials these are relatively poor. It is therefore important that a substantial fraction of the superconductor should switch in a short time to limit the heat generated. Because of this, it may also be necessary to open the series circuit breaker quickly to prevent damage to the limiter. Another drawback is that it may require resistive and/or inductive shunts to be used to assist energy dissipation, although these could be expected to add to the complexity and cost of such devices and additional losses [2.4], [2.6].

- **Air gap FCL**

The secondary winding is replaced by a strip of superconductor inserted into an air gap in the iron core. During normal operation, the superconductor expels the field from the gap causing a high reluctance and a low primary inductance; during a fault the superconductor can no longer support the currents necessary to expel the field and the magnetic reluctance drops causing the primary inductance to rise [2.6].

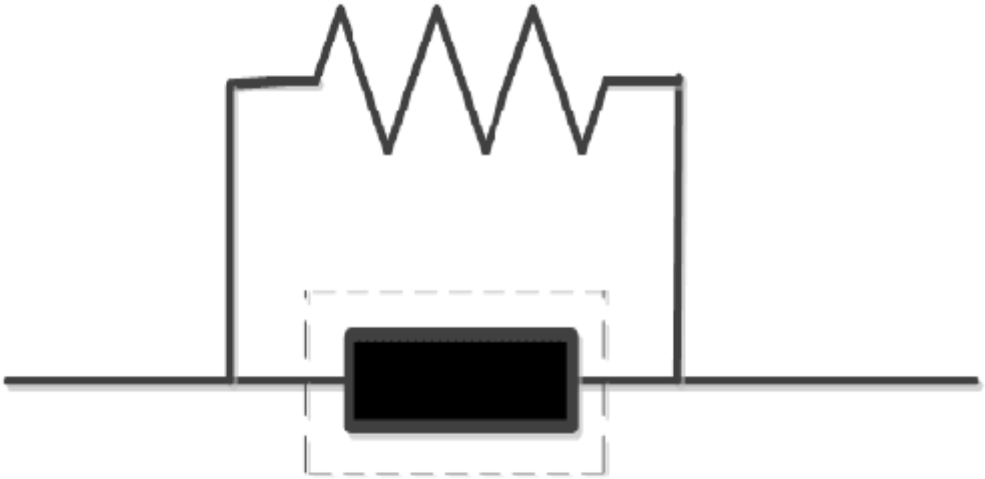

Figure 2- 5 Superconducting series resistance FCL

The scheme presented is not clear whether is suitable for transmission applications because of the probably low normal/abnormal impedance ratio [2.6].

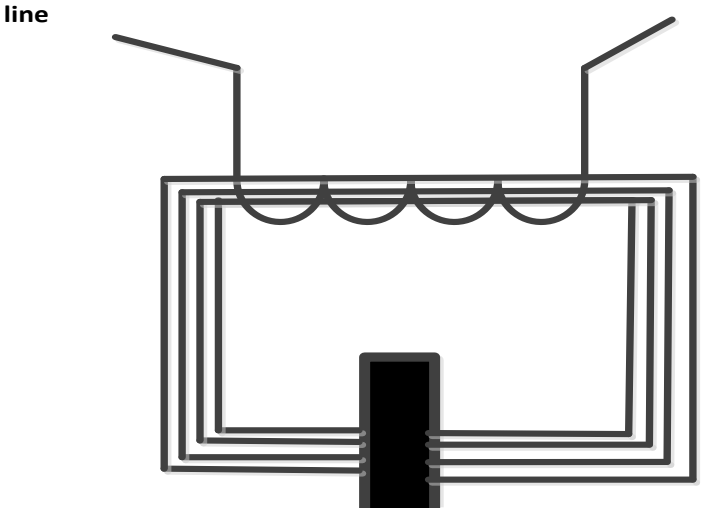

Figure 2- 6 Air gap FCL

- **Transformer with shorted secondary winding/shielded iron core**

This device is essentially a transformer with the primary winding connected in the line and a superconducting secondary winding, which is shorted. Because of the inductive coupling between the line and the SC, this device is often referred to as "inductive" SCFCL. This SCFCL needs no current-leads. Since the number of turns of the secondary windings can be much smaller than the primary turns, only short SC are needed, and the voltage drop in the cryogenic part of the device is reduced. During normal steady state operation, the superconducting secondary winding balances the ampere- turns from the primary winding so that flux does not penetrate the iron. At fault onset the superconductor current necessary to achieve amp-turns balance exceeds the critical current and thus flux can penetrate the iron; this causes the inductance of the primary winding to increase rapidly, affecting the fault limiting action. The heat loss from the line into the superconducting is eliminated even though this device is not popular due to high amount of mass of iron and copper required for the core and the windings. Till today the shielded iron core FCL incurs high estimated cost, the cost of iron, copper and in addition to the cost of superconducting material [2.4], [2.6].

The ABB pursued the concept of shielded iron core SCFCL based on HTS [2.4]. It mainly consists of a normal conducting coil, a superconducting tube, a cryostat, and an iron core, all of which are concentrically arranged. The device is essentially a transformer in which the secondary winding is the superconducting tube. The primary winding (coil) is connected in series to the line which must be protected. Only the superconducting tube is cooled with liquid nitrogen (77 K). This prototype based on HTS-tubes with a rated power in the 100-kVA range has been built and successfully tested. The device limits fault currents to about 5 times the nominal value without showing any over voltages or degradation of the HTS [2.4].

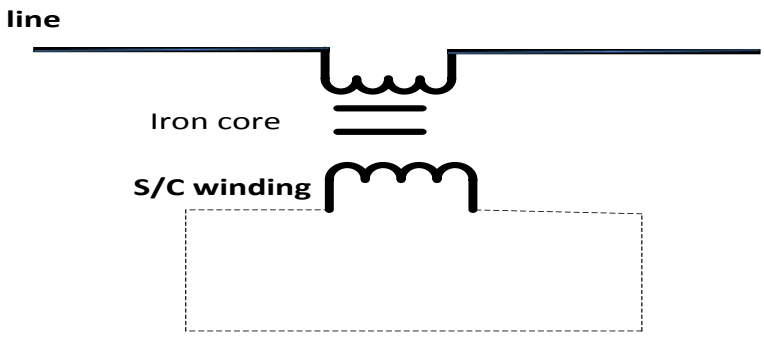

Figure 2- 7 Shielded inductance FCL

- **Saturated iron core reactor**

In this method the line current is passed through a series winding around an iron-cored reactor. The iron of this reactor is held in saturation by a second DC superconducting winding. During a fault the iron core departs from saturation and thus increases the impedance of the reactor. The superconducting winding detects only a DC-current and always stays in the superconducting state so that it needs no recovery time after a fault. The main disadvantage of the device is its mass, which is about two times that of a transformer with the same rated power [2.6].

The saturating inductive design has been demonstrated using low temperature superconducting material (LTc) materials and is a proven concept [2.6]. A successful prototype of saturated iron core reactor was tested taking into consideration the superconducting coil possible vital damage elimination [2.12].

The device consists of two iron-cored reactors in series per line, which are biased with DC to saturate the cores. The iron cores of the device are saturated by DC bias during normal operation and offer low impedance. The onset of a severe fault desaturates the core thereby increasing the impedance, thus limiting the fault current [2.12].

However, it never reached the market place for several possible reasons; (i) high costs; (ii) requires a large volume of iron; and (iii) concern of reliability and maintenance requirements associated with liquid helium refrigeration [2.1], [2.4]. Extensive study of applying LTS was conducted and the conclusion was that it was too expensive and the heat loss (refrigeration cost) made it impractical [2.9].

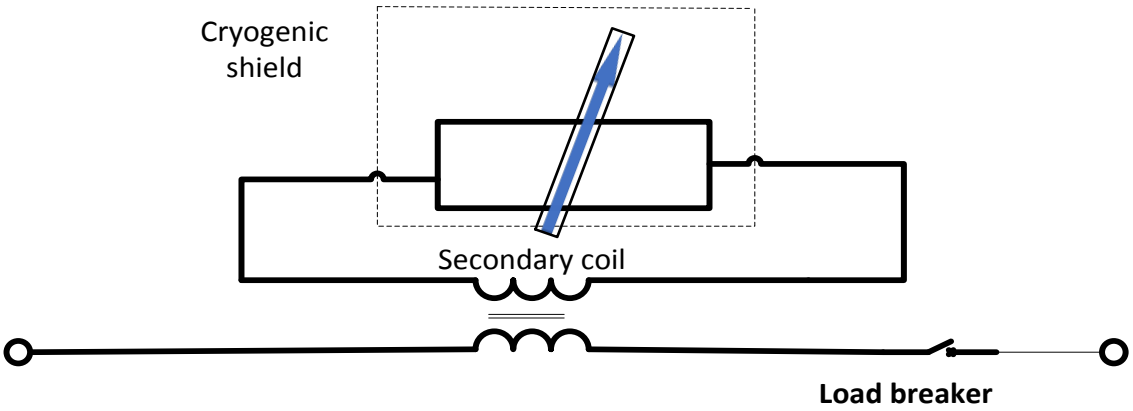

Figure 2- 8 Saturated inductance FCL

The Lockheed Martin team completed the testing of a 2.4 kV, 2.2 kArms fault current, 150 A_{rms} continuous current [2.9]. The principle of operation is that the HTS coil is quickly inserted into the circuit by a patented solid-state switch. Under normal operation, ac load current passes through the network unimpeded. However, during a fault condition, the excessive fault current is diverted into the current limiting inductor, which is sized to provide a predetermined reduction in fault current. The reduced fault current would then be cleared by a conventional (lower-rated) circuit breaker [2.9].

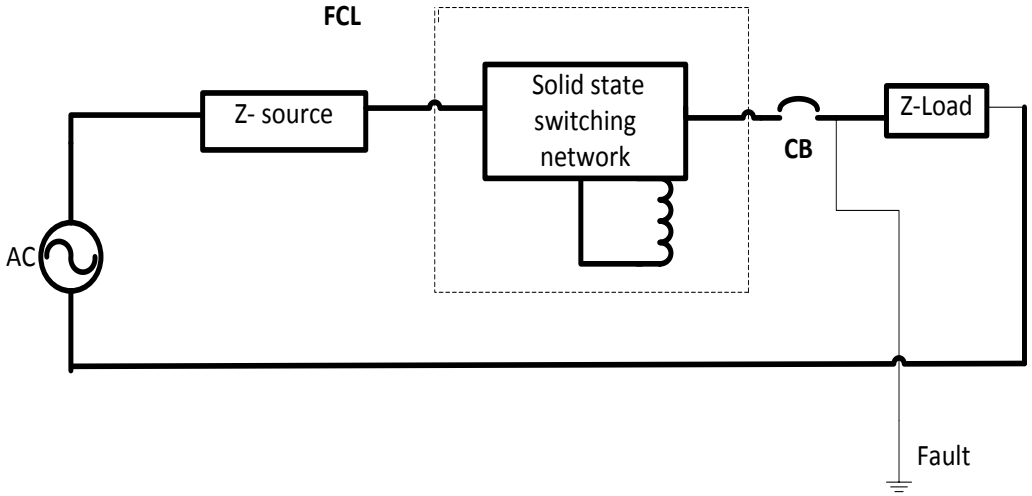

Figure 2- 9 High temperature superconducting fault current limiter

A group of researchers from Nigata and Nitsu universities, Japan, proposed a single DC reactor type fault current limiting interrupter (FCLI) for a three-phase power system [2.8]. The device uses a high temperature superconducting coil that operates in combination with a modified half control bridge composed of four thyristors and two diodes. The dc power supply is connected to the reactor coil in series. DC current flow throughout the bridge is maintained from the moment power is applied, enabling thyristors to transmit it without a gate pulse. The load current does not flow to the dc reactor and is therefore unaffected by the dc reactor, if it is smaller than the dc bias current. Line current flows continuously from Th1 to D1 and from Th2 to D2, as shown in Figure 2-10, bypassing the dc reactor altogether. The loss within the dc reactor coil is negligible, since only dc current flows within the coil. In the event of a fault, the flow of line current would be greater than that of the bias current. This excess current would naturally flow to the dc reactor, limiting any such increase rate. Thyristors automatically interrupt the flow of current at the zero-intersect of the fault current, after approximately one-half cycle.

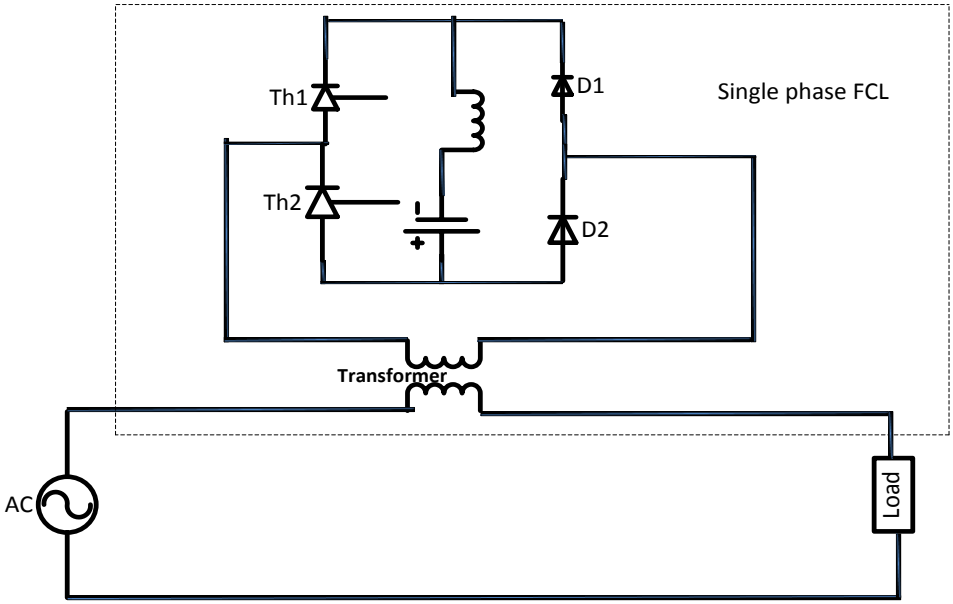

Figure 2- 10 One DC reactor type three phase FCL

Following the same concept of saturated iron core reactor, Zenergy Power designed a 15 KV distribution class superconducting fault current limiter using FEM (Finite Element Methods).

In Zenergy Power's FCL, each AC phase consists of two coils connected in series and wound around two core regions. An HTS coil provides the DC bias to saturate the two cores of every phase. The windings are oriented such that, in one core, positive AC current counteracts (bucks) the superconducting DC bias while, in the other core, negative AC current assists (boosts) the superconducting DC bias [2.2].

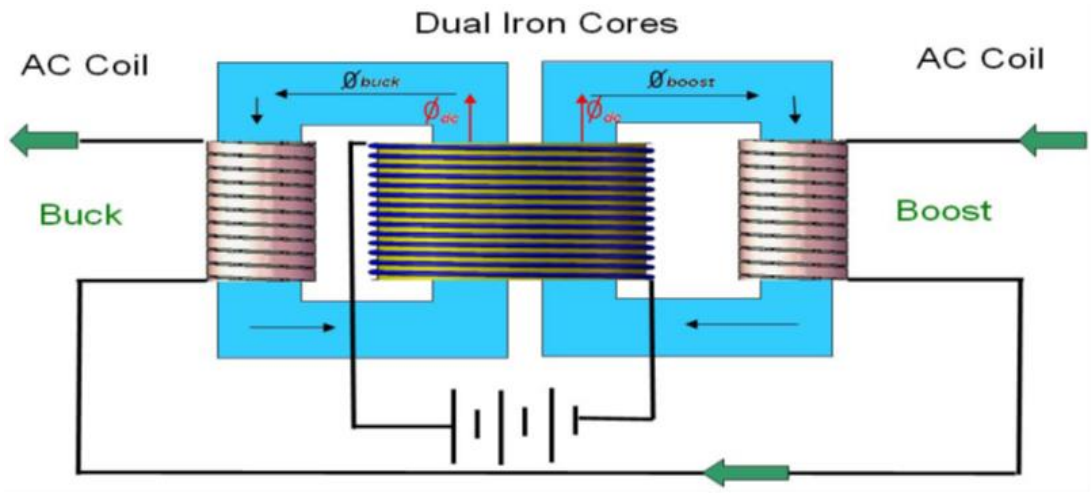

Figure 2- 11 Dual iron cores saturated by an HTS DC coil in a single-phase FCL [2.2]

This prototype performed extremely well in early fault current testing and showed exceptionally low insertion impedance at maximum load current. The device was delivered to Southern California Edison (SCE) in January 2009 and on March 2009 SCE energized the first superconducting FCL in US electrical grid [2.2].

Although the use of superconductor HTS instead of LTS would potentially result in both technical and economic benefits, the following comments are made: -

- A large volume of iron and copper is still required.
- Normal operating voltage across the limiter is about 4% of the normal rated line voltage.
- The superconducting DC field winding will probably need to be protected against the electromagnetic fields of the AC windings - an electromagnetic screen will be required which will be a source of energy loss.
- Due to the large m.m.f. required to saturate the iron cores, the DC bias field at the superconducting field winding will be relatively high [2.1].

2.3.3 Single phase saturated core open core

Recently, Jonathan C. Knott and Jeffrey W. Moscrop, [2.19] presented two designs for small-scale saturated-core fault current limiters, one uses DC coils to saturate the cores; single phase open core saturated core, and the other uses a hybrid design with DC coils and permanent magnet blocks; Open-Core saturated-core with two DC Biasing Coils and Permanent Magnets.

The open core saturated core consists of two coils wound and connected such that they set up flux in opposite directions are placed in series between an AC source and load. Laminated steel cores are inserted in to the coils and one or more additional DC coils are placed around the cores to drive the material in to saturation during normal operating conditions. The device is designed so that current in the AC coils is not sufficient to desaturate the core material during normal operation, which leads to a device impedance that is low and approximately equal to that of an equivalent sized air-core reactor. When a fault event occurs, the increased current in the AC coils can drive the cores out of saturation, which results in an increase in the permeability of the material and subsequently an increase in the coil impedances [2.19].

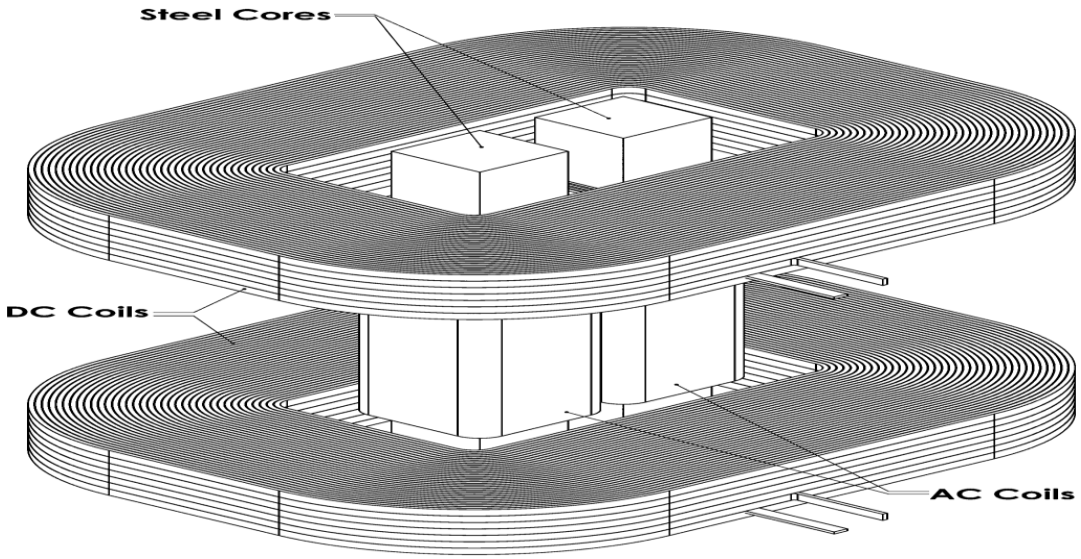

Figure 2- 12 Basic configuration of a small scale single-phase saturated core FCL [2.19]

Open-core FCLs have several key advantages over closed core (i.e. where a high permeability magnetic return path is provided) designs. From a practical standpoint, using an open-core requires significantly less material than a closed-core of equivalent performance. Furthermore, while closed-core designs allow for a much smaller biasing current to achieve saturation of the core, the ability of these FCLs to limit current is similarly reduced. The biasing of open-core FCLs presents both a challenge and an opportunity as although an open-core FCL requires higher magneto-motive force (MMF) from the DC coils to fully saturate the cores, this also leads to a significant clipping potential for very high fault currents. In commercial-scale devices the high DC MMF required can typically only be achieved using superconducting DC coils, which greatly increase the complexity and ancillary equipment required for the FCL [2.19]. In late 2010, after successfully validating the performance of a new "compact" saturated-core FCL, Zenergy Power received contracts to install a 11 kV, 1250 A FCL in the CE Electric UK Malleable substation, Stockton, UK, and a 138 kV, 1300 A HTS FCL in the American Electric Power Tidd substation, Steubenville, OH, USA in late 2011 [2.20].

2.3.4 Solid state fault current limiter

The solid-state distribution fault current limiter device (CLD) must meet the following functional requirements: -

1. Limit the available system short circuit current so that it does not exceed the momentary or interrupting rating of any downstream protective device.
2. Maintain the limited fault current without interruption until the fault is cleared by a downstream device.
3. Reset automatically after the fault is cleared by another device.
4. Permit sufficient fault current to flow during the limiting mode so that the time to clear a fault is within the user's guideline limit for each circuit.
5. Maintain performance throughout a normal sequence of operations of downstream protective devices (duty cycle).
6. Permit an acceptable number of operations in the current limiting mode before maintenance is required.
7. Operate in the current limiting mode while maintaining coordination among protective devices.

8. Limit current when first energized, and switch to non-limiting if control power is present and its current is less than the rated full current for 3 cycles.
9. Trip an upstream switch if CLD internal temperature after operation is too high to operate again immediately.
10. Have continuous and overload ratings which match the capabilities of the circuit to which the CLD is applied.
11. Meet the frequency, maximum continuous voltage and dielectric strength ratings prescribed by ANSI/IEEE standards for the voltage class to which the CLD is applied.
12. Limit transient voltages to the same level as permitted by other protective devices, such as circuit breakers or reclosers [2.20].

2.3.4.1 Thyristor based devices

In the solid-state FCLDs, semiconductor AC switch (two GTO thyristors connected in inverse parallel) is placed in series with each phase of the power line. In parallel with each switch is current limiting impedance as shown in figure 2-13. When a fault is detected, the normally conducting switch is turned off and the current is diverted to the parallel impedance which limits the current. A voltage arrester (Varistor) and a snubber circuit are connected in parallel with a switch to limit the level and the initial rate of rise of the transient voltage across the thyristors [2.10]. GTO thyristors now available can block forward and reverse voltages of up to 4500 V, carry continuous currents of up to 1100 A (rms) and interrupt peak currents of up to 3000 A [2.10].

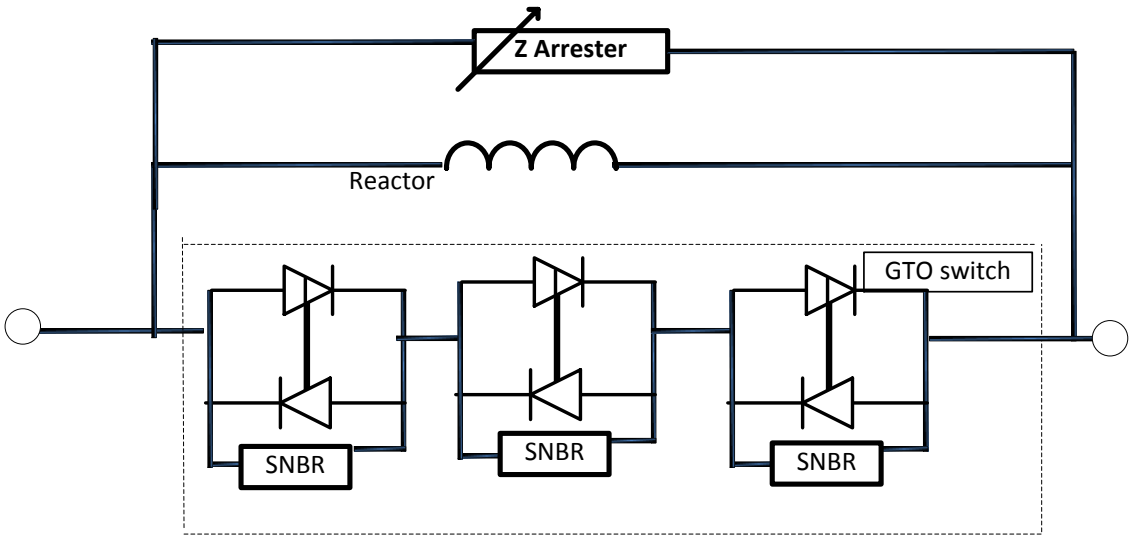

Figure 2- 13 GTO based CLD for a 15 KV circuit

Different circuit configurations based on the same principle were suggested. The parallel impedance was replaced by an inductor. Under normal load conditions, the GTO's are gated continuously and maintained in full conduction. When a fault occurs, the fault current initiates a turn-off for the GTO's. The GTOs of this type were connected in series to block the voltage, as the one used previously for 15 kV distribution system voltage class [2.20].

Then the inductor was replaced by a resistance, and in both cases the FCL does not utilize the full switching capabilities of GTO thyristors employed. This is because the current limiting action is essentially carried out by the parallel high-power impedance when the GTOs turn off at the event of the fault current [2.10]. Another development of FCL of this kind was the fault current interrupting device (FCID) for use at power distribution voltage levels. They have the advantages of very fast operating speed, produce no arc and incur very little maintenance [2.10].

Different types of FCIDs employing SCRs (silicon-controlled rectifier) or GTO thyristors have been investigated and employed in some applications [2.10] such as the main incoming transformer source leads, feeder applications, and bus tie position [2.20].

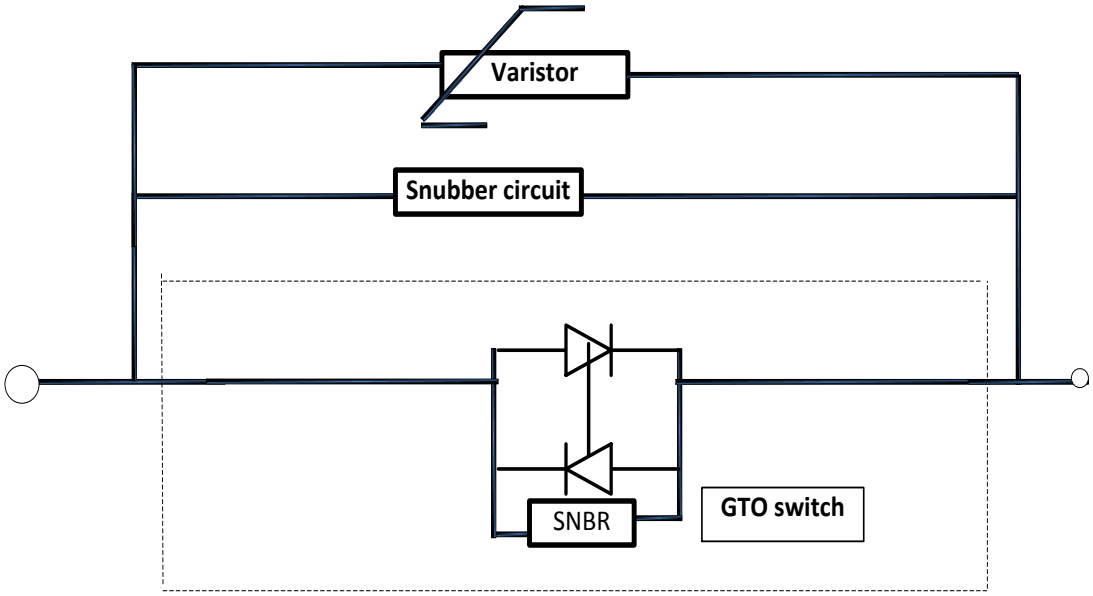

Figure 2- 14 Fault current interruption devise (FCID)

The current limiter interrupting device should have the following requirements: -

1. Interrupt the current in less than 1/2 cycle.
2. Reset only when both buses are healthy or by operator command.
3. Include isolating switches to keep it open when it is needed to be isolated.
4. Include bypass switches to carry current when no interruption by the CLID is desired.
5. Have continuous and overload ratings which match the capabilities of the circuit to which the CLD is applied.
6. Meet the frequency, maximum continuous voltage and dielectric strength ratings prescribed by ANSI/IEEE standards for the voltage class to which the CLD is applied.
7. Limit transient voltages to the same level as permitted by other protective devices, such as circuit breakers or reclosers.

Basically, the circuit layout of a FCID, shown in Figure 2-14, is like that of a FCLD except that the parallel current limiting impedance is not used. This enables the FCID to completely interrupt the current [2.10]. The FCID in existing power distribution network, although possible and advantageous as far as speed and maximum through current are concerned, suffers from the disadvantage of lacking coordination with downstream devices. On the contrary, the FCLD provides the possibility of limiting the fault current to safe limits and enable coordination with downstream devices. However, due to their inherent structure (the parallel low impedance), they do not have the capability to completely interrupt the fault

current. As a result, a hybrid solid-state breaker using a combination of GTO thyristors, SCR's and current limiting impedance was proposed. The fault current limiting and interrupting device (FCLID) is very similar to FCLD, instead of switching the GTO thyristors off for the complete period of overcurrent and leaving the parallel element to bear whole limiting duty, the GTOs thyristors is continuously switched on and off. Although the fault current can be shared by both GTOs thyristors and the parallel element, this device still does not utilize the full capability of GTO and incorporates more losses. Hence, for the sake of a better performance, the parallel element was replaced by a nonlinear resistor (Varistor). During normal operation the Varistor is short circuited by the GTO thyristors, which are in the on state. On detection of fault current, the conducting GTO thyristor is switched off and the fault current is diverted to Varistor. When the transient overvoltage is suppressed and the Varistor current decreases, the GTO switch is turned on again. When the current reaches the pre-set value, the GTO thyristor is turned off again, and so on. The state of operation is maintained for a specific period. If the overcurrent continuous for a longer period, the GTOs thyristors are permanently switched off. The FCLID can limit the fault current as well as being able to interrupt it. It has a simple structure and fast response. Contrary, the FCLID suffers from the thyristors operating losses and the fault current takes several cycles prior to a complete interruption [2.10].

2.3.4.2 Thyristor controlled reactor.

Contrary to the conventional reactor, which is in the system all the time, the thyristor-controlled devices can be introduced into transmission systems to reduce the down-time of the system during installation and commissioning. Additionally, they reduce losses as they are only inserted if a short circuit is detected. The reactor is connected in series with thyristor branch 1 during normal system operation and bypassed by thyristor branch 2 in case of a fault.

A surge arrester, which is designed for high energy absorption is placed in parallel with these two branches to protect the system from voltage surge during this transition. The fault current is therefore reduced by the limiting reactor.

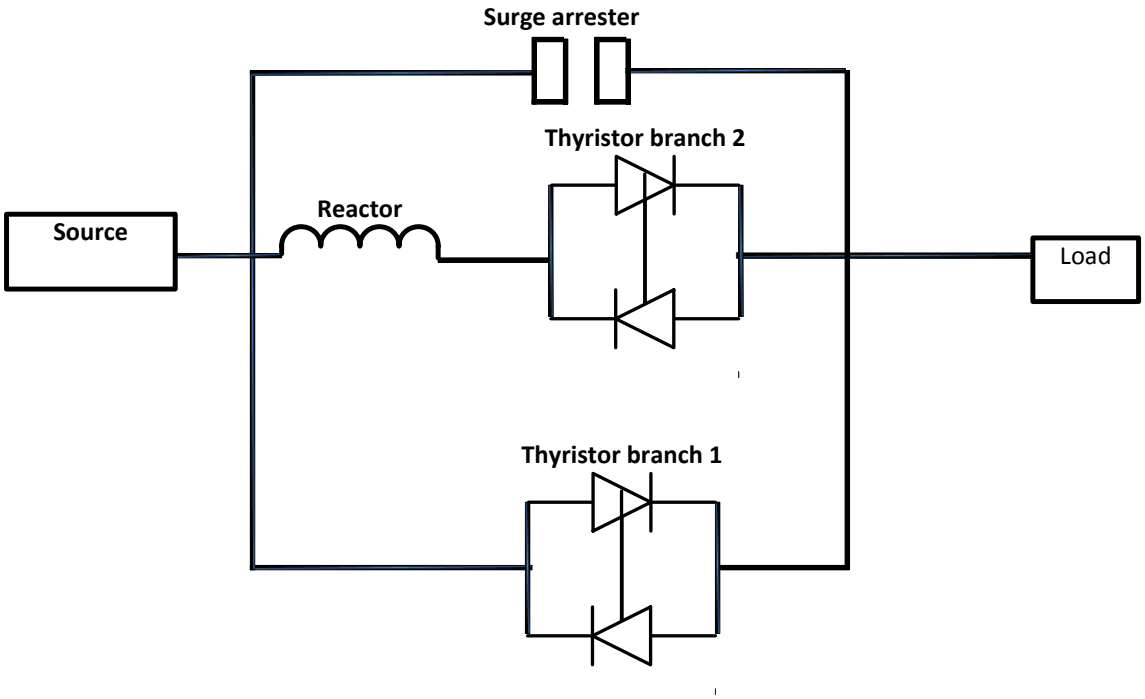

Figure 2- 15 Thyristor controlled reactor as a fault current limiter

This type of fault current limiter device encounters the problem of voltage drop and losses caused by the thyristors internal impedance. In addition, the control of the thyristors firing angle associated with harmonic distortion issue requires further study in the future [2.3].

2.3.4.3 Advanced series compensation (ASC)

The ASC thyristor protection scheme uses solid state devices which can react instantaneously to system conditions to turn on the thyristor-switched reactor and quickly insert an inductive element into the line to reduce fault currents (Figure 2-16). Protective features of electronic circuits using Break Over Diode (BOD) elements further enhance the self-protective feature of the scheme by automatic insertion of the thyristor-switched reactor. The ASC fault current feature is used at the Kayenta Substation, USA. The merits of this protection method can give additional benefits to utilities when increasing short circuit levels approach limits of existing equipment within the system [2.15].

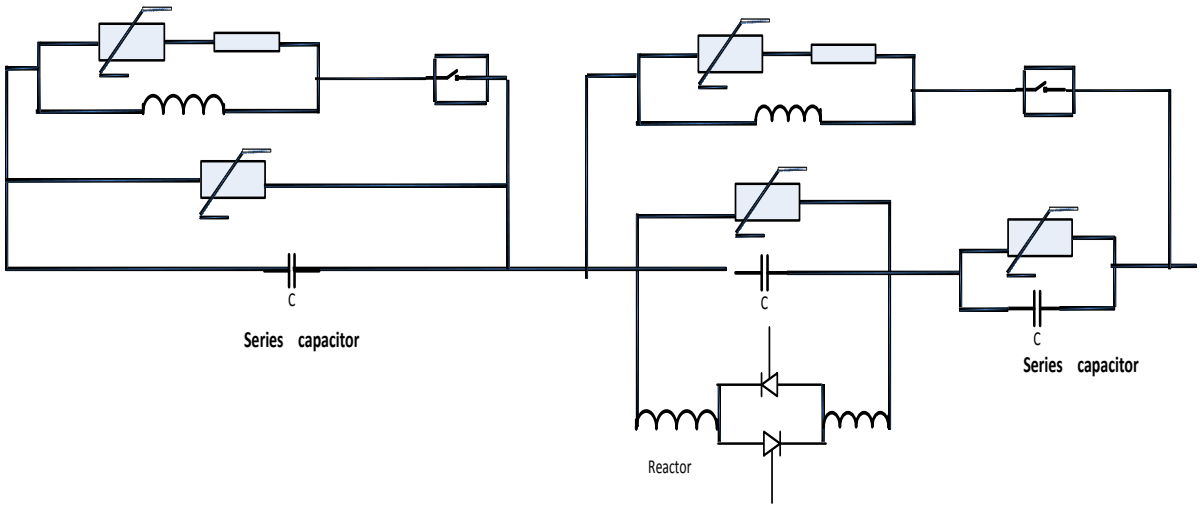

Figure 2- 16 ASC schematic diagram.

2.3.4.4 Thyristor controlled phase-shifting transformer

Phase-shifting transformers (quad boosters) can be built which insert capacitive or inductive voltages into the transmission line. This feature can be used to increase or decrease currents in a transmission line. To achieve fault current limitation quick insertion of the inductive part is required which can't be realised by slow mechanically switched phase-shifting transformers [2.15].

2.3.4.5 Thyristor controlled series tuned circuit.

A series capacitor is inserted in the line and a thyristor-controlled reactor is placed in parallel with it. During normal operation, the thyristor backs-off' the capacitance, providing the required amount of line compensation. The effective impedance of the line can thus be dynamically controlled which helps to increase the maximum power transfer capacity of the line. The first scheme of this type has been commissioned by Siemens at Kayenta in the USA (230 kV, 330 Mvar). If designed correctly it is possible that when a fault occurs, the firing angle of the thyristors can be adjusted (e.g. to less than 140 in the figure below) so that the net impedance inserted into the line becomes inductive rather than capacitive, thus reducing the fault current. This feature is an attractive by-product of a controlled series capacitor installation [2.6].

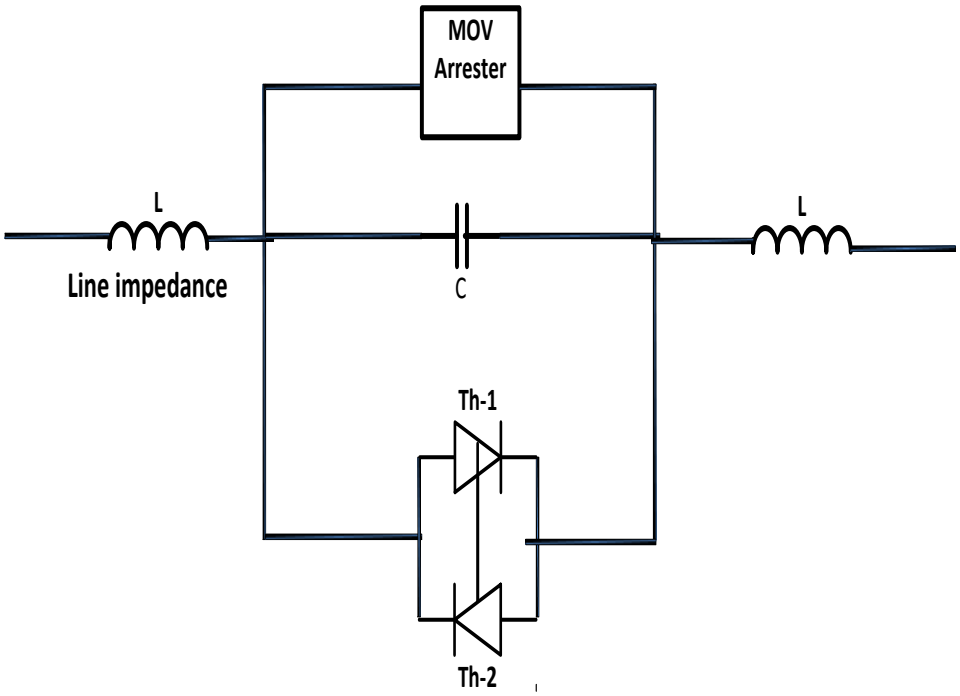

Figure 2- 17 Thyristor controlled series tuned circuit

2.3.4.6 Thyristor controlled resonant lc circuit fault current limiter

Two circuits are used for this type, the Thyristor-controlled resonant current limiter and the GTO (gate turn on) controlled resonant current limiter. In thyristor-controlled resonant current limiter the capacitance C is connected in series with the line and provides series compensation. When a short circuit occurs, the thyristors TH-I and TH-2 are fired, which connects inductance L in parallel with the capacitor. The resulting resonant circuit limits the fault current.

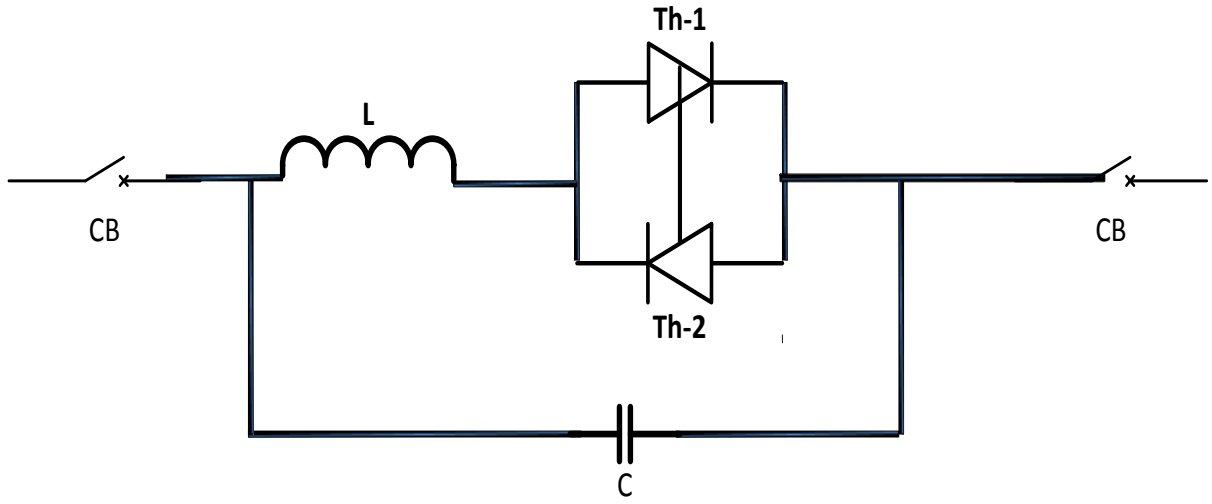

Figure 2- 18 Thyristor-controlled resonant current limiter

The second circuit utilises GTO switches, which are on under normal operating conditions. When a fault occurs, the GTO switches are turned off, and the current is diverted into the resonant circuit, which limits the fault current. The thyristors in the above circuit are conducting only during the fault. Capacitance C, which is connected in series with the line in normal operation, compensates the line voltage drop. The GTOs in Figure 2-19 carry the load current continuously, which generates losses during normal operation and requires larger, more expensive switches [2.5].

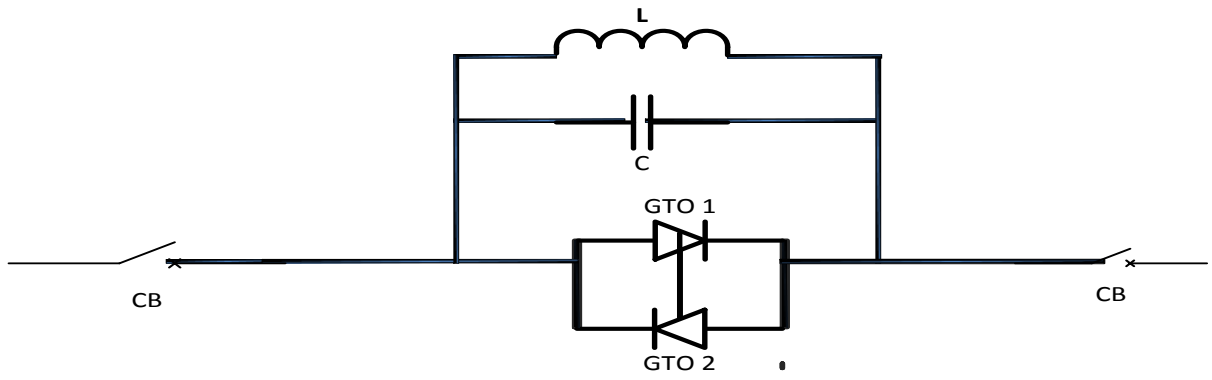

Figure 2- 19 GTO-controlled resonant current limiter

2.4 Motivation for novel magnetic fault current limiter

The candidate FCLDs currently being investigated are the re-healing fuse, the superconducting limiter, and the solid-state (thyristors based) limiter. The first has the main disadvantage of a limited number of operations. The second is restricted by the technical and economic limitations of producing high temperature superconducting materials [2.10]. These limitations involve the need for a refrigeration system to remove the heat generated by eddy current losses and to compensate for heat leakage into the cryogenic container, the need for additional sensors and control circuits, and the need for a reset time after clearing the fault. The above limitations affect the reliability and the overall efficiency of the system [2.23]. The solid state FCLD, however, in addition to the losses incurs, it cannot be placed in a situation where it would be subjected to a fault current for more than a cycle which, results in the destruction of the semiconductor devices.

For some semiconductor circuit topologies, specifically a voltage source inverter, the traditional methods of protection do not ensure the safety of the solid-state devices. However, if the rate of current rise could be reduced during a fault, then before current could rise to a destructive level, the solid-state devices could be turned off safely [2.23], [2.24]. In commercial-scale devices the high DC MMF required can typically only be achieved using superconducting DC coils, which greatly increase the complexity and ancillary equipment required for the FCL. Reducing the required DC-coil-generated MMF in FCLs has been the topic of considerable interest recently, and attention has been focused on using permanent magnets as a source of magnetic flux to “top up” or completely replace DC coil MMF [2.19].

Therefore, existing fault current limiting devices systems still fall short of addressing one or more of the following concerns; economic, current capacity, efficiency or reliability. Hence, there is currently a motivation to explore alternative approaches to fault current limiting, the magnetic fault current limiter Device (MFCLD) [2.24] - [2.38].

2.5 Introduction to permanent magnetic fault current limiter (PMFCL).

With the development of magnetic materials as well as topology design research, Fault Current Limiter based on permanent magnet biased saturation (PMFCL) has recently attracted a lot of interests of researchers and scientists. PMFCL shows low impedance during normal condition and renders high impedance during fault condition, which will change from

one state to the other automatically. With simple configuration and easy for manufacturing, this approach eliminates the need for an additional winding or a power supply, and thus addresses the issue of reliability, in addition, its response to a fault and the subsequent recovery process is automatic and instantaneous. With unique attributes including compactness, small size, reliable and fail-safe operation, and zero reset time, presently PMFCL has been one of the most promising current limiting technologies. In this new type of fault current limiters, the scheme has a permanent magnet as a source, which feeds a soft magnetic material iron core and keeps it in saturation during normal operating condition. The permanent magnet saturates the iron core so that the load current is not affected by the insertion of the device [2.13]- [2.14], [2.24]- [2.40]. This means the magnetic domains in the iron core are aligned in the direction of the magnetic field by means of the state of the art soft and hard magnetic materials [2.22]. In 1990s onwards, many researchers have reported on development of passive type magnetic current limiter using permanent magnet [2.27]. The PMFCL has a promising practicality and economy in applications with two pivotal features based on its operation principle. Firstly, the bias magnetic field is generated by the permanent magnet without employing any superconducting system or DC sources. Secondly, The PMFCL achieves fault current suppression through dynamic transition of the nonlinear permeability of iron-core within

a very quick response time excluding additional expensive control devices. Consequently, with preferable competence in both technological and economic advantages [2.39]. Quite

a few of research institutes, such as Toronto University in Canada, Kanazawa University in Japan, AREVA T&D technology Centre in Europe, Tsinghua University and Shandong University in China, have done both simulating and experimental studies with low voltage prototypes. These fundamental work and invaluable achievements establish a milestone for further research. However so far, the available research results on PMFCL are mainly based on the low voltage prototypes. Hence, how to design a PMFCL for high voltage and especially large capacity applications remains a great concern nowadays. For a large capacity design, the principal aspects that require further research of PMFCL lie in the static and dynamic operating characteristics, fault current limiting characteristics, equivalent magnetic circuit modelling, topology optimization and so on [2.14], [2.25].

2.6 The Passive Fault Current Limiter

The passive type fault current limiter composed of permanent magnets and a low saturation flux density material was proposed [2.29].

AREVA T&D Technology Centre in the U.K designed a magnetic fault current limiter using soft and hard magnetic materials. The basic design is that a laminated 'C' core inductor has a piece of un-magnetised permanent magnet bridging its poles. Its coil is connected in series with the power circuit that it is protecting as shown in figure 2-20 [2.13].

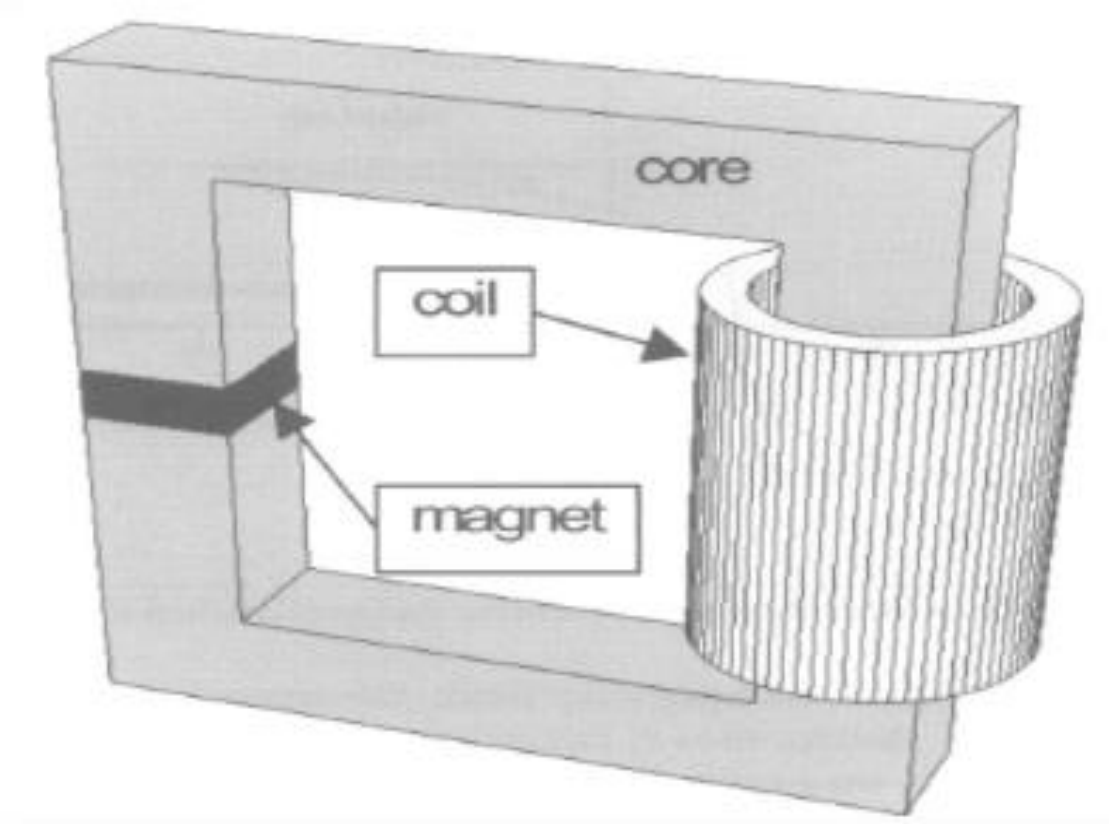

Figure 2- 20 A Magnetic fault current limiter [2.13]

Later, in Kolghat, India, a group of researchers conducted a research into the analysis of parallel biased MFCL, Figure 2-21, using ferrite core and N_dFeB magnet. They concluded that the MFCL is a way to provide affordable and quality power to the consumers [2.28].

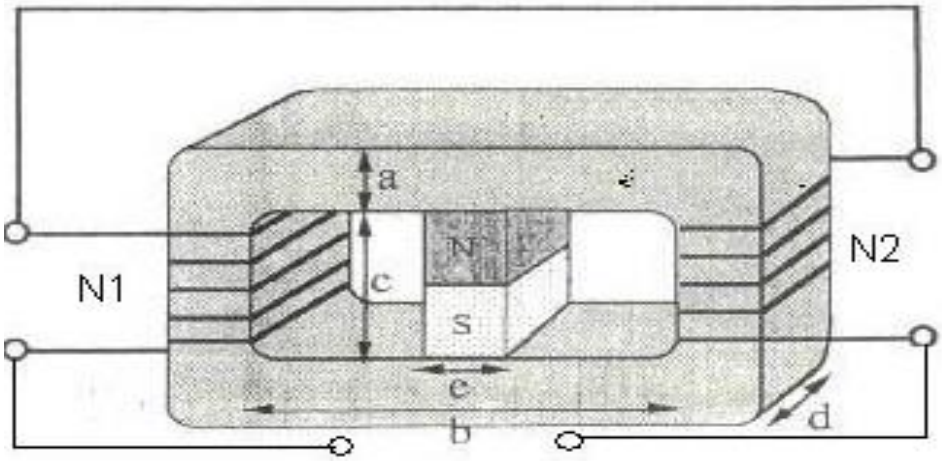

Figure 2- 21 Parallel biased magnetic fault current limiter [2.28]

Another development to the MFCL was the introduction of a new topology of PMFCL [2.26]. As for the new topology, the conventional PMFCL is generally divided into two types, the series connection and the parallel connection as shown in Figure 2-22. The series connection topology with two identical magnetic devices is connected with opposite magnetomotive forces to limit the positive and negative half-wave currents respectively. In the parallel connection topology, the permanent magnets are employed to generate a strong magnetic field as to bias the iron-cores into deep saturation. Under normal conditions, the AC magnetic field generated by coil is not enough to drive iron-core out of saturation, so the PMFCL behaves like an air-cored reactor with a low inductance. While a fault comes, either of the iron-cores comes out of saturation on alternate half-waves of the short current within a very sharp time duration, and the inductance of the PMFCL rises considerably to a big value, which is a summation of the inductances of a saturated core plus the other un-saturated core. However, the iron-core may go in to the reverse saturation and lose the fault current limiting capability if the fault current continues increasing to a very high value.

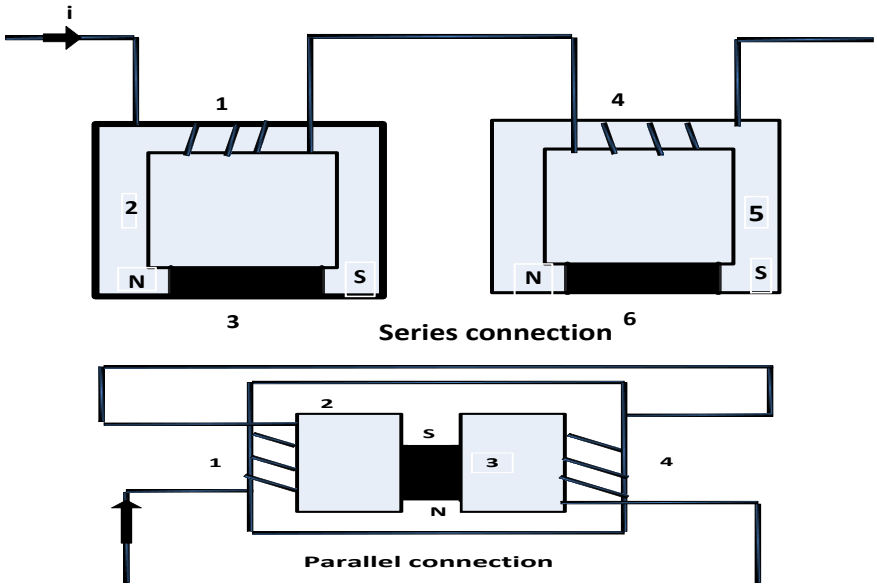

1,4- coil; 2,5- iron core; 3,6 - permanent magnet

Figure 2- 22 Conventional topology principles of PMFCL models

The new topology in [2.26] was simulated by 2D FEM [2.41] and verified by experiments to present effective basis and guide towards the design of high voltage and large capacity permanent magnet fault current limiter (PMFCL) [2.26]. The new topology was consisting of a permanent magnet and iron core, which has the same principle as the conventional series topology of Figure 2-22. Compared with the conventional PMFCL topology, yoke section of iron-core is removed to optimize the magnetic circuit. Two methods are presented apparently accounting for improving the bias capability of the permanent magnet. The first one is changing magnetic materials of better magnetic performance, such as the iron core and the permanent magnet. The second method, which is adjusting the configuration of the magnetic circuit and adjusting the main geometrical parameters like structural parameters of the PMFCL. Specifically, the permanent magnet including decreasing length or increasing section area is strongly recommended with reference to the convenient practical adjustment based on the novel topology.

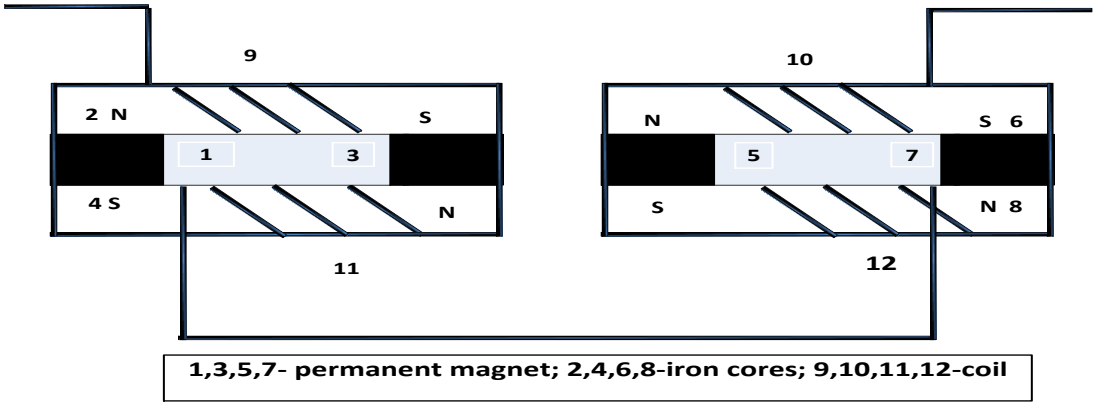

Figure 2- 23 Schematic diagram of a novel PMFCL topology

Liang Zou, et al. (2009), [2.26] simulated a large capacity 10KV PMFCL model, based on saturation depth ratio concept [2.26], [2.35], with a high number of turns (800) in 2D (FEM). The effect of the PMFCL on the fault current according to 2D (FEM) transient results showed that the fault current was reduced from analytically calculated of 4000 A to numerically calculated of 1700 A [2.26].

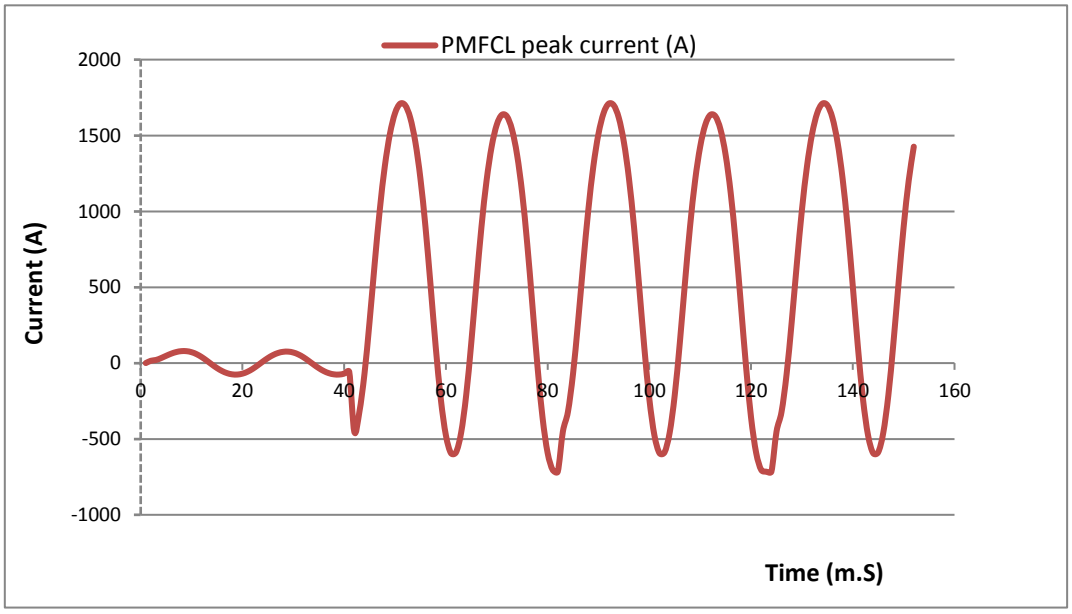

Figure 2- 24 Simulated transient current in 2D FEM

A further study was the design of hybrid FCL for the FREEDM system by means of substituting the iron core by a neodymium permanent magnet, which is the ferromagnetic core, as Figure 2-25 illustrated. The ferromagnetic core is connected in parallel with a fast-mechanical switch, which is operated by a controller in abnormal conditions to provide rushed impedance, and a surge arrester for overvoltage protection [2.37]

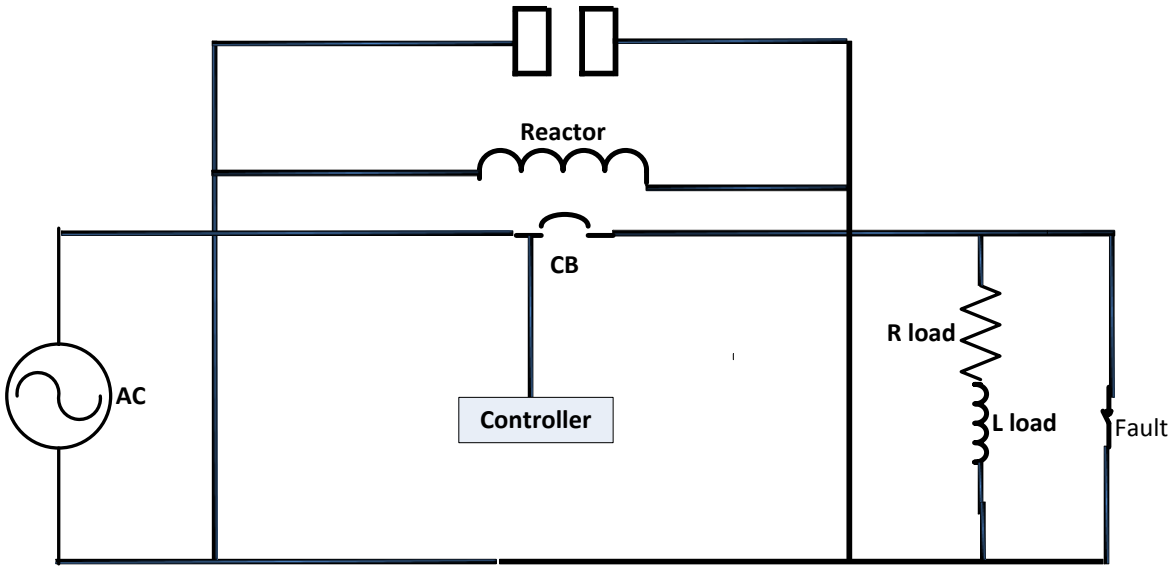

Figure 2- 25 Schematic of the proposed hybrid FCL

W S Siew with the same group of Chinese researchers, in addition to Li Zhang, Shandong University, China, [3.14] studied four types of PMFCL topology, which are named according to the mode how the permanent magnet biases the core, as indicated in Figure 2-26.

A Parallel biased PMFCL is consisted of two sets C-shape cores, one permanent magnet and two AC current windings**.** The permanent magnet in the middle biases the two C-shape cores and forces them into saturation under normal conditions. Each C-shape core is used for one of the half power cycles. The two windings around the two core limbs arranged magnetically in opposite direction function as a bipolar current limiter to suppress the large current flow in the AC circuit [2.14].

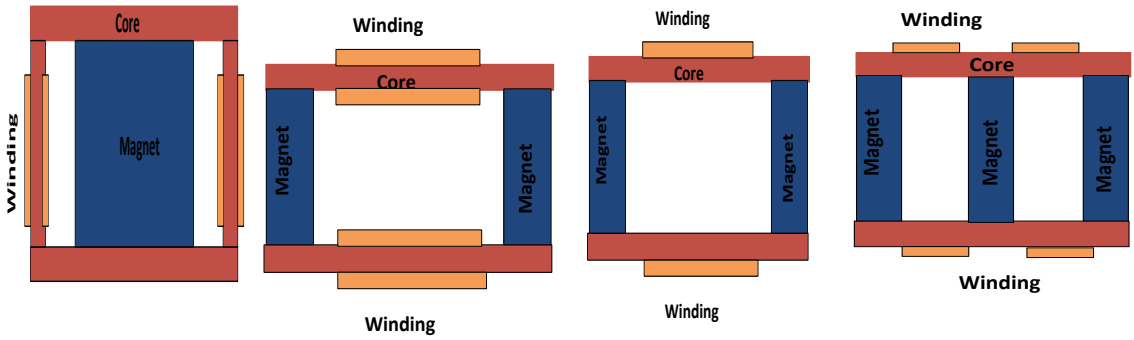

Figure 2- 26 A parallel, series I, series II and comprehensive design

The series biased design I is much more economical than the parallel biased PMFCL in term of the topology design. The permanent magnet is divided into two pieces in series with the two cores. As the magnetic field direction in the two cores is opposite, the windings around the two cores are magnetically in the same direction.

The magnetic structure of the series biased design II is like that of the series biased design I, however, there is only one winding around the two cores for the series biased design II, where the winding functions to limit the fault current at every alternative power cycle. A comprehensive design PMFCL is the synthesis of a parallel biased design and a series biased design II, in which the permanent magnet is separated into three parts and its middle limb is twice bigger than the other two side limbs.

The AC windings of the above four topologies are wounded around the cores and thus the magnets in these configurations are exposed only to the magnet's own DC flux. Therefore, the impact incurred from demagnetization or eddy current losses does not play a significant role for the above modes. The researchers used NdFeBN35 as a magnetic material and cold-rolled steel DW360-50 with higher permeability as the core material and found that the flux density through the magnet of the comprehensive design PMFCL is the biggest while through that of the parallel biased design is the smallest. The comparison of the results demonstrates that the comprehensive design configuration always gets the deepest saturation extent of the four types. Apart from the core saturation and operating point of the magnetic flux density in the permanent magnet, the leakage flux should not be ignored. The leakage flux directly influences the static magnetic field distribution and indirectly influences the fault current limiting characteristics of the PMFCLs. The analytical results obtained by the researchers show that, the PMFCLs with one-winding topology, especially the comprehensive design PMFCL, is

much preferable for large capacity design compared with the two-winding topology, such as the parallel biased design and the series biased design I. Based on detailed study on both the static and dynamic magnetic characteristics of different modes of PMFCLs, the derived equivalent magnetic circuits present fundamental basis for further study of the operating mechanism of the PMFCLs as well as optimization of the fault current limiting topology design. The actual magnetic field distribution of the PMFCLs is quite complicated, and the flux leakage phenomenon in windings and the cores must be fully accounted, which needs further investigation in the future, combining both theoretical and experimental studies [2.14].
In [2.24] a new structure of parallel type permanent magnet fault current limiter (PPMFCL) was introduced.

The previous related work on PMFCL are mainly based on the low voltage prototypes, hence, how to design a PMFCL for high voltage and especially large capacity applications [2.26] remains a great concern nowadays.

2.7 Conclusion

Different types of fault current means of limitation have been studied. There are the rehealing fuse, superconducting limiter, and the solid-state (thyristors based) limiter. The first has the main disadvantage of a limited number of operations. The second is currently restricted by the technical and economic limitations of producing high temperature superconducting materials. The limitations of superconductor fault current limiters affect the reliability and the overall efficiency of the system and were previously discussed in section 2.4. The solid state FCLD, however, in addition to the losses incurs, it cannot be placed in a situation where it would be subjected to a fault current for more than a cycle which, results in the destruction of the semiconductor devices.
Therefore, existing fault current limiting devices systems still fall short of addressing one or more of the following concerns; economic, current capacity, efficiency or reliability. Hence, there is currently a motivation to explore alternative approaches to fault current limiting, the magnetic fault current limiter Device (MFCLD). The proposed PMFCL is designed to be used with the distribution transformers to improve the reliability, cost effectiveness and safety of power distribution system by limiting the short circuit current. The aim of this research is to limit or eliminate the short circuit current flowing through distribution transformers primary

circuit by means of the permanent magnet fault current limiter (PMFCL). This study is also focusing on reducing the momentary voltage drop and co-operating with the protective relays in a power system.

The Finite Element Method MagNet will be used in the simulation to design and implement the new distribution transformers permanent magnet fault current limiter for the power grid. The new device is expected to offer almost the sufficient requirements of the fault current limiter.

References

[2.1] J. R. S. S. Kumara, et al. (2006). Over current protection coordination of distribution networks with fault current limiters. *2006 IEEE power engineering society general meeting,* 8 pp.

[2.2] MORICONI, F., et al. (2010). Modelling and test validation of a 15kV 24MVA superconducting fault current limiter. Transmission and Distribution Conference and Exposition, 2010 IEEE PES, 1-6.

[2.3] J. P. Sharma and V. Chauhan (2015). Analysis and control of fault current by firing angle control of solid state fault current limiter. *2015 international conference on energy systems and applications,* 527-530.

[2.4] D. Sharma and K. B. Sahay (2016). Basic concepts of superconducting fault current limiter. 2016 IEEE 1st international conference on power electronics, intelligent control and energy systems (ICPEICES), 1-5.

[2.5] M. Rezaee and R. G. Harley (2016). Performance analysis of parallel-type resonant fault current limiters. *2016 Clemson university power systems conference (PSC),* 1-5.

[2.6] S. Patil and A. Thorat (2017). Development of fault current limiters: A review. *2017 international conference on data management, analytics and innovation (ICDMAI),* 122-126.

[2.7] S. Nam, J. Lee, W. S. Lee, Y. G. Park, S. Song, H. Jin, et al. (2015). Operational characteristics of a small-scale novel hybrid resistive-type SFCL with controlled power electronics. *IEEE Transactions on Applied Superconductivity, 25*(3), 1-5.

[2.8] S. H. Lim, H. S. Choi and B. S. Han (2006). Fault Current Limiting Characteristics of DC Dual Reactor Type SFCL Using Switching Operation of HTSC Elements. *IEEE transactions on applied superconductivity,* 16 (2), 723-726.

[2.9] T. R. Blackburn, et al. (2013). The performance of a power system high Tc superconducting fault current limiter with saturable core under symmetrical fault conditions. In: *2013 IEEE international conference on applied superconductivity and electromagnetic devices,* 245-249.

[2.10] C. C. Marouchos, et al. (2017). An investigation of the switched-capacitor circuit as a solid-state fault current limiting and interrupting device (FCLID) with power factor correction suitable for low-voltage distribution networks. 2017 52nd international universities power engineering conference (UPEC), 1-5.

[2.11] GANG, C., et al. (2003). Simulation study of bridge type solid state fault current limiter. Power Engineering Society General Meeting, 2003, IEEE, 2526 Vol. 4.

[2.12] J. B. Cui, et al. (2013). Safety Considerations in the Design, Fabrication, Testing, and Operation of the DC Bias Coil of a Saturated Iron-Core Superconducting Fault Current Limiter. *IEEE transactions on applied superconductivity,* 23 (3), 5600704-5600704.

[2.13] Design and Construction of a Magnetic Fault Current Limiter, J-L. Rasolonjanahary, J.P. Sturgess*, E.F.H. Chong, A.E. Baker, C.L. Sasse

[2.14] FARHOODNEA, M., MOHAMED, A. and SHAREEF, H. (2014). A comparative study on the performance of custom power devices for power quality improvement. Innovative Smart Grid Technologies - Asia (ISGT Asia), 2014 IEEE, 153-157.

[2.15] A. Abramovitz and K. Ma Smedley (2012). Survey of Solid-State Fault Current Limiters. *IEEE transactions on power electronics,* 27 (6), 2770-2782.

[2.16] H. Samet, et al. (2017). Fault current limiter versus series reactor. In: 2017 IEEE international conference on environment and electrical engineering and 2017 IEEE industrial and commercial power systems Europe (EEEIC / I&CPS Europe), 1-5.

[2.17] RANJAN, R. and KALKSTEIN, E. W. (1994). Design, development and application of smart fuses-part 1. Industry applications, IEEE transactions on, 30 (1), 164-169.

[2.18] T. Hazel, B. Leforgeais and E. Savary (2015). Operation of power systems incorporating fault current limiting devices. *2015 petroleum and chemical industry conference Europe (PCIC Europe),* 1-8.

[2.19] KNOTT, J. C. and MOSCROP, J. W. (2013). Increasing energy efficiency of saturated-core fault current limiters with permanent magnets. *Magnetics, IEEE transactions on,* 49 (7), 4132-4136.

[2.20] MORICONI, F., et al. (2011). Development and deployment of saturated-core fault current limiters in distribution and transmission substations. *Applied superconductivity, IEEE transactions,* 21 (3), 1288-1293.

[2.21] J. A. Sa'ed, et al. (2017). Control of solid-state fault current limiter for DG-integrated distribution systems. *2017 IEEE international conference on environment and electrical engineering and 2017 IEEE industrial and commercial power systems Europe (EEEIC / I&CPS Europe),* 1-5.

[2.22] F. G. Balakrishnan, S. K. Sreedharan and J. Michael (2013). Transient stability improvement in power system using unified power flow controller (UPFC). *2013 fourth*

international conference on computing, communications and networking technologies (ICCCNT), 1-6.

[2.23] David Jiles, Magnetism and Magnetic Materials, second edition.

[2.24] J. Yuan, et al. (2015). Performance Investigation of a Novel Permanent Magnet-Biased Fault-Current Limiter. *IEEE transactions on magnetics,* 51 (11), 1-4.

[2.25] C. Tian, et al. (2017). A Coupled Method for Evaluating Eddy Current Loss of NdFeB Permanent Magnets in a Saturated Core Fault Current Limiter. *IEEE transactions on magnetics,* 53 (6), 1-4.

[2.26] Liang Zou, et al. (2009). Study on the feasibility of developing high voltage and large capacity permanent-magnet-biased fault current limiter. Universities Power Engineering Conference (UPEC), 2009 Proceedings of the 44th International, 1-5.

[2.27] HALL, J. and CHEER, A. (2013). Fault current limiter surge protection device for the power grid based upon zero power consumption ceramic ferrite permanent magnets. Electricity Distribution (CIRED 2013), 22nd International Conference and Exhibition on, 1-4.

[2.28] SANTRA, T., et al. (2009). Analysis of passive magnetic fault current limiter using wavelet transform. Power Systems, 2009. ICPS '09. International Conference on, 1-6.

[2.29] L. Hong-shun, et al. (2008). Operating characteristics of the Permanent-Magnet-Biased Saturation Based Fault Current Limiter. In: *2008 international conference on high voltage engineering and application,* 503-507.

[2.30] C. Tian, et al. (2017). A Coupled Method for Evaluating Eddy Current Loss of NdFeB Permanent Magnets in a Saturated Core Fault Current Limiter. *IEEE transactions on magnetics,* 53 (6), 1-4.

[2.31] Q. Li, et al. (2012). Modelling methodology and experimental verification of the permanent-magnet-biased saturation-based fault current limiter, *IET electric power applications,* 6 (8), 504-512.

[2.32] B. Chen, et al. (2016). Investigation on a modified hybrid compact saturated-core fault current limiter based on permanent magnets. 2016 IEEE conference on electromagnetic field computation (CEFC), 1-1.

[2.33] J. Yuan, et al. (2015). Investigation of the performance of a novel permanent magnet biased fault current limiter. *2015 IEEE magnetics conference (INTERMAG),* 1-1.

[2.34] Shah, S. S. A., Khan, F., & Mutalib, P. A. Fault current limiter for a distributed power system.

[2.35] Liang Zou, Yuan Ma, Hong-shun Liu, Qing-min Li, & Shu-min Sun. (2008). Impact of saturation depth ratio of iron-core on the PMFCL. 2008 International Conference on Electrical Machines and Systems, pp. 4338-4343.

[2.36] J. C. Knott, et al. (2014). Design Considerations in $hbox{MgB}_{2}$-Based Superconducting Coils for Use in Saturated-Core Fault Current Limiters. *IEEE transactions on applied superconductivity*, **24** (5), 1-4.

[2.37] G. G. Karady, J. R. Prigmore, & J. A. Mendoza. (2012). A neodymium permanent magnet fault current limiter for use in the FREEDM project. 2012 3rd IEEE PES Innovative Smart Grid Technologies Europe (ISGT Europe), pp. 1-7.

[2.38] L. Wei, B. Chen, J. Yuan, C. Tian, Y. Zhong, X. Li, et al. (2017). Performance and optimization study of a novel compact permanent-magnet-biased fault current limiter

[2.39] Limiter, F. C. (2014). FEM simulations of permanent-magnet-biased saturation based.

[2.40] R. Patwary, S. Datta, & S. Ghosh. (2011). Harmonics and interharmonics estimation of a passive magnetic fault current limiter using coiflet wavelet transform. 2011 International Conference on Communication and Industrial Application, pp. 1-6.

[2.41] Magnet user manual by Infolytica, www.infolytica.com.

Chapter 3: - Magnetism, magnetic materials and related issues

3.1 Introduction

Magnetic materials cover a wide variety of materials, which are used in a different range of applications. Magnetic materials are utilized in the generation and distribution of electricity, and in most cases in the appliance that use that electricity. The need for efficient generation and uses of electricity is dependent on improved magnetic materials and designs.

Non-polluting electric vehicles will rely on efficient motors utilizing advanced magnetic materials. The state-of-the-art soft magnetic materials (SMM) are those which can be easily magnetized and demagnetized [3.1]- [3.2].

The term hard magnetic material is used to describe materials that have sufficiently high resistance to demagnetizing fields. The hard-magnetic materials maintain a large amount of residual magnetism after exposure to a magnetic field.

This chapter begins with the classification of magnetic materials. Then, it will look at the properties of magnetic materials such as permeability, coercivity, remanence, saturation magnetization, etc. It also will deal with magnetic materials types and applications [3.2]- [3.3]

3.2 Classification of magnetic materials

The materials can be classified according to their hysteresis loop and the magnetic field behaviour.

3.2.1 Classification of materials based on hysteresis loop

The hysteresis loop is a curve, a name given to the curve drawn between induced magnetic field (B) and the applied magnetic force (H), as shown in Figure 3-1. In the SI unit of measurement, the magnetic field (B) is measured in Tesla (T) and the magnetic force (H) is measured in Amber per meter (Am^{-1}) [3.1].

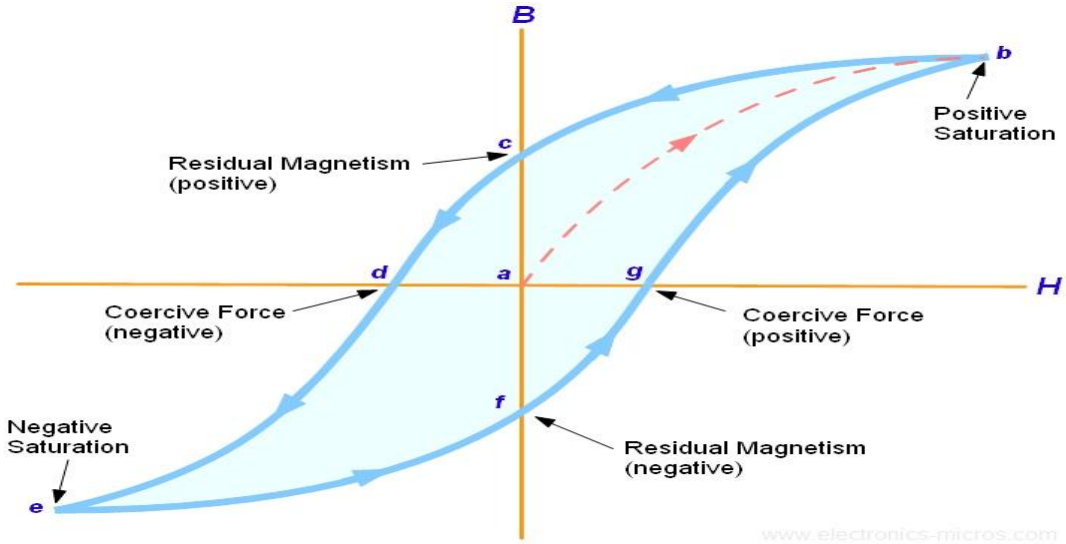

Figure 3- 1 Typical B-H loop of a ferromagnetic material [3.1]

Starting with demagnetised core, both B and H will be at zero, point (a) on the magnetisation curve. If the magnetisation current I is increased in a positive direction to some value, the magnetic field strength H increases linearly with I and the flux density B will also increase as shown by the curve from point (a) to point (b) as it heads towards saturation. Now, if the magnetising current in the coil is reduced to zero, the magnetic field circulating around the core also reduces to zero. However, the coils magnetic flux will not reach zero due to the residual magnetism present within the core and this is shown on the curve from point (b) to point (c). To reduce the flux density at point (c) to zero we need to reverse the current flowing through the coil. The magnetising force which must be applied to null the residual flux density is called a “Coercive Force”. This coercive force reverses the magnetic field re-arranging the molecular magnets until the core becomes demagnetised at point (d). An increase in this reverse current causes the core to be magnetised in the opposite direction and increasing this magnetisation current further will cause the core to reach its saturation point but in the opposite direction, point (e) on the curve [3.1]. This point is identical to point (b). If the magnetising current is reduced again to zero the residual magnetism present in the core will be equal to the previous value but in reverse at point (f) Again reversing the magnetising current flowing through the coil this time into a positive direction will cause the magnetic flux to reach zero, point (g) on the curve and as before increasing the magnetisation current further in a positive direction will cause the core to reach saturation at point (b). Then the B-H curve follows the path of b-c-d-e-f-g-b as the magnetising current flowing through the coil

alternates between a positive and negative value such as the cycle of an AC voltage. This path is called a Magnetic Hysteresis Loop. The effect of magnetic hysteresis shows that the magnetisation process of a ferromagnetic core and therefore the flux density depends on which part of the curve the ferromagnetic core is magnetised on as this depends upon the circuits past history giving the core a form of “memory”. Thus, ferromagnetic materials have memory because they remain magnetised after the external magnetic field has been removed. However, soft ferromagnetic materials such as iron or silicon steel have very narrow magnetic hysteresis loops resulting in very small amounts of residual magnetism making them ideal for use in relays, solenoids and transformers as they can be easily magnetised and demagnetised. Since a coercive force must be applied to overcome this residual magnetism, work must be done in closing the hysteresis loop with the energy being used and dissipated as power in the magnetic material. This power is known as hysteresis loss and the amount of loss depends on the material’s value of coercive force. By adding additive to the iron metal such as silicon, materials with a very small coercive force can be made to have a very narrow hysteresis loop. Materials with narrow hysteresis loops are easily magnetised and demagnetised and known as soft magnetic materials. Magnetic hysteresis results in the dissipation of wasted energy in the form of heat with the energy wasted being in proportion to the area of the magnetic hysteresis loop. Hysteresis losses will always be a problem in transformers where the current is constantly changing direction and thus the magnetic poles in the core will cause losses due to the constantly reverse direction. Rotating coils in DC machines will also incur hysteresis losses as they are alternately passing north the south magnetic poles. The shape of the hysteresis loop depends upon the nature of the iron or steel used and in the case of iron which is subjected to massive reversals of magnetism, for example transformer cores, it is important that the B-H hysteresis loop is as small as possible. In general, the soft magnetic materials are characterised by a steeply ascending magnetization curve; that is, large values of flux density are produced by small magnetizing forces. For certain applications where the flux density is low, the initial portion of the curve is important for intermediate flux density applications, the steeply ascending portion is of a dominant interest while for higher densities, the upper portion is of higher importance [3.1- [3.2].

3.2.2 Classification of magnetic materials on account of behaviour in a magnetic field

The various types of magnetic materials are traditionally classified according to their susceptibility. The susceptibility (χ) indicates the degree of magnetization (M) of a material in response to an applied magnetic field (H).

$$\chi = \frac{M}{H} \tag{3.1}$$

The first group are materials for which χ is small and negative. These materials are called diamagnetic; their magnetic response opposes the applied magnetic field. The diamagnetic materials for which their susceptibility is approximately -10^{-5} are silver, gold, bismuth and beryllium. The atoms in this type have no magnetic moment. Superconductors from diamagnetic materials are for which $(\chi) = -1$. A second group of materials are paramagnetic for which (χ) is small and positive and typically (χ) approximately in the range 10^{-3} to 10^{-5}. The magnetization of paramagnetic is week but aligned parallel with the direction of the magnetic field. Examples of paramagnetic materials are aluminium, platinum and oxygen. It also includes various salts of the transition metals such as chloride, sulphates and carbonates of manganese- chromium-iron and copper. Furthermore, it includes hydrated salts such as potassium-chromium. The atoms in paramagnetic materials have randomly oriented magnetic moments. In diamagnetic and paramagnetic materials, the magnetic susceptibilities at constant temperature and for relatively low value of magnetic field are constant. Under these conditions the materials are called linear, that magnetization is proportional directly to the applied field. The diamagnetism and paramagnetism do not have linear relationship between magnetic induction (B) and magnetic field (H) at high field due to the exhibition of saturation magnetization. Another group which is the most widely recognised magnetic materials are the ferromagnetic solids for which (χ) is much greater than 1 and typically can have values $(\chi) \approx$ 50 to 10,000. Examples of these materials are iron, cobalt and nickel and several rare earth materials and their alloys, magnets, helimagnets and supermagnets. In ferromagnetic materials both permeability and susceptibility are strongly affected by prevailing magnetic field (H). They do not have a constant value. The atoms have parallel aligned magnetic moments. Ferromagnetism acquires a large magnetization in relatively small magnetic fields. This magnetization corresponds to all magnetic moments being aligned. The ferromagnetic and ferromagnetic materials are used in many engineering applications

because of their high permeability which enable high magnetic induction to be obtained with only modest magnetic fields. They have ability to retain magnetization and they act as a source of field. The ferromagnetic materials are also used in permanent magnets, magnetic recording, power generation and inductors, transformers and relays applications.

The antiferromagnetic materials have antiparallel magnetic moment and hence the magnetic field cancels out and the materials behave in the same way as paramagnetic materials. Ferrimagnetic materials have atomic magnetic moments aligned parallel and antiparallel. The material breaks down into magnetic domains just like a ferromagnetic material [3.2].

Table 3-1 Susceptibility at room temperature for each type of magnetic material [3.1]

Type of magnetism	**Susceptibility**	**Example**	**Susceptibility (T.m/A)**
Diamagnetism	Small and negative	Aluminium (Au) Cupper (Cu)	-2.74×10^{-6} -0.77×10^{-6}
Paramagnetism	Small and positive	Pentium (Pt) Manganese (Mn)	21.04×10^{-6} 66.10×10^{-6}
Ferromagnetism	Large and positive, function of applied field, microstructure dependant	Iron (Fe)	Up to $\sim 100{,}000$
Antiferromagnetism	Small and positive	Chromium (Cr)	3.42×10^{-6}
Ferrimagnetism	Large and positive, function of applied field, microstructure dependent	Barium Ferrite (Ba Ferrite)	Up to ~ 3

Diamagnetic materials are typically those which are considered non-magnetic. Most organic compounds fall in this classification, as well as many metals such as copper, mercury, and gold. Metals which are typically diamagnetic are heavy metals with core electrons.

In paramagnetic materials, each atom possesses a permanent dipole moment, resulting from incomplete cancellation of the electron spins or orbital magnetic moments. These atomic magnetic moments are randomly oriented. Paramagnetic material has no net macroscopic magnetization and exhibit magnetic behaviour only in the presence of a magnetic field and retains no magnetism when the field is removed. The dipoles of paramagnetic materials do not affect the surrounding dipoles within the material [3.1].

3.3 Magnetic properties of magnetic materials

3.3.1 Hysteresis loop

The Magnetic Hysteresis loop previously shown in Figure 3-1 illustrates the behaviour of a ferromagnetic core.

3.3.2 Permeability

The permeability is a property of the specific medium through which the (H) field passes and in which (B) is measured. The permeability of a material is a measure of the degree to which the material can be magnetized, or the ease with which a (B) field can be induced in the presence of an external (H) field. The magnetic flux density (B) is given by

$$B = \mu_0 H \quad (3.2)$$

In SI system of measurement, the permeability is measured in Weber per ampere-meter (Wb/A-m), (T m/A) or henry per meter (H/m) as (B) is measured in $^{wb}/_{m^2}$ or tesla (T).

$$\mu = \mu_0 \mu_r \quad (3.3)$$

where(μ) is the permeability, $(\mu_{0)}$ is the permeability of a vacuum, it equals $4\pi \times 10^{-7}$(Wb/Am) or (H/m) and $(\mu_{r)}$ is the relative permeability, which is the ratio of the permeability in a material to the permeability in a vacuum and hence it has no unit. In a vacuum, $(\mu_r) = 1$.

The linear relationship between (B) and (H) and is,

$$B = \mu_0 \mu_r H \quad (3.4)$$

However, in other media particularly ferromagnetic and ferrimagnetic materials, B is no longer a linear function of H and hence (μ_r) varies rapidly with (H). This means the permeability (μ) is not constant as a function of magnetic field in the way that the permeability of paramagnetic is [3.2]. In order to characterize the properties of a given magnetic material it is necessary to measure the magnetic induction (B) as a function of (H) to obtain a hysteresis curve. The permeability ranges from the initial permeability, which is the initial slope of the magnetization curve to the maximum permeability, which is the maximum value at the saturation's point. The initial relative permeability for ferromagnets usually lie in the range of 10 - 10^5. The highest values occur for special alloys such as permalloy and supermalloy, which are nickel-iron alloys. These materials are used as flux

concentrators. For soft magnetic materials the permeability is a large quantity at low magnetizing force. In the original state the bulk magnetization of ferromagnets is zero, but on an application of a magnetic field they become magnetically polarized; that is, they acquire a magnetization. However, the magnetization of ferromagnets is mostly orders of magnitude greater than the field strength which produce them [3.2].

3.3.3 Differential permeability

As any value of permeability μ can be obtained including (μ) = ∞ at the remanence (B)= (B_R), (H)=0 and (μ) = 0 at the Coercivity (B)=0, (H) = (H_c). The permeability (μ) is not a particularly precise parameter for characterisation of ferromagnets. The differential permeability is known as the incremental permeability, (μ) = (dB/dH), is a more useful quantity although this value varies with the field. The initial or apparent permeability is the slope of the initial magnetization curve at the origin [3.2].

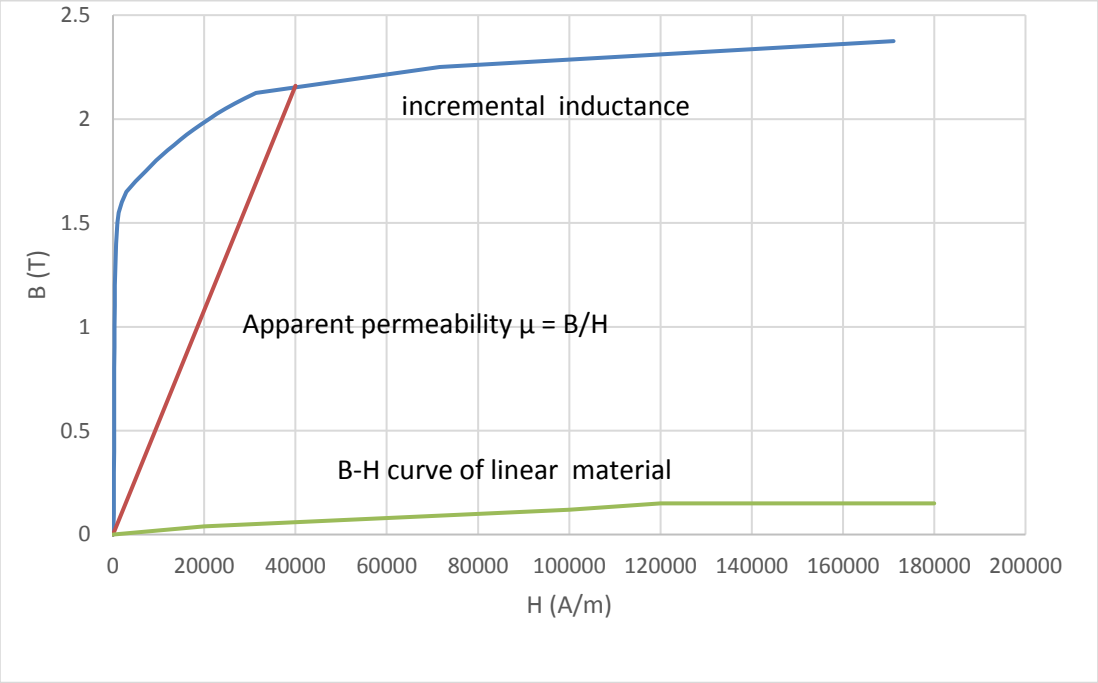

Figure 3- 2 Typical magnetic characteristics of different materials

3.3.4 Retentivity

The retentivity or remanence is a material's ability to retain a certain amount of residual magnetic field when the magnetising force is removed after achieving saturation. The ferromagnetic materials retain their magnetization once they exposed to a magnetic field even when the field is removed. It is the most widely recognised property of ferromagnets. The retention of magnetization distinguishes ferromagnets from paramagnets which although they acquire a magnetic moment in an applied field (H), they can not maintain the magnetization after the field is removed [3.3]. When the field is reduced to zero after magnetizing a magnetic material, the remaining magnetic induction is called the remanent induction (B_R), (B_R) = (μ_0 M_R) [3.3]. The remanence is the value of remaining induction or magnetization when the field has been removed after the magnetic material has been magnetized to saturation. The remanence is the upper limit for all remanent induction or magnetization [3.2].

3.3.5 Coercivity

If sufficient magnetic field is applied to produce complete saturation inside the ferromagnet and then start reducing the field back to zero, it will be found that at zero applied field some residual magnetization “remnant induction “will remain and it will take a significant field “coercive field” to completely demagnetize the material. The magnetic induction can be reduced to zero by applying a reverse magnetic field of strength (H_c). This field strength is known as the coercivity and it is defined as the magnetic field needed to reduce the magnetisation to zero from saturation [3.2].

3.3.6 Electrical losses

Core losses occur in magnetic cores of ferromagnetic materials under alternating magnetic field excitations. It comprises of hysteresis loss and eddy current loss. The hysteresis energy loss per unit volume per cycle due to an AC excitation in an iron ring is equal to the area of the B-H loop.

$$P_{hyst} = \oint H \,.\, dB \quad {}^{W}/_{m^3} \tag{3.5}$$

The hysteresis loss for magnetic materials commonly used in the construction of electric machines is given by the following equation: -

$$P_{hyst} = C_h f B_p^n (1.5 < n < 2.5)\ (W/kg) \quad (3.6)$$

Where (C_h) is a constant determined by the nature of the ferromagnetic material, (f) is the frequency of excitation, and (B_p) is the peak value of the flux density [3.4] - [3.6].

The eddy current loss is caused by the induced eddy currents in a magnetic core and is expressed by: -

$$P_{eddy} = C_e (f B_p)^2 (W/kg) \quad (3.7)$$

Where (C_e) is a constant determined by the nature of the ferromagnetic material and the dimensions of the core. Since this kind of loss is caused by the induced eddy currents in a magnetic core, it can be reduced by increasing the resistivity of the soft magnetic material. The hysteresis loss increases linearly with frequency while the eddy current loss increases with frequency squared. There is usually a discrepancy between the measured loss and the loss expected from the sum of the hysteresis and eddy current losses and this is usually referred to as the excess loss (P_{ex}).

$$P_{ex} = C_{ex} (f B_p)^{3/2} \quad (3.8)$$

The core loss or total electrical power loss is the summation of the foresaid losses [3.4], [3.6].

$$P_{core} = P_{hyst} + P_{eddy} + P_{ex} \quad (3.9)$$

$$P_{core} = C_h f B^n{}_p + C_e (f B_p)^2 + C_{ex} (f B_p)^{3/2} \quad (3.10)$$

The core losses can be reduced if the conductivity of the material is reduced. This is exploited in transformer material such as silicon-iron, which silicon is added principally to reduce the conductivity, although it has adverse effect on the permeability but does reduce the coercivity. The losses in Ni-fe alloys are lower than for silicon-iron, and this is also used in AC applications such as induction coils and transformers, but silicon-iron has a higher saturation magnetization [3.2].

3.3.7 Curie temperature

The transition temperature from ferromagnetic to paramagnetic behaviour is called the Curie temperature or Curie point. All ferromagnets when heated to sufficiently high temperatures above the Curie temperature they become paramagnetic as the magnetic domains select

random alignment. At this temperature the permeability of the material drops suddenly and both coercivity and remanence become zero [3.2].

3.3.8 Magnetic anisotropy

Anisotropy is the property of being directionally dependent, as opposed to isotropy, which implies identical properties in all directions. It can be defined as a difference when measured along different axes. In the absence of an applied magnetic field, a magnetically isotropic material has no preferential direction for its magnetic moment, while
a magnetically anisotropic material will align its moment with one of the easy axes. In this case the demagnetizing field will not be equal for all directions, creating one or more easy axes. The easy axis is an energetically favourable direction of spontaneous magnetization that is determined by the sources of magnetic anisotropy. The ferromagnetic single crystals exhibit 'easy' and 'hard' directions of the magnetization, as shown in figure 3- 3. The easy axis is the direction inside a crystal, along which a small applied magnetic field is sufficient to reach the saturation magnetization. Hard axis is the direction inside a crystal, along which large applied magnetic field is needed to reach the saturation magnetization. From the technological viewpoint magnetic anisotropy is one of the most important properties of magnetic materials. Depending on the type of application, material with high, medium or low magnetic anisotropy will be required, for respective application as, for example, permanent magnets, information storage media or magnetic cores in transformers and magnetic recording heads [3.4].

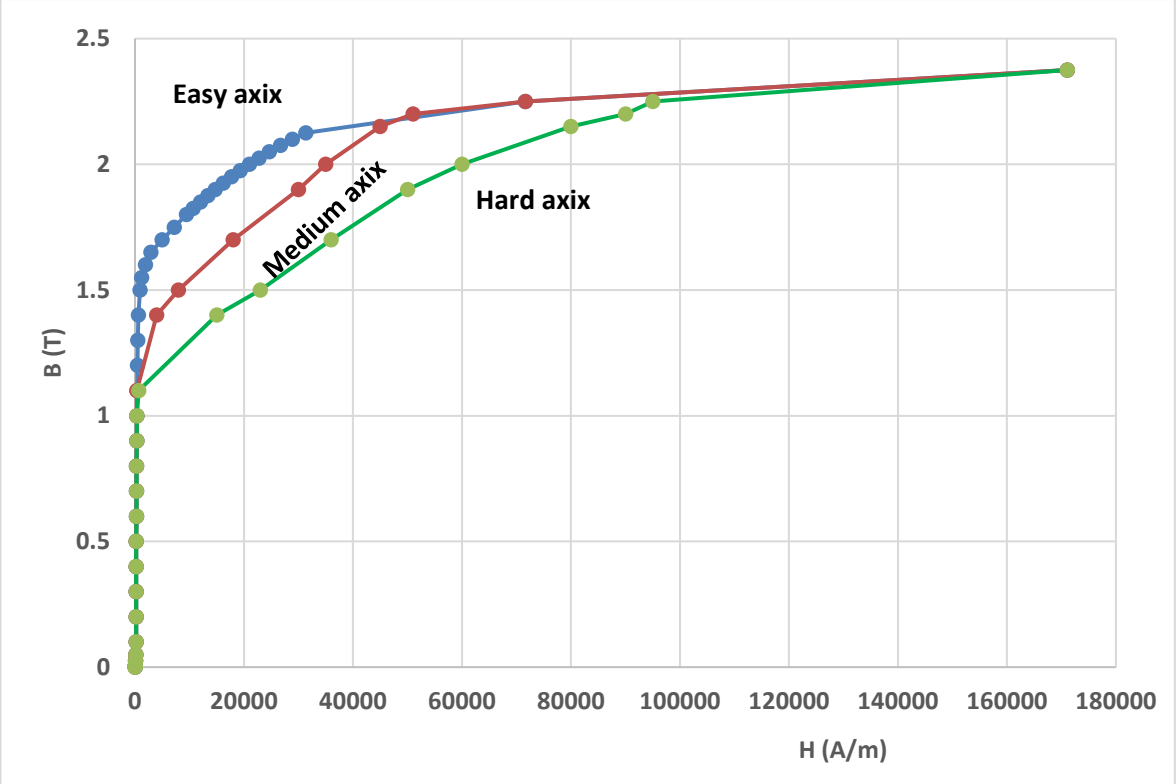

Figure 3- 3 Magnetization curves for iron along the three axes (100), (110), (111)

3.3.9 Magnetostriction

Magnetizing a core material usually changes its dimensions by a few parts per million. This dimensional change is called magnetostriction. Longitudinal magnetostriction is the dimensional change in the direction of magnetization and may be positive or negative. It is generally considered the most significant dimensional change of the core material. Its magnitude depends on the core material and the angle between the direction of magnetization and the rolling direction under the cyclic excitation; magnetostriction causes core vibration which creates noise. During cyclic excitation, this vibration has a fundamental frequency twice the excitation frequency. Since the magnetostriction does not vary linearly with induction level, higher frequency harmonics are also generated. Although there are other sources of noise in transformers, magnetostriction makes a significant contribution. The noise amplitude increases with core size as well as induction level and is a function of core design. Configuration, clamping, and other constructional features of the complete transformer can also have a large effect on noise levels [3.7].

3.4 Soft magnetic materials types

3.4.1 Steel

Two types of steel are used as cores in transformers, generators and motors. These are grain-oriented and non-oriented electrical steel. Grain oriented silicon-iron is done be techniques called cold and hot rolling followed by annealing (heat treatment). Grain-oriented steel is used in large power and distribution transformers. The hot and cold rolled techniques make the steel magnetized in the easy axis (100), which is the direction of the applied magnetic field. This means the magnetic moments or magnetic domains of the iron align in the easy direction (1,0,0) instead of medium axis (1,1,0) or hard axis (1,1,1) as shown in Figure 3-3.
The Cold Rolled Grain-Oriented Electrical Steel (CRGOS) is the one which made with special arrangement to control the crystal orientation. It is processed in such a way that the optimum properties are developed in the rolling direction, due to a tight control of the crystal orientation relative to the sheet. The magnetic flux density is increased by 30% in the coil rolling direction, although its magnetic saturation is decreased by 5%. It is used for the cores of power and distribution transformers. CRGO is usually supplied by the producing mills in coil form and it must be cut into "laminations" which are then used to form a transformer core, which is an integral part of any transformer [3.2], [3.8]. Cold-rolled grain-oriented steel is a 3-4 per cent silicon iron, cold reduced to develop a high degree of grain orientation, which gives increased flux for a given magnetising force and decreased size for a given rating, hence reduced weight. The difference between cold and hot rolled is the temperature at which they are processed. Hot rolled is processed above the re-crystallization temperature while cold rolled is processed below its re-crystallization temperature. Re-crystallization is the process in which destroyed grains of a crystal structure are replaced by the new strain free grains. Non-oriented electrical steels are silicon steels in which magnetic properties are practically the same in any direction of magnetism in the plane of the material and have high loss characteristics (isotropic). Cold Rolled Non-Grain-oriented Electrical Silicon [CRNGO] is made without special processing to control crystal orientation. It usually has a silicon level of 2 to 3.5% and has similar magnetic properties in all directions (isotropic). CRNGO is less expensive than CRGO and is used when cost is more important than efficiency and for applications where the direction of magnetic flux is not constant, as in electric motors and generators. It

can be used when there is insufficient space to orient components to take advantage of the directional properties of grain-oriented electrical steel [3.9].

Non-orientated silicon steels are extensively used for machine laminations. Normally cores are produced in a number of material lamination thicknesses as follows: -

- 0.3 mm for frequencies up to 200 Hz
- 0.1mm for frequencies between 200 Hz to 2 kHz and
- 0.05 mm for higher frequencies and pulse applications.

Steel laminations for low frequency applications are available in different shapes. E and I laminations or strip C cores or toxoids are extensively used for mains transformers and ac line inductors [3.4].

3.4.2 Iron powders

Two general forms of iron powder cores are employed

- Cores are made by highly compacting insulated high-quality spongy iron powder.
- High resistivity is required to reduce eddy current losses and so the iron powder is subjected to an acid treatment to produce an insulating oxide layer on the surface of each individual particle. This fine carbonyl iron is mixed with a bonding material and highly compressed. The bonding material used limits the maximum core temperature. Minute gaps appear between the particles, severely reducing the permeability. It is difficult to saturate such materials [3.10].

3.4.3 Ferrimagnetic materials - soft ferrites

Ferrites are black, hard, brittle, chemically inert ceramic materials, which have a magnetic cubic structure. The most general ferrites are polycrystalline magnetic ceramic oxides, which are compounds of iron oxide, Fe203 mixed with one or more oxides of bivalent transition metals such as Fe0, Ni0, Zn0, Mn0, Cu0, Ba0, Co0, and Mg0. At lower frequencies, below a few MHz, a Mn-Zn combination is added to iron oxide, while for higher frequencies, above a MHz, Ni-Zn is the additive. The raw oxide materials are mixed, pre-sintered at 1000°C if required, and ground. The powder material is shaped by means of pressing and sintering at between 1150°C and 1300°C. The sintering process involves raising the temperature to 1300°C in about 3 hours, with 15 per cent oxygen present. The cores are cooled slowly without oxygen present to about 200°C in 20 h after entry. A 15 per cent linear and 40 per cent by

volume shrinkage occurs during sintering. A diverse range of ferrite core shapes is available, which include, E, I, U, toroid, drum, pot, rod, tube, and screw [3.10], [3.11].

Table 3- 1 Typical comparative data of soft magnetic materials [3.12]

		Silicon steel	**Iron powder**	**Alloys**	**Ferrite, Ni-Zn**
Frequency	Hz	20-1k	400-10k	40-70k	200k-10M
Temperature	°C	-55 to 300	-55 to 125	-55 to 200	-55 to 250
Initial permeability, μ_1		500	90	160	100
Flux density @ 25 c^0	T	1.75	0.86	0.63	0.24
Remanence	T	1.2	0.2	0.02	0.12
Intrinsic coercivity	A/m	440	2560	1448	350
Resistivity	Ωcm	0.1			10^5 - 10^6
Curie temperature, T_c	°C	300	200	500	450

3.5 Applications of soft magnetic materials

The types of applications for soft magnetic materials fall into two main categories: AC and DC [3.2]. In DC applications the material is magnetised to perform an operation and then demagnetised at the end of the operation, e.g. an electromagnet on a crane at a scrap yard will be switched on to attract the scrap steel and then switched off to drop the steel. In AC applications the material will be continuously cycled from being magnetised in one direction to the other, throughout the period of operation, e.g. a power supply transformer. A high permeability will be desirable for each type of application, but the significance of the other properties varies [3.2].

3.5.1 Electromagnets

In consideration of materials for electromagnets, the core material should have high permeability to enable high magnetic induction to be achieved, while having a low coercivity so that the induction can be easily reversed. Soft iron is used almost exclusively in electromagnets. Its coercivity is typically $80Am^{-1}$ and when coupled with its high saturation magnetization of $1.71 \times 10^6 Am^{-1}$ makes the ideal material. Sometimes the pole tips of the electromagnet are made from cobalt-iron alloy which has a higher saturation magnetization in order to achieve slightly higher fields in the air gap ($m_0 = 1.95 \times 10^6 Am^{-1}$ for an alloy

of 35% co, 65%fe compared with $m_0 = 1.95 \times 10^6$ for iron). The materials most often used for electromagnet pole tips is an alloy containing 49% fe, 49% co, 2% V. Electromagnets are not very useful for magnetic induction above 3T because the iron can not contribute much additional field. Therefore, for higher field strengths either water-cooled iron –free magnets, known as Bitter magnets or superconducting magnets are used [3.2].

3.5.2 Transformers

Although high permeability of the core material is desirable for transformers, it is necessary to reduce the eddy current losses by employing as low a conductivity material as possible. The material that is used exclusively for transformer cores is grain oriented silicon iron. This contains about 3-4% by weight silicon to reduce conductivity. The material is usually hot-rolled then cold -worked twice followed by an anneal to improve the grain orientation, increasing permeability along the rolling direction. The total core loss in watts per kilogram at 50 or 60 HZ is an important parameter for transformer steels. Losses decrease with increasing silicon content, but the material becomes more brittle. In recent years there has been an attempt to develop amorphous metal for use in electromagnetic devices [3.2]. These alloys such as Metglas, have found applications in some smaller devices but have not been successful in replacing silicon-iron except in some cases where distribution transformers have been required where fuel costs are high. Several thousands of metglas transformers have been built and sold, however this remains a very small fraction of the market for transformers. In view of the recent contributions such as non-oriented and grain oriented to improve the properties of silicon-iron, there does not seem to be any likelihood of large- scale adoption of metglas materials as transformers cores [3.2].

3.5.3 Electromagnetic Relays

The control circuit of the relay consists of a coil with a magnetisable core and a movable component called the armature, which is used to make or break the circuit. The yoke and core materials of relays have much the same requirements as electromagnets, that is low Coercivity, low remanence, and high magnetic induction. This leads in addition to low core loss and high permeability. Relays materials are almost always iron or iron-based alloys. The addition of silicon to iron reduces the Coercivity from $100Am^{-1}$ to a few amperes per meter. The addition of Nickel to iron reduces the coercivity to as low as $1Am^{-1}$ [3.2].

3.5.4 Induction Cores

Soft magnetic materials are also needed as cores of induction coils. They enhance the flux density inside the coil and thereby improve inductance. When inductors are required to operate at high frequencies then due to the skin depth, only non-conducting or finely laminated magnetic materials can be used [3.13]. This usually means soft ferrite which is magnetic materials with high electrical resistivity and high permeability, which for many years were thought to be ferromagnets. This was because their bulk magnetic properties are very similar to ferromagnets. Another application of soft ferrite is in antenna for radio receivers. These have an internal ferrite-cored antenna consisting of a short solenoidal coil which enhances the emf in the circuit for given amplitude of field. Typical values of (μ_r) for these applications are μ_r ~100 – 1000. Soft ferrites consist of a compound oxide consisting of iron oxide ($F_{e2}O3$) together with other oxides such as manganese, nickel or magnesium, which have a complicated chemical composition. For example, nickel ferrite has the composition of N_iO and $F_{e2}O3$. It has B_s of 0.25 T with coercivity of the order of $8Am^{-1}$and maximum permeability μ_r= 1500 [3.2].

3.6 The characteristics of permanent magnet materials

The hard-magnetic materials have wide hysteresis loop, high remanence flux density and high coercive field. Due to the great improvement of magnetic materials such as coercivity and maximum energy product, the materials that more considered hard magnetic in the past are in many instances are not recognised as hard material, today [3.1].

3.6.1 Maximum energy product of permanent magnet materials

The maximum energy product is used to specify the performance characteristic of a permanent magnet. It is the maximum value of BH in the second quadrant. This is closely related to the total hysteresis loss or area enclosed by the hysteresis loop. The maximum energy product is simply a measure of the maximum amount of useful work that a permanent magnet can do outside the magnet [3.1].

3.6.2 Permanent magnet materials demagnetizing curve

The maximum energy product only gives limited information about the properties of a permanent magnet. A more useful way of displaying the magnetic properties of

a permanent magnet is to plot the portion of the hysteresis loop in the second quadrant from the remanence point to the coercivity. This demagnetization curve indicates the magnetization under various demagnetizing fields. Such a curve contains information about the maximum energy product [3.1]. The strength of the demagnetizing field of a permanent magnet in open-circuit configuration depends on the shape of the permanent magnet. Therefore, the performance of permanent magnet material as a field source is dependent as much on the geometry as on the intrinsic material properties [3.1].

3.7 Hard magnetic materials

3.7.1 Magnetite or lodestone

The first permanent magnet material to be recognised wasFe_3O_4 , which a naturally occurring oxide of iron but it is no longer in use [3.1].

3.7.2 Permanent magnet steels

The first commercially product permanent magnets were high-carbon steels containing about 1% carbon. These were also mechanically hard while the low carbon steels and iron were mechanically soft. The classification “hard” and “soft” later came a measure of coercivity rather than of mechanical properties. Later the coercivity improved better by adding tungsten and chromium. Later still came the cobalt steels. These permanent magnet steels have coercivity of up to 20KAm^{-1} and maximum product of up to $7\ \mathrm{KJm^{-1}}$ [3.1].

3.7.3 Alnico alloys

The Alnico alloys consist mainly of iron, cobalt, nickel, and chromium with small amount of other materials such as copper. These composed of a strongly magnetic α_1 phase ($\mathrm{F_e}$-$\mathrm{C_o}$) and a very weakly magnetic α_2 phase ($\mathrm{N_i}$-Al). The magnetic properties of the alloy are improved by suitable heat treatment involving quenching followed by tempering at 700℃. They are also improved by annealing in a magnetic field. This rises the coercivity and maximum energy product. They have remanences in the range 50-130 $\mathrm{KAm^{-1}}$ with maximum energy product of 50-75$\mathrm{K\ Jm^{-1}}$. These alloys represent a mature technology and no significant improvements in their magnetic properties have occurred in recent time [3.1].

3.7.4 Hard ferrites

The hard-hexagonal ferrites in widespread use are usually either barium or strontium ferrite ($\mathrm{B_aO.6F_{e2}O_3}$ or $\mathrm{S_rO.6F_eO_3}$), these materials are relatively cheap to produce and commercially remain the most important magnetic materials. The coercivities are larger than Alnico, being typically 150-250 $\mathrm{K\,Am^{-1}}$ and romances are 200-300 $\mathrm{K\,Am^{-1}}$but their maximum energy product is low, being typically 20 75$\mathrm{K\,Jm^{-3}}$ [3.1].

3.7.5 Platinum –cobalt

Due to the availability of other cheaper materials, the platinum-cobalt permanent magnet materials are no longer in use. However, it has coercivity of typically $400\mathrm{KAm^{-1}}$ and a maximum energy product of typically $80\mathrm{KJm^{-3}}$ [3.1].

3.7.6 Samarium-cobalt

This kind of material was developed by the combination of high anisotropies of some earth materials with the high curie temperature of the 3^{rd}transition metals iron, cobalt and nickel. It had high coercivity which could operate at ambient temperature and above. It was found that the cobalt-rare earth alloys had higher anisotropies than nickel or iron rare earth alloys. Furthermore, the alloys with the light rare earths generally had higher saturation magnetizations. The first of those alloys to be developed wasSmC_{O5}, which has a saturation magnetization of $800\mathrm{KAm^{-1}}$, a coercivity of typically B$H_c = 760KAm^{-1}$, a maximum energy product of $150 - 200\mathrm{KJm^{-3}}$, a remanence of ($B_r$)=0.9T and a curie temperature of 720℃. This is was followed by Sm_2F_{e17}which has a saturation magnetization of $1MAm^{-1}$, a coercivity of typically (BH_c) $= 500KAm^{-1}$, a maximum energy product of$240 - 260\mathrm{KJm^{-3}}$, a remanence of ($B_r$)=1T and a curie temperature of T_c= 820℃. The higher coercivity of SmC_{O5} ensures that it maintains a position as a material of choice for high coercivity applications at temperatures beyond which Ndf_eB is no longer viable [3.1].

3.7.7 Neodymium-iron-boron

The $Nd_2f_{e14}B$ alloys have become the materials of choice for a large number and wide diversity of applications requiring hard magnetic materials. Coercivities and energy products of these materials rival those of the samarium–cobalt alloys. The magnetization–demagnetization behaviour of these materials is a function of domain wall mobility, which, in

turn, is controlled by the final microstructure- that is, the size, shape, and orientation of the crystallites or grains, as well as the nature and distribution of any second-phase particles that are present. Microstructure will depend on how the material is processed. Two different processing techniques are available for the fabrication of $Nd_2f_{e14}B$ magnets: powder metallurgy (sintering) and rapid solidification (melt spinning). As for the powder metallurgical approach, the alloy, in molten form, is quenched very rapidly such that either an amorphous or very fine grained and thin solid ribbon is produced. This ribbon material is then pulverized, compacted into the desired shape, and subsequently heat treated. Rapid solidification is the more involved of the two fabrication processes; nevertheless, it is continuous, whereas powder metallurgy is a batch process, which has its inherent disadvantages. These high-energy hard magnetic materials are employed in a host of different devices in a variety of technological fields. One common application is in motors. Permanent magnets are far superior to electromagnets in that their magnetic fields are continuously maintained and without the necessity of expending electrical power; furthermore, no heat is generated during operation. Motors using permanent magnets are much smaller than their electromagnet counterparts and are utilized extensively in fractional horsepower units. Familiar motor applications include the following: in cordless drills and screw drivers; in automobiles (starting, window winder, wiper, washer, and fan motors); in audio and video recorders; and in clocks. Other common devices that employ these magnetic materials are speakers in audio systems, lightweight earphones, hearing aids, and computer peripherals [3.13].

Table 3- 2 The properties of some important permanent magnet materials [3.14]

Property	**Remanence B_r (T)**	**Intrinsic Coercivity (kA/m)**	**Max. Energy Product (kJ/m^3)**
Alnico	0.6 – 1.35	40 – 130	20 – 100
Ferrite	0.35 – 0.53	180 – 400	24 – 36
SmCo	0.7 – 1.05	800 – 1500	1600 – 4000
NdFeB	1.0 – 1.5	800 – 1900	2000 – 3000

The working temperature has a great effect on the magnets' ability to resist demagnetization. The maximum acceptable internal field for an amount of demagnetization depends on the temperature. Figure 3-4 shows the demagnetization curve for NdFeB [3.15].

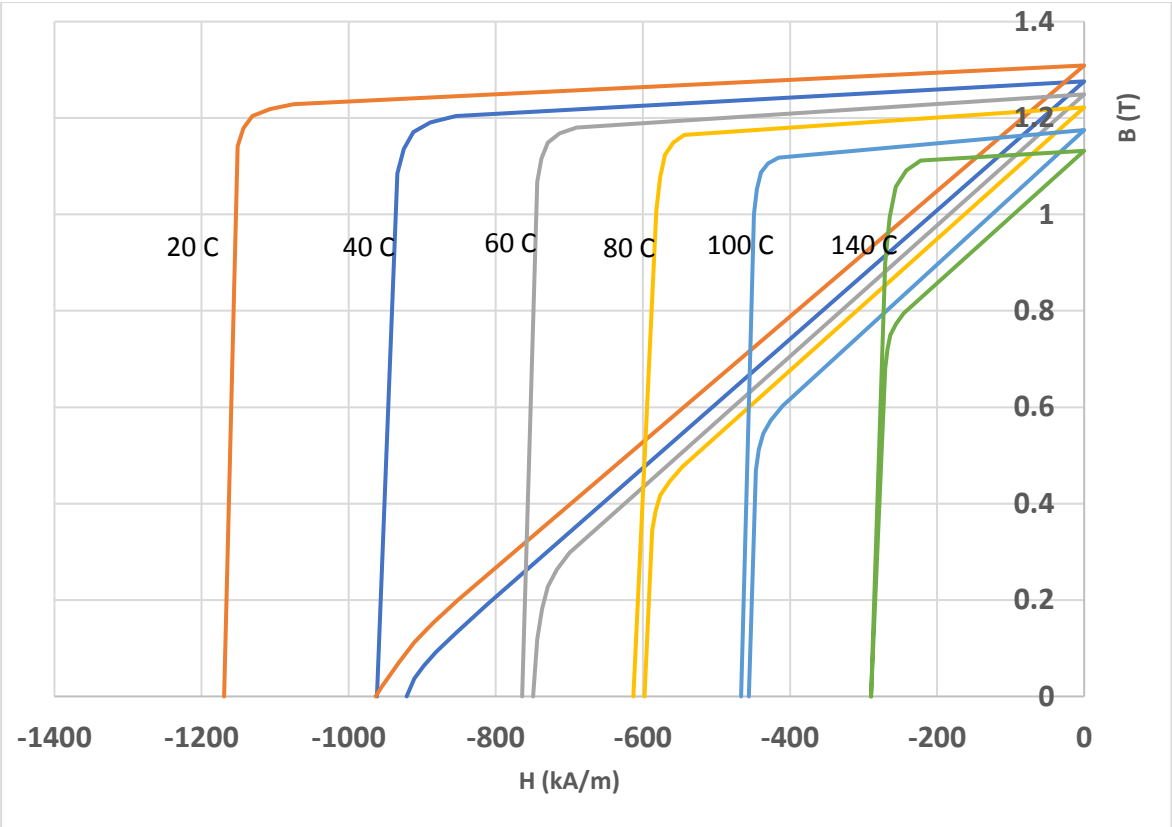

Figure 3- 4 Demagnetization curve for NdFeB at various temperatures

3.8 Stability of permanent magnet materials

It is important to know under what conditions a permanent magnet will perform to its design specifications. There are two problems which may affect the performance of the permanent magnet. One of the problems is the temporary effect due to operating at temperature beyond those for which the material was designed. The other problem is the deterioration of the magnetic properties caused by exposure to very high fields (demagnetization) or by alteration of microstructure caused by exposure to elevated temperature (ageing). The temporary or reversible changes in the magnetic properties with temperature are caused by the reduction of the spontaneous magnetization within the domains as the temperature is raised. This becomes more significant the closer the temperature to the Curie point. Permanent changes which occur as a result of exposure to elevated temperature are caused by acceleration of the aging process. Many permanent magnet materials exist in metastable metrological state so that a phase transformation does occur, but at room temperature this proceeds very slowly. The transformation proceeds more rapidly at higher temperature. There are other

factors that can alter the properties of permanent magnet such as mechanical treatment, corrosion and radiation [3.1].

3.9 Conclusion

Some magnetic materials require a magnetic field to be applied to align the magnetic moments throughout the whole material (soft magnets) and others produce significant magnetic field without an applied field (hard magnets). The state-of-the-art soft magnetic materials (SMM) are those which can be easily magnetized and demagnetized. A good SMM should have large saturation magnetization, and the magnetization should be large even in relatively small applied field. Silicon steels and ferrites dominate soft magnetic materials. For high power applications silicon-iron is widely used for the sake of low coercivity, anisotropy, magnetostriction and increases resistivity and hence reduces losses and cost.

Neodymium magnets have good physical properties and become the materials of choice for a large number and wide diversity of applications where strong permanent magnets are required. However, one of the difficulties for NdFeB in practice is the irreversible demagnetization due to high temperature and strong inverse magnetic field, which should be considered when designing a permanent magnet (PM) device.

References

[3.1] J.P.Jakubovics, Magnetism and Magnetic Materials, second edition.

[3.2] Jiles D. Introduction to magnetism and magnetic materials. 2nd Ed. London & New York: Chapman and Hall, 1998.

[3.3] Parker RJ. Advances in permanent magnets. New York: Wiley, 1990.

[3.4] M. Amar and R. Kaczmarek, "A general formula for prediction of iron losses under non-sinusoidal voltage waveform," IEEE Trans. Magn.,
vol. 31, no. 5, pp. 2504–2509, Sep. 1995.

[3.5] 48531 EMS – Chapter 7. Magnetic Materials and Magnetic Circuit Analysis

[3.6] *Bertotti, G., General properties of power losses in soft ferromagnetic materials, IEEE Trans Volume: 24, Issue: 1, Page(s): 621 – 630, 1988*

[3.7] Joule,J.P. (1847). "On the Effects of Magnetism upon the Dimensions of Iron and Steel Bars".The London, Edinburgh and Dublin philosophical magazine and journal of science (Taylor & Francis). 30, Third Series: 76–87, 225–241. Retrieved 2009-07-19.

[3.8] R. K. Ray, J. J. Jonas, and R. E. Hook, "Cold rolling and annealing textures in low carbon and extra low carbon steels," *Int. Mater. Rev.*, vol. 39, no. 4, pp. 129–172, 1994.

[3.9] Melcher, James R. Solutions Manual for Continuum Electromechanics. (Massachusetts Institute of Technology: MIT Open CourseWare). http://ocw.mit.edu

[3.10] K.Aska, C.Ishihara, M.L. Marucci, Innovative electric devices using iron-polymer materials, Magn. Mater, Euro PM207-212(2003)

[3.11] D. Stoppels, "Development in soft magnetic power ferrites," J. Magn. Magn. Mater., vol. 160, 1996, pp. 323-328.

[3.12] Field Precision LLC, "Saturation curves for soft magnetic materials", http://www.field.com/magneticproperties.html, Accessed 26-Aug-16.

[3.13] Rodewald W, Wall B, Katter M, Uestuener K, Steinmetz S. In: Hadjipanayis GC, editor. Proceedings of the 17thInternational Workshop on rare earth magnets and their applications, Newark, Delaware. Princeton, New Jersey:

[3.14] J. Hendershot and T. J. E. Miller, Design of Brushless PM Motors: Oxford Science Publications, 1994.

[3.15] Mishra, Raja K., et al. "Microstructure and properties of step aged rare earth alloy magnets." *Journal of Applied Physics* 52.3 (1981): 2517-2519.

Chapter 4: - Modelling, analysis and comparative work on existing FCL

4.1 Introduction

In the previous related work dealing with the simulation of 10 kV PMFCL model, only the 2D (FEM) fault current modelling results were reported in the published literature. The reported results were highlighted in chapter two in Figure 2-26.

In this chapter, the10 kV permanent magnet fault current limiter model has been simulated according to the material and geometry provided in [4.1] by a commercial Finite Element software (FEM MagNet) in 2D and 3D. The (FEM) divides the magnetic field domain into a group of smaller elements called finite elements. (FEM) MagNet solves time dependent Maxwell's equations to simulate the flux density and magnetic field distribution within the model. The advantage of breaking the domain down into a number of small elements is that the problem becomes transformed from a small but difficult to solve problem into a big but relatively easy to solve problem [4.2] - [4.6].

The aim of this work is to verify and ensure the validity of the reported 2D (FEM) modelling results, evaluate the performance of the model and to develop the analysis techniques.

An analytical approach was used in the PMFCL preliminary design to calculate the main governing parameters such as the core saturation state and the topology of the permanent magnet. The analytical approach is based on the relationship between the saturation depth ratio of the magnetic core and the model structural parameters and is presented in Section 4.3. The mathematically calculated magneto static flux density in the core is then verified with 2D and 3D (FEM) simulation.

A new proposed method to design the PMFCL was used based on establishing the relationship between the operating current and the inductance of the (PMFCL). The steady state inductance/current profiles, which are given in Section 4.4.3.1 and Section 4.4.3.2, are obtained using 2D and 3D (FEM) magneto static solver to predict the PMFCL device fault current limitation in the abnormal condition. The 2D (FEM) transient behaviour of the PMFCL is verified in Section 4.5. The obtained 2D (FEM) transient results have been validated by 3D (FEM) time-step solver. Due to magnetic symmetry of the (PMFCL) under investigation, a quarter of the device was modelled to obtain a cost-effective solution from the computational

prospective. The model design verifications provided theoretical basis and guidelines towards the effective design of the PMFCL for the power grid.

4.2 The PMFCL model specifications

The PMFCL model consists of iron-core (silicon steel sheet), permanent magnet (N_dF_eB) and coil (copper) with turns of 800. The model design specifications are given in Table 4-1.

At normal operation of the device the AC magnetic field generated by coil is not enough to drive iron-core out of saturation, so the PMFCL behaves like an air-cored reactor with a low inductance. While during the fault condition either of the cores comes out of saturation and thus inherently rushed to a high impedance state that limits the high short circuit current.

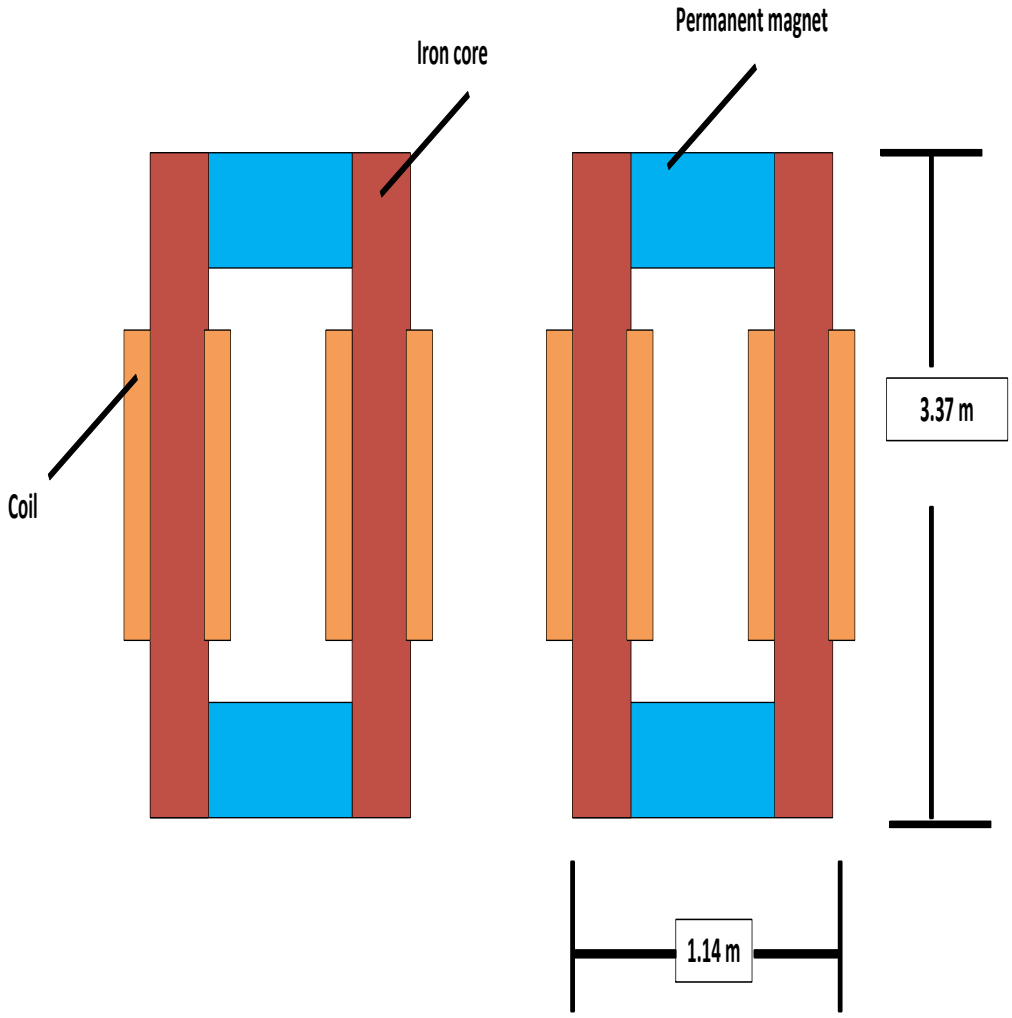

Figure 4- 1 Schematic diagram of 10KV PMFCL

Table 4- 1 Model details

Magnetic material	**Magnetic parameters**	**Topology parameters**
Permanent magnet, Neodymium Iron Boron, (N_d F_e B, N35)	Coercivity, $\mathrm{H_c} = 8.68 \times 10^5 \frac{\mathrm{A}}{\mathrm{m}}$ Intrinsic coercivity, $\mathrm{H_c^-} = 9.55 \times 10^5 \frac{\mathrm{A}}{\mathrm{m}}$ Remanence, $\mathrm{B_r}$ = 1.22T	length =0.64m, Depth = 0.25m Area = 1.06*0.25= $0.265\mathrm{m}^2$
Core, M4	Saturated permeability, $\mu_2 = 1.2 \times 10^{-4}\ H/m$ Relative permeability, μ_r =95	length = 3.37 m Area =0.25*0.25 =0.0625 m^2

4.3 The PMFCL model analytical approach

The characteristics of a permanent magnet and the limiter core are obtained by considering a magnetic circuit model of a magnet in Figure 4-2. The permanent magnet has a uniform cross-sectional area of (A_m) and a length (l_m). The magnet has demagnetization curve of a straight line with a coercive force of (H_c), a remanent flux density of (B_r), where (H_c) is the magnetic field intensity (A/m), which is the value of (H) at (B) equals zero [4.1], [4.7] – [4.8].

The permanent magnet demagnetization curve can be expressed analytically as

$$B_m = \mu_m H_m + B_r \quad (4.1)$$

$$B_m = \frac{B_r}{H_c}(H_m + H_c) = \mu_m (H_m + H_c) \quad (4.2)$$

where (μ_m) is the permeability of the permanent magnet. ($\mu_m = \frac{B_r}{H_c}$) , (B_m) is the permanent magnet flux density, and (H_m) is the permanent magnet magnetic field intensity [4.1], [4.7].

The magnetomotive force across the magnet can be expressed as: -

$$H_m l_m = \left(\frac{B_m}{\mu_m} - H_c\right) l_m = \frac{l_m}{\mu_m A_m}\Phi_m - H_c l_m = R_m \Phi_m - F_m \quad (4.3)$$

Where ($R_m = \frac{l_m}{\mu_m A_m}$) and ($F_m = H_c l_m$) [4-1], [4-10].

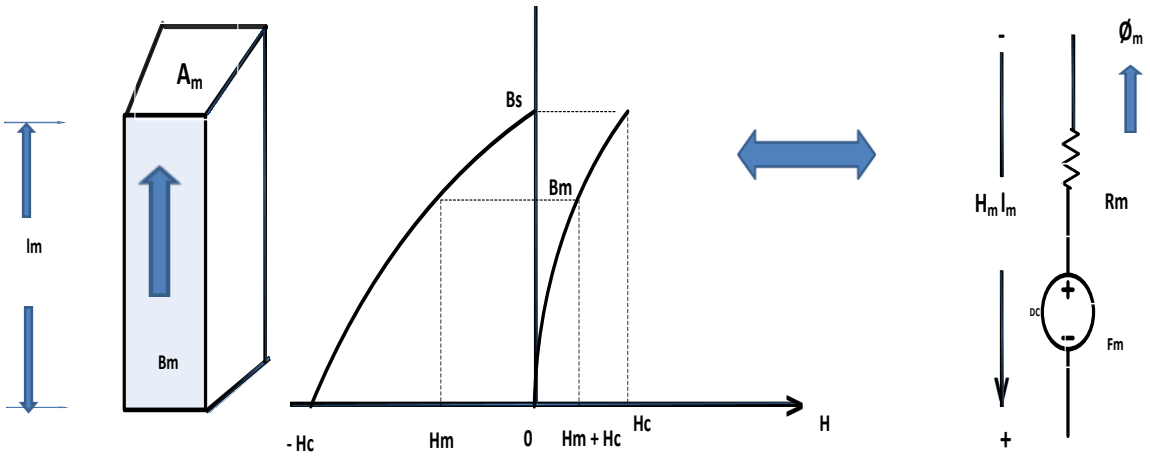

Figure 4- 2 Magnetic circuit model of a magnet with demagnetization curve

During fault conditions, the following equation should be considered so that the permanent magnet as a source does not lose its capability when the fault exists.

$$H_c * l_m \geq IF_{max} * N \quad (4.4)$$

Where (IF_{max}) is the maximum fault current and (N) is the number of turns.

Studying the material properties is essential to choose the most appropriate material for the core of the PMFCL [4.8].

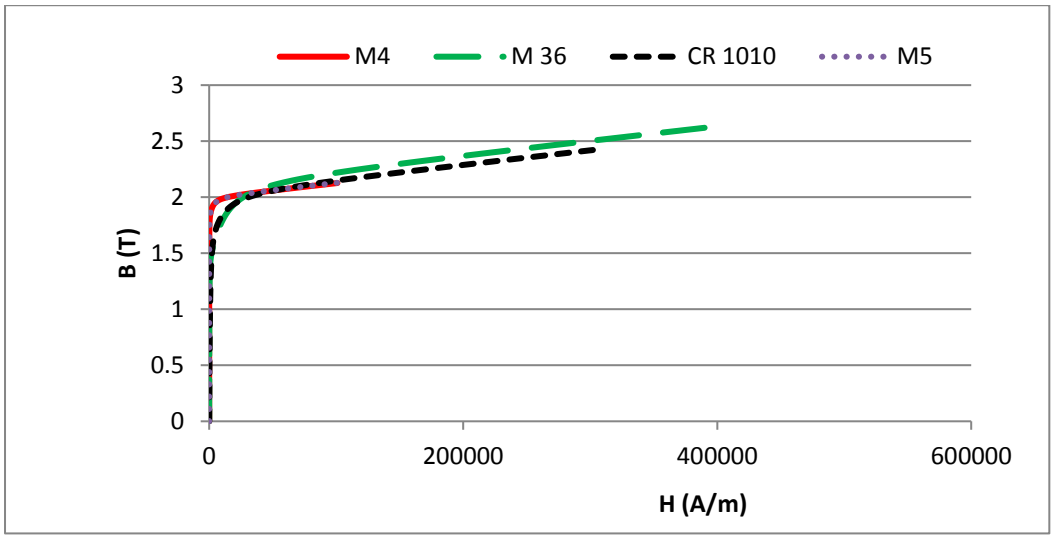

Figure 4- 3 B-H curve for various electrical steel materials

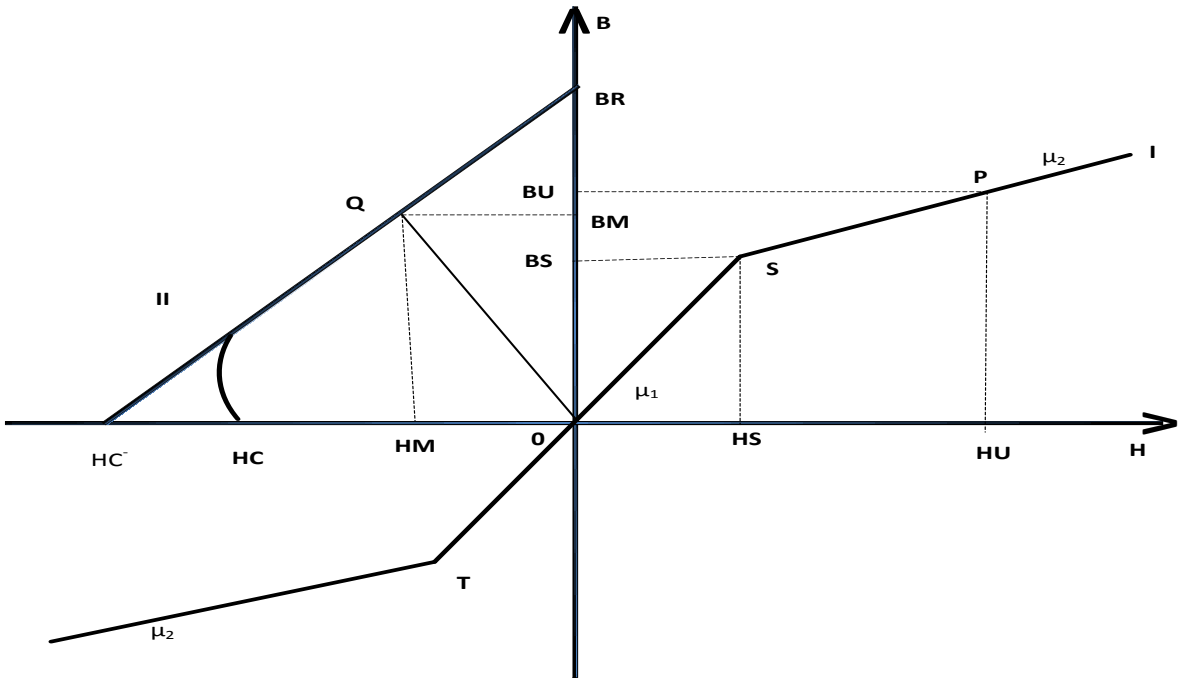

Figure 4- 4 B/H curves of the iron-core and the permanent magnet

The B-H curve for various electrical steel materials in Figure 4.3 and the magnetization curve I of the iron core in Figure 4.4, show that the flux density increases in proportion to the field strength until it reaches a certain value up to the saturation level. When the materials reach the saturation level, any increase in the magnetic field strength, the flux density does not increase significantly. This is because all the domains in the steel material are perfectly aligned. Any further increase will have little considerable effect on the value of the flux density (B).

It can be noticed from Figure 4-3 that the both the (M4) and (M5) have almost the same B-H characteristics but with fewer points on the B-H curve in comparison with M36 and cold rolled steel (CR1010). The relative permeability of the electrical steel (M4, M5, M36 and CR1010) at 2 T are 95, 105, 57 and 49 respectively [4.2]. This means each magnetic property of these materials has different effect on the PMFCL' performance [4.9]. The cold rolled steel CR1010 is not preferred to be used, though, it has relatively low strength.

Figure 4-4 represents the B-H curve for the iron core and the permanent magnet. On the magnetization curve (I, P) represents the working point of the iron core with (B_u) and (H_u) denotes the corresponding magnetic flux density and magnetic field intensity. (B_s) and (H_s) denote the saturated magnetic flux density and saturated magnetic field intensity at point S.

On the magnetization curve (II, Q) represents the working point of the permanent magnet with (B_m) and (H_m) denoting the magnetic flux density and magnetic field intensity correspondingly. (B_r) and (H_s) denote the remanent flux density and the coercivity respectively. (H_c^-), the intersection coordinates of the extended reversion trace line of the curve (II) with the -H axis, denotes the equivalent coercivity of the permanent magnet. (μ_m) represents the permeability of the permanent magnet which contains the following relation with (Hc^-) [4.1].

$$B_r = \mu_m H_c^- \quad (4.5)$$

Under normal condition, the iron core works at the deep saturation region of curve (I) in which (Hu) larger than (H_s).

The magnetic flux density of the iron-core at point P (B_u) could be divided into two parts, the linear part and the saturated part.

$$B_u = B_s + \Delta B = B_s + \mu_2 \Delta \quad (4.6)$$

Where ($\Delta B = B_u - B_s$) and (ΔH) is the saturation depth of the iron core.

$$\Delta H = H_u - H_s \quad (4.7)$$

$$B_u = \mathrm{B_s} + \mu_2 (\mathrm{H_u} - \mathrm{H_s} \quad (4.8)$$

$$\mathrm{H_u} = \frac{B_u - \mathrm{B_s}}{\mu_2} + \mathrm{H_s} \quad (4.9)$$

The bias capability of the permanent magnet was based on the saturation depth ratio (K_s).

$$K_s = \frac{\Delta_H}{H_s} = \frac{\Delta_H}{\Delta_{H+H_s}} \times 100\% \quad (4.10)$$

The saturation depth ratio (SDR) [4.1], [4.10] measures the bias capability of the permanent magnet PM at zero steady state current. It determines the percentage of how much additional saturation the PM can supply. The big value of (K_s) means that the permanent magnet can reduce higher fault current under the transient situation. In some situations, with a low value of (K_s) or SDR, the PM may lose the capability of fault current limiting. The value of (K_s) is always less than 100%. Saturation depth ratio as an important parameter is fit for quantifying the bias capability of the permanent magnet, and to improve the bias capability of the permanent magnet is in effect equivalent to increasing saturation depth ratio of the iron core. However, the (SDR) concept assumed that the actual 3-D field problem was idealised and transformed into a 2-D field problem. Moreover, the leakage flux, the eddy current loss of the

magnetic material and the angular frequency (ω) in the time-varying field are ignored [4.1]. At zero AC current, the summation of the magnetomotive force of the core and the magnet at the working points (P) and (Q), equals the amber- turns of the AC coil (Ni), which is zero.

$$H_u l_u + H_m l_m = Ni = 0 \quad (4.11)$$

$$H_u l_u = -H_m l_m \quad (4.12)$$

From equation 4.3 and by substituting (H_c) with (H_c^-), equation 4.11 becomes as follows,

$$H_u l_u = H_c^- l_m - \Phi_m R_m \quad (4.13)$$

$$\Phi_u R_u = H_c^- l_m - \Phi_m R_m \quad (4.14)$$

The magnetic flux of the core and the permanent magnet are considered the same, hence,

$$B_u S_u \left[\frac{l_u}{\mu_2 S_u} + \frac{l_m}{\mu_m S_m}\right] = H_c^- l_m \quad (4.15)$$

The following equation is obtained by substituting equation 4.8 into equation 4.14,

$$B_s + \mu_2 \Delta_H . \left(\frac{1}{\mu_2} . \frac{l_u}{l_m} + \frac{1}{\mu_m} . \frac{S_u}{S_m}\right) = H_c^- \quad (4.16)$$

The core saturated permeability (μ_2) and the permanent magnet permeability (μ_m) are both constant holding the relationship connected by constant ratio (n),

$$\mu_2 = n\mu_m \quad (4.17)$$

$$\Delta H = \frac{H_c^-}{\frac{l_u}{l_m} + \frac{nS_u}{S_m}} - \frac{B_s}{\mu_2} \quad (4.18)$$

Equation 4.17 links the geometrical parameters of the core with the magnetic materials used. The equation revels that the bias capability of the permanent magnet can be improved by two methods. The first one is changing the magnetic materials, such as the permanent magnet and the iron core of better magnetic performance. The second method is adjusting the structural parameters of the PMFCL, especially the Permanent magnet including decreasing length and increasing section area [4.1], [4.10].

Based on the mathematical equations previously stated, the core flux density was calculated using the model specifications in Table 4.1 and was found to be 2.17 T.

Though, the SDR assumed that the actual 3-D field problem was idealised and transformed into a 2-D field problem [4.1]. Hence, the SDR is not considered to provide a correct estimation to the calculated flux density due to the leakage flux.

However, by considering the core is saturated and hence the value of core saturated permeability (μ_2) is known, the preliminary design specifications such as the required PM magnet and core dimensions can be easily estimated. More accurate results taking the leakage flux components and the non-linearity of the core excitation could be obtained using the (FEM) approach [4.1]. 2D & 3D FEM magneto static solvers are enough to calculate the core saturation state. Thus, the calculated flux density needs to be compared with the numerical value obtained by 2-D and 3-D (FEM) to ensure adequate saturation extent of the limiter core.

4.4 Magnetic circuit calculations by 2D and 3D (FEM)

Due to limitations of analytical equations to model the non-linear core material properties, the (FEM) modelling techniques are being widely used by researchers and engineers. (FEM) MagNet is one of the most advanced packages currently available for modelling electromagnetic devices on a personal computer. It provides a virtual laboratory in which the user can create models from magnetic materials and coils, view displays in the form of field plots and graphs and get numerical values for quantities such as the flux linkage [4.2].

The (FEM) is an approximate method for solving differential equations. It is based on the concept of dividing the original problem domain into a group of smaller elements called finite elements. (FEM) MagNet solves time-dependent Maxwell's equations over each element to find the magnetic field within the model. The Maxwell's equations use the magnetic vector potential to serve the magnetic field and for (B) to be calculated, the magnetic vector potential (A) must be found. The magnetic vector potential is a vector field. Its utilization allows simplification of the mathematical approach of many physical problems. The derivative of the magnetic vector potential gives the flux density (B)

$$B = \nabla \mathrm{A} \tag{4.19}$$

The differential form of a Gauss's law for magnetic field is given by,

$$\nabla B = 0 \tag{4.20}$$

This means the divergence of the magnetic field at any point is zero.

According to Ampere's law, the derivative of the magnetic field intensity is the current density.

$$\nabla \mathrm{H} = J \tag{4.21}$$

The Maxwell field equations are extended to allow treatment of hysteresis by including the constitutive equation for magnetic material. The general equation for a ferromagnetic material can be expressed as [4.5].

$$B = \mu_0 \ (H + M) \tag{4.22}$$

$$\nabla \frac{1}{\mu_0} B = \nabla \ (H + M) \tag{4.23}$$

$$\nabla \frac{1}{\mu_0} \ \nabla \mathrm{A} = J + \nabla \ M \tag{4.24}$$

In (FEM) modelling, it is important to choose the right mesh to calculate the magnetic field and flux density. A good mesh refinement especially for the core provides excellent results for evaluating the PMFCL performance. Generally, building and activating of the 2D and 3D (FEM) model goes through the following steps [2]: -

1- Building the geometry according to the model specifications.

2- Meshing (subdivision of the whole model for triangular elements).

3-Assuming material properties (M4) or (M36) electrical steel, permanent magnet, copper wire).

4- Applying field normal boundary conditions along the line of symmetry for a part of the model in 2D and 3D (FEM) modelling.

5- Applying current density on the coil area.

As the elements for the core are made smaller and smaller, as the mesh is refined, the computed solution will approach the true solution.

The air box was made large enough so that to cater for the flux outside the core essentially and thus, Flux Tangential boundary conditions (specified by default) are applied. The surrounding air box had to be made to coincide with symmetry planes to specify the field normal boundary conditions when simulating a quarter of the model. The field normal boundary condition depends on the plain whether the magnetic flux cross perpendicularly.

An appropriate maximum element size of the cores was selected to make the mesh fine. However, with increasing the elements and nodes, the calculation in 3D (FEM) will be more time-consuming and hence the elements and nodes should be compromised as far as possible

while ensuring the calculation accuracy. A larger number of elements were chosen for the permanent magnets region where the solution changes a little, smaller elements were selected for the cores where the solution is very important and changes dramatically.

For the sake of increased accuracy, the following factors were taken into considerations in modelling the 3D (FEM) model: -

1. More mesh refinement in the area of the coils where flux linkage calculations were performed.
2. Solutions were sought at higher polynomial order.
3. The B-H curve of the core materials was extended to the higher region of the flux density.

The initial mesh in Figure 4-5 provides immediate feedback upon editing refinement controls. Figure 4-6 shows the solution mesh. In addition to manual mesh refinements, the solution mesh includes the nodes automatically added by Mesh Adaption [4-2].

The core material initially used was (M4) electrical steel, however, due to some incorrect inductance values obtained at low problems or low current, the M4 was replaced by (M36), which has more data points along the B-H curve.

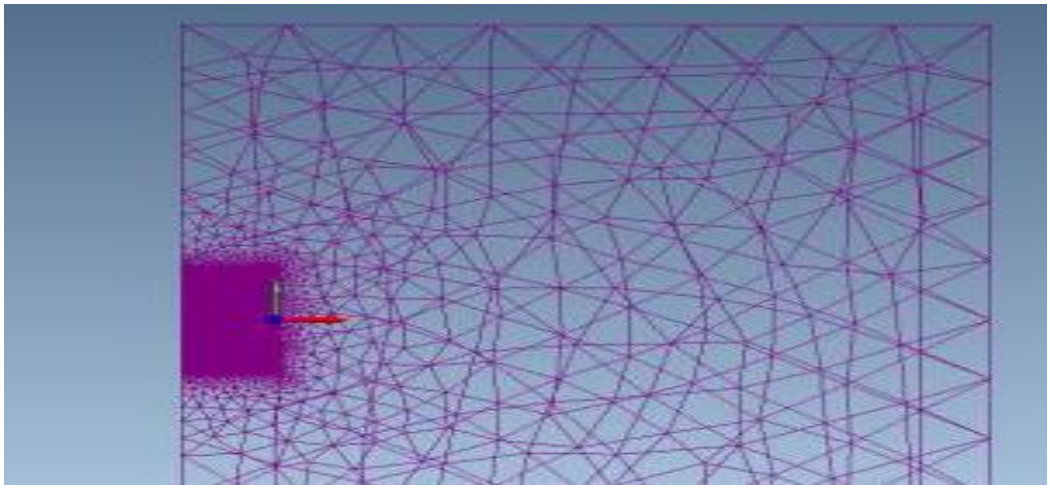

Figure 4- 5 Initial 3D (FEM) mesh

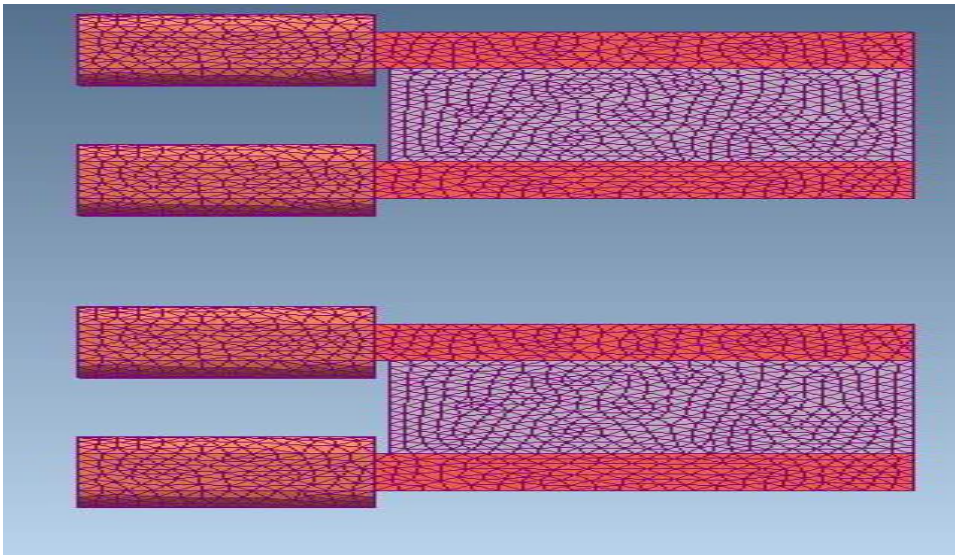

Figure 4- 6 The 3D (FEM) solution mesh

4.5 Core flux density calculations by 2D FEM

The permanent magnets were used to generate a strong magnetic field to saturate the core. With no current in the coils, a contour line was taken along the cores for 800 turns per coil to check the saturation extent. Figure 4-7 shows that the core is in saturation state. The flux density in the middle of the core is almost 2.1 Tesla.

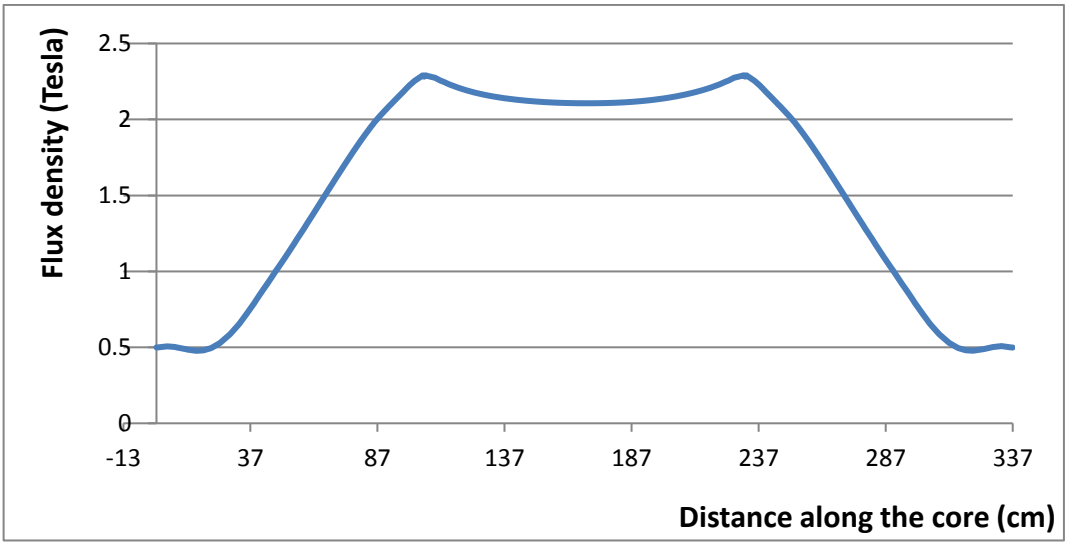

Figure 4- 7 Core magneto static flux |B| in 2D (FEM)

Figure 4-8 indicates the magneto static flux density lines distribution in the cores in 2-D modelling. It can be seen from the figure that the whole core is almost in saturation state. This means that the permanent magnets can generate a strong magnetic field to saturate the cores to an acceptable level.

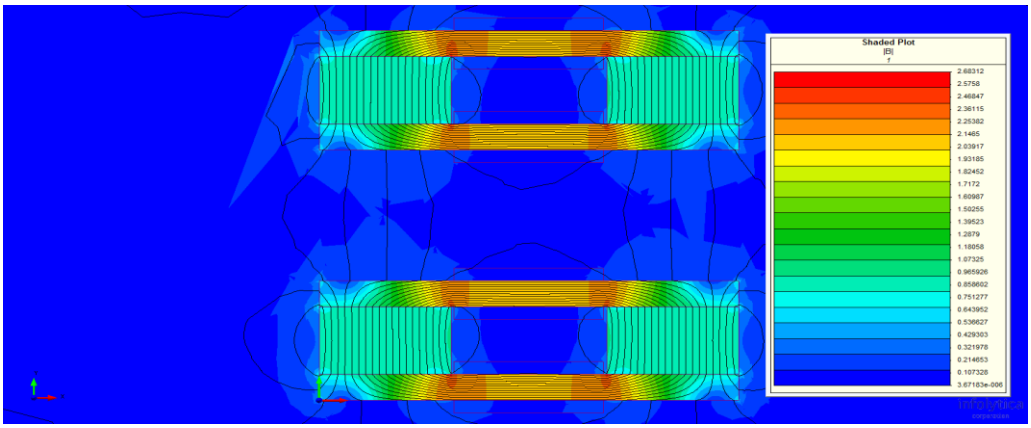

Figure 4- 8 Core magneto static flux density distribution in 2D

Although the 2D (FEM) requires less computational time, the results are inadequate due to the limitation of 2D (FEM) modelling in addressing the end effects of both the PMFCL coils and core as the 2D neglects the field variations along the model's depth.

In 3D modelling, as the model was large, only a quarter of the model was modelled, and the result indicated that the core region within the coils was in saturation.

The flux density in the middle of the core is 2.02 Tesla. This value is just above the saturation level of the core material (M36) (2.0 T).

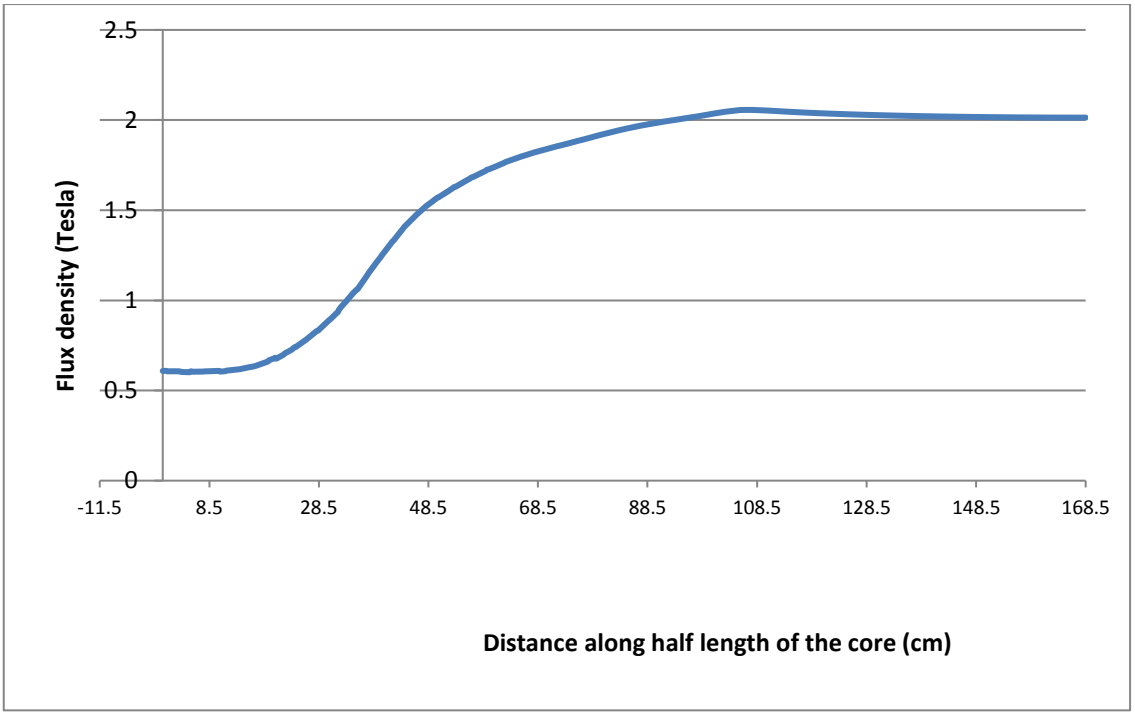

Figure 4- 9 Core magneto static flux |B| in 3D(FEM)

Figure 4.9 illustrates the magneto static flux density distribution along the cores in 3D modelling. The figure indicates that both cores are in saturation level.

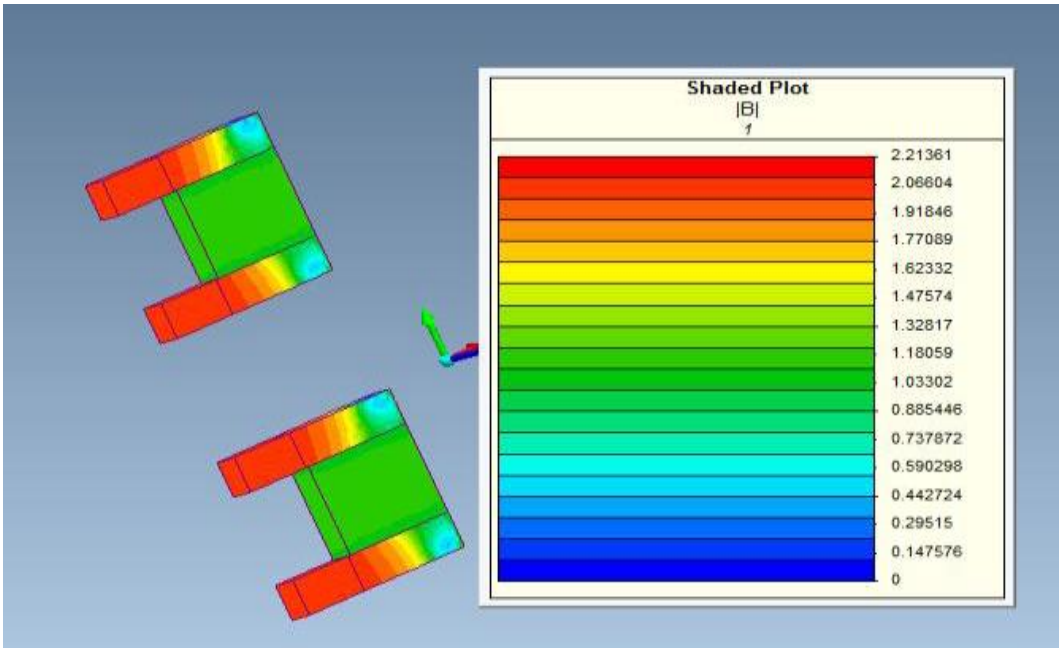

Figure 4- 10 The 3-D(FEM) core magneto static flux density distribution

Table 4-2 gives the analytical and numerical average flux density in the core. The average values obtained by 2D and 3D modelling are low, although the magnetic flux densities within the coils regions are above the flux density required for (M36) material.

Table 4- 2 The analytical, 2-D and 3-D magneto static flux values

Component	Analytical	2-DMagNet	3-DMagNet
Core	2.17	2.06	2.02

4.6 Steady state inductance calculation by 2D & 3D FEM

The inductance calculations using (FEM) approach could be evaluated using different techniques, among those are the stored energy and the flux linkage methods [4.11]. The inductance can be calculated using stored magnetic energy method [11], which is given by,

$$W = \frac{1}{2}\int AJdV \tag{4.25}$$

In 2D (FEM), the depth has no dependence on the model depth and hence

$$W = \frac{1}{2}h\int AJda \tag{4.26}$$

$$L = \frac{2W}{i^2} \tag{4.27}$$

$$L = h\int \frac{Ajda}{i^2} \tag{4.28}$$

The stored energy can also be given by: -

$$w = \frac{1}{2}\int BHdV \tag{4.29}$$

$$L = h\int \frac{BHda}{i^2} \tag{4.30}$$

A new proposed method to design the PMFCL was used based on establishing the relationship between the operating current and the inductance of the (PMFCL). In this approach, the magnetic status of the device at each current value would be obtained by (FEM) modelling. The ac current acting against the (PM) field excitation drive the core back from saturation to lower reluctance status and hence higher inductance.

Therefore, the total inductance would be evaluated from the magneto static (FEM) module at each current value, and the current inductance profile would be established. An accurate predication of the operating fault current values could be determined from the characteristics corresponding to high inductance value.

In this model where it has multiple coils, the stored energy method is not suitable to be used.

The flux linkage method is the more appropriate one. In this context the flux linkage (λ) and the inductance (L) is defined as following: -

$$\lambda = L\, I + \lambda_o \qquad (4.31)$$

Where L is the absolute inductance and (λ_0) corresponds to a constant flux linkage through the coil, caused by the presence of permanent magnet.

4.6.1 Inductance/current evaluation in 2D FEM

The 2D solver was initially used to model the device, this due to the magnetic circuit symmetry, computing resources and to verify the reported results. The flux linkage for each coil in the model was evaluated from the (FEM) solution by calculating the average flux linkage over the coil cross sectional area Sc. as follows: -

$$\lambda = \int_{S_c} \oint_{C} A \,.dl\; n\, dS \qquad (4.32)$$

Figure 4-11 shows the 2D results of the inductance-current profile for the PMFCL under consideration. The figure shows where such device could operate at normal low reactance region and where it will exhibits higher inductance.

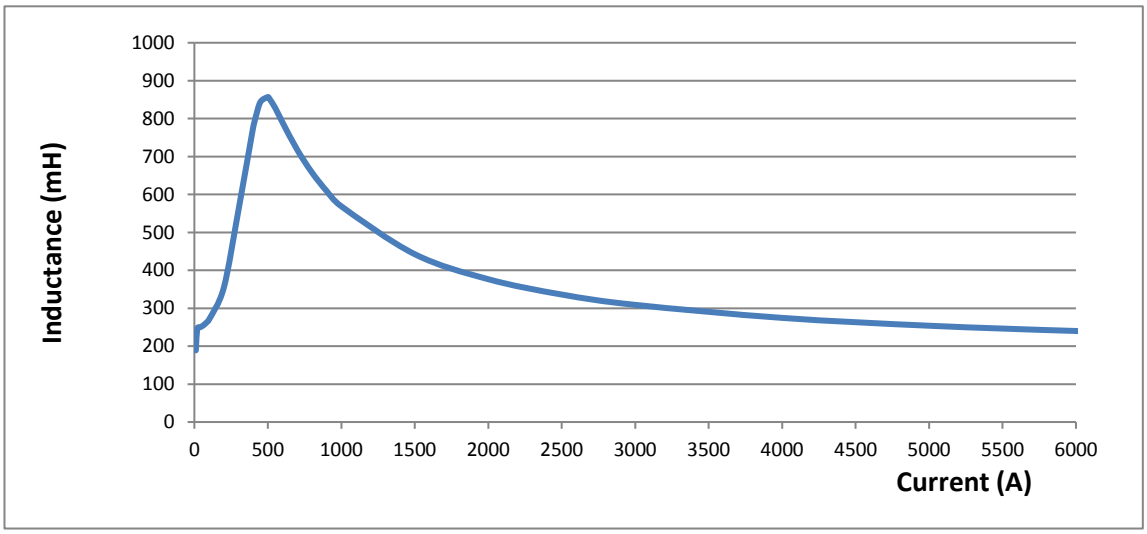

Figure 4- 11 Inductance vs current profile obtained from 2-D *(FEM)*

Figure 4-11 also shows the region where the PMFCL go back to saturation at higher current values. This figure also shows a relatively higher values of inductance due to higher number of turns (800 turns/coil) chosen for this design.

During a fault condition, one of the cores come out of saturation to reduce the dangerous fault current as in Figure 4-12 displays the flux density distributions of the magnetic circuit at fault current.

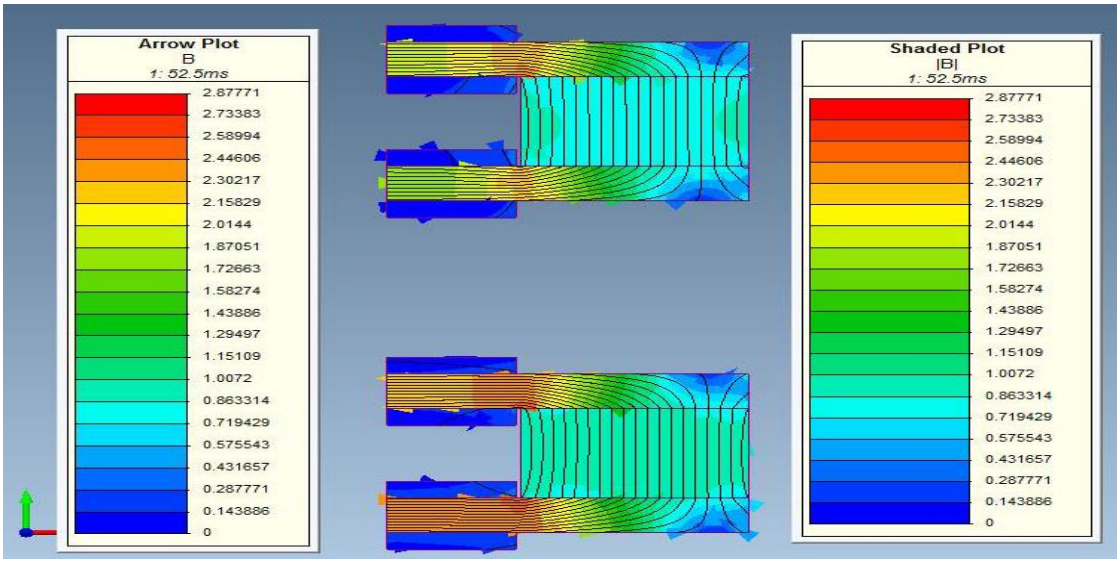

Figure 4- 12 Flux density distributions at fault current obtained from 2D (FEM)

4.6.2 Inductance/current evaluation in 3D FEM

The 3D solvers were used to explore the limitations of the 2D design tool. In 3D tool, (λ) for a single coil is calculated as following: -

$$\lambda = \frac{1}{I}\int_{Vc} A.\, J_o \; dv \qquad (4.33)$$

The adapted model under investigation was modelled using 3D tools. The inductance calculation was performed, and the results are shown in the figure below.

Figure 4-13 shows the calculated inductance-current profile in 3D (FEM). The inductance is much higher in comparison to hat obtained by 2D (FEM).

Figure 4-14 shows the flux density distributions of the magnetic circuit at fault current, it shows one of the cores at saturation when the coil current field in the same direction as the PM field, and the other core driven out of saturation when the coil current field in opposite to the (PM) field.

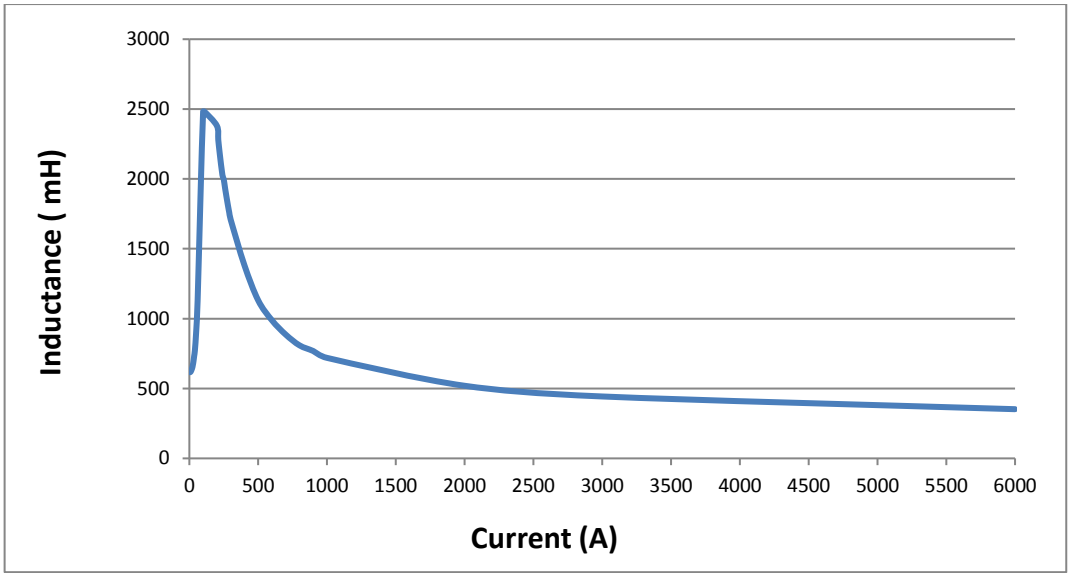

Figure 4- 13 Inductance vs current profile obtained from 3-D (FEM)

There is a clear discrepancy between the results obtained from 2D and 3D. This is not only related to the classical limitation of the 2D solvers in taking the coils end effects into consideration. However, it is mainly attributed, as shown in Figure 4-14, to the core no-uniform flux density distributions along its axial length which cannot be considered in 2D approach.

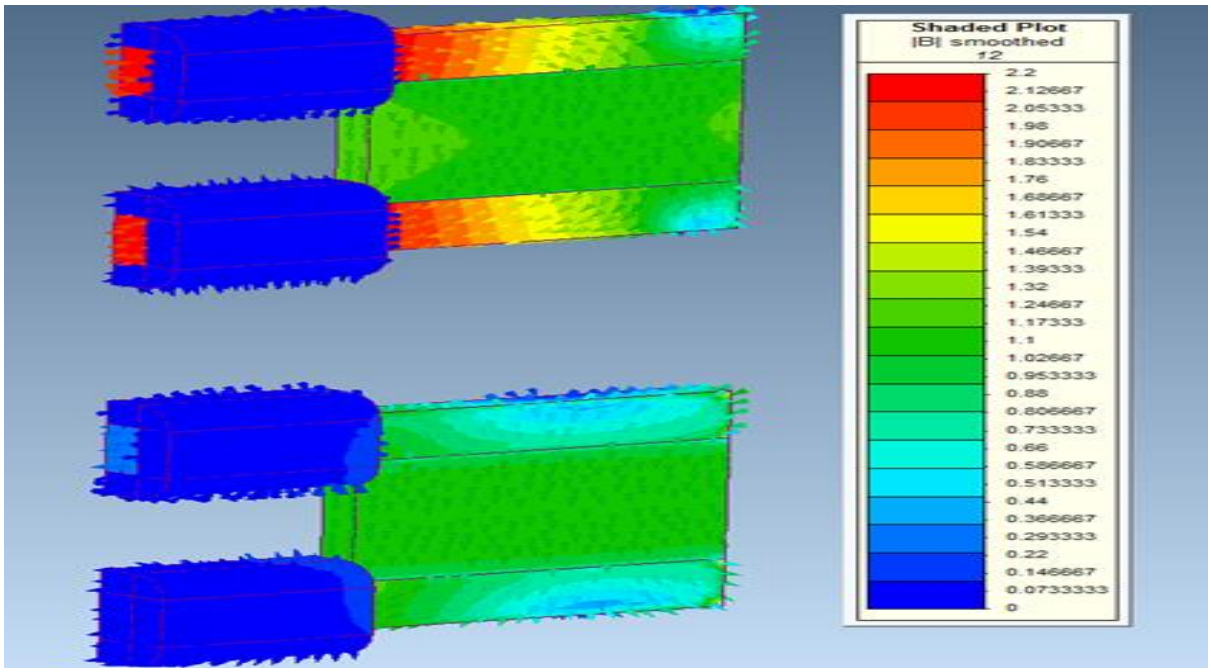

Figure 4- 14 Flux density distributions at fault current obtained from 3D (FEM)

4.7 Simulation of transient performance in 2D and 3D(FEM)

The transient FEM solver was used to model the dynamic response of the PMFCL. In this approach the driving current is the unknown and the model is driven by a given voltage of 10 KV, 50Hz. A time step solution was sought where the voltage across each coil is calculated by Faraday's law.

The model of the PMFCL is coupled to electrical circuit model as shown in Figure 4-15. For such approach, the time steps were chosen according to the coils time constant.

The value of the supply voltage, source internal resistance (R_1) and the load resistance R_2 were divided by 4, as only a quarter of the model was simulated. In modelling of the quarter of the model, it was found that the outer air box has a great effect on obtaining the transient results of the PMFCL. The outer air box height and depth should be made long and deep enough so that the feature of flux density boundary condition can easily force the magnetic flux lines at the outer surface and make them change their direction along the line of symmetry.

The model was allowed to run for two ac excitation cycles and the switch set to close at time corresponding to 0.04s to short circuit the load resistance (RL) of 100 Ω.

Prior to modelling the PMFCL in transient condition, the system fault current level was calculated for the case of air-cored model, in which the windings only are defined in the model and no presence of magnets and magnetic cores. This is to obtain a set of results for equivalent air-cored inductors. The air-cored for the same size of the PMFCL model was modelled to check the fault current level without the use of the current limiter device.

The maximum ground fault current between the input voltage terminals and the ground is only limited by the internal resistance (R_1). Hence, this value is 10000V/2.5Ω =4000A.

Figure 4-14 shows the results obtained by the transient solvers, this figure also shows the simulated current obtained from a model where only air-cored a coil of exactly the same dimensions of the PMFCL coils. This is to the current limitation capability of the PMFCL.

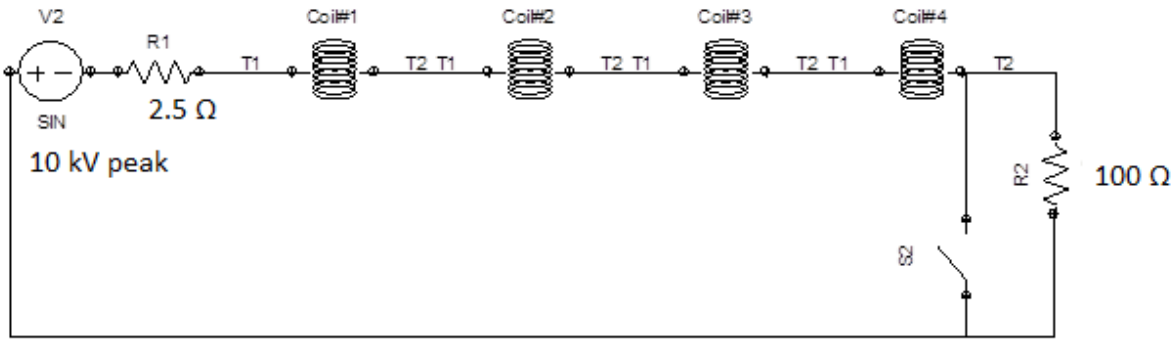

Figure 4- 15 Single phase circuit diagram of the transient (FEM) model

At the time of fault, the fault current is reduced by the rushed inductance of the PMFCL device L_{pmfcl} limits the fault current to an acceptable value as follows: -

$$\mathrm{If} = \frac{\mathrm{v2}}{\mathrm{R1+R2+j\ 2\pi f\ L_{pmfcl}}} \qquad (4.34)$$

The value of L_{pmfcl} depends on the device number of turns and the reluctance of the magnetic core,

$$L_{pmfcl} = \frac{N^2\ \mu\ A}{l} \qquad (4.35)$$

The permeability (μ) is the degree of magnetization, which depends on the core material, (l) and (A) are the length and the cross-sectional area respectively [4.8].

The PMFCL fault inductance stores energy without loss and returns it to the system at the end of each cycle. Therefore, the PMFCL does not introduce excessive power losses should the normal operation of the system is restored without interrupting the load current. However, if the line is interrupted, only the energy that is stored in the last cycle is dissipated in the CB. Before the fault occurred, the load current as Figure 4-16 indicates, had been 86.6 A.

At 40 milliseconds the air-cored model transient current was 320A, which shows a major reduction to the fault current. However, this value is far away from the maximum fault current (4000A). The significant reduction to the fault current was mainly attributed to the coils number of turns and there was no presence to the magnets and cores.

However, the air-cored calculated fault current value is then compared with the PMFCL devise transient current to check the influence of the device on fault current profile. In either positive or negative half cycle of the fault current, the magnetic flux in the lower core was reduced, and thereby the lower core unsaturated inductance increased to a high value. The fault current was reduced by both the high unsaturated inductance of the lower core and the low

saturated inductance of the upper core. The result shows that the fault current was reduced to 186A with the presence of the PMFCL. These results proof the concept of the PMFCL in limiting fault current. However, the published results in [2.26] reported a fault current 1700A which is a way far from the results obtained in this chapter.

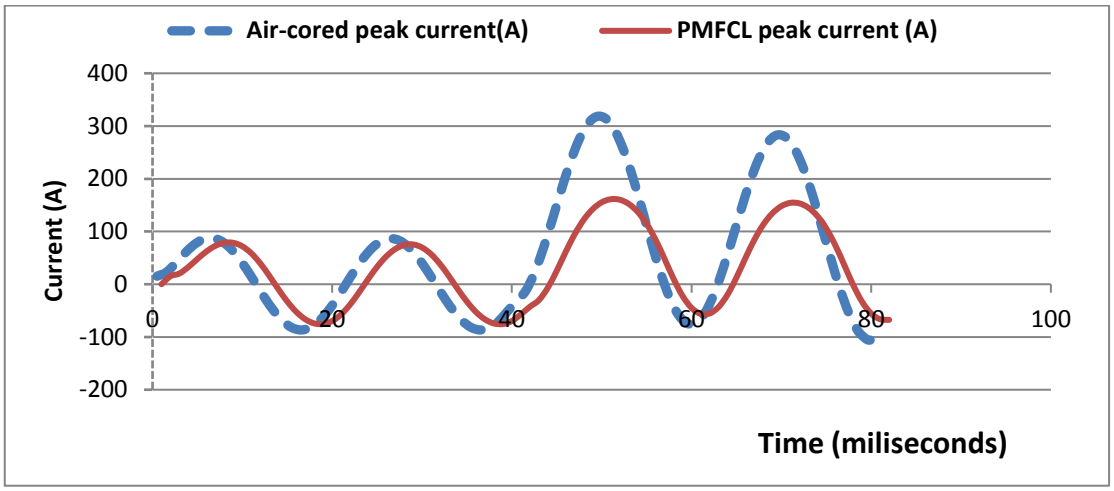

Figure 4- 16 Simulated current with PMFCL and air-cored

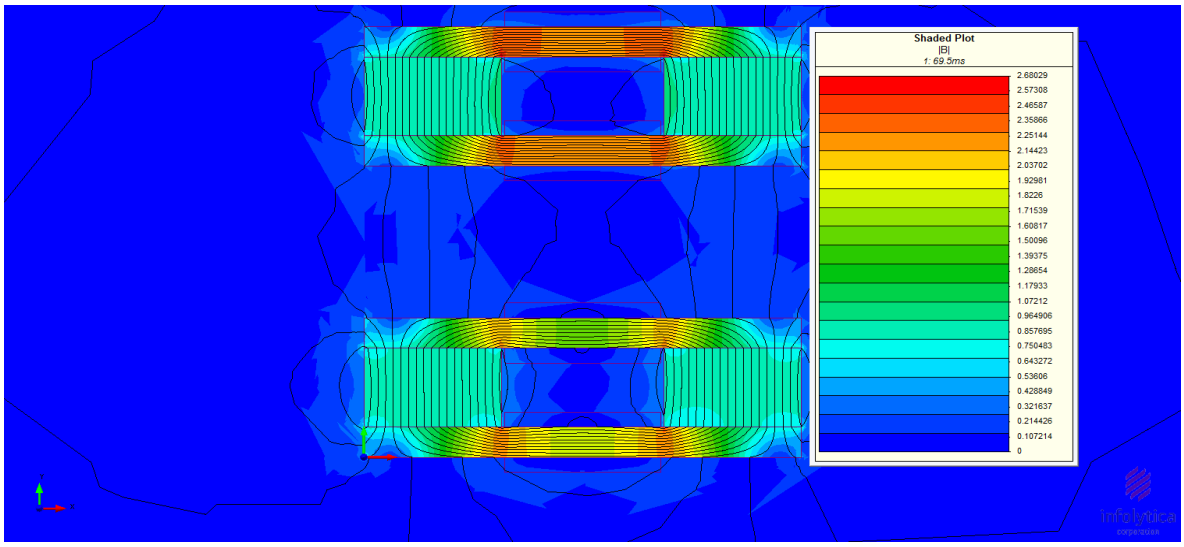

Figure 4- 17 Flux density distribution in transient 2-D (FEM)modelling

The figure above shows that the lower core was out of saturation because of high fault current.

4.8 Discussions of results

The PMFCL's performance has been investigated. The preliminary design of the device was done by the analytical approach. The analytical approach could be used to estimate the saturation level in the core and to estimate the dimensions of the required permanent magnets. However, the investigations show that this approach will falls short of accurate estimations of the leakage flux. The leakage flux was not considered because of the saturation depth ratio (SDR), which neglects the need for 3-D field problem [4.1], [4.10].

In the published literatures dealing with the analysis of PMFCL, only the core saturations and the fault current profile were reported. However, the inductance and the inductance calculations of the PMFCL are important in the design considerations. In this work, it is believed that the inductance profile of the PMFCL is one of the important design parameters. It provides the required information of the PMFCL behaviour in steady state and at fault situation. It also could be used as comparison parameters between various PMFCL configurations also, this parameter is essential in the introduction of PMFCL to power system calculations software.

In this work an approach of calculating the inductance of the PMFCL was introduced, and the results were reported. In such devices which operate at high saturation level, classical inductance calculations will not provide accurate results. Therefore, (FEM) modelling should be used in both 2D and 3D approaches. The results presented in Fig. 4.11 & 4.13 shows the inductance profile of the PMFCL, which were obtained using 2D and 3D magneto static solvers, hence where the input current to the model is not a time dependant. The inductance calculations also show an expected discrepancy between 2D and 3D approach. This is due to the 2D limitations in addressing the end effects of both coils and core. Hence, the 3D (FEM) approach is the accurate tool to obtain more accurate results.

The transient behaviour of the PMFCL under consideration was obtained using 2D (FEM). The aim was to obtain comparable results to that reported one in literature. Therefore, 2D transient (FEM) model was carried out accordingly. The obtained results from this task were far away from the reported in [4.1] as shown in Figure 4.16. Hence, the model is unrealistic to operate at 10 KV and therefore the 3D (FEM) transient modelling is not possible to perform. There were some issues related to the model under discussion. In the first place, there were an issue in the inductance/current profile. The core material used initially was M4 electrical

steel, however due to unfeasible results in obtaining the inductance/current profiles in both 2D and 3D (FEM), the material type M36 was used instead.

Another issue was related to the 3D (FEM) transient solution, which was not possible to perform as the model was unrealistic. The model was checked for messing issues, the cores element size, the air box, materials type and sweep distances were considered. The model symmetry and the field normal boundary condition were checked to be applied accurately. The coils were ensured to be properly modelled in 3D (FEM). In transient analysis, the material type was checked to be set to nonlinear from the solve menu/set solver option. Furthermore, the time steps from the menu solve/ set transient option was ensured to be made short enough and set to 0.1 second.

An investigation to the parameters used in the model revealed that a figure of higher number of turns per coil was used (800 turns). It is believed that such figure is unrealistic design parameter as the coil number of turns has a great effect on the performance of the PMFCL in both steady state and transient conditions. The high number of turns as reported in [4.1] had a major influence on the normal operation of the PMFCL, which incorporated in high voltage drop from both resistive and reactive components.

With respect to the previous published results, two important causes must have led to the inconsistent results. One important factor was related to the 2D (FEM) modelling technique, which was the sweep distance in z-direction (the depth of the components). The actual depth of the component should be always considered in 2-D voltage driven circuit modelling. Another essential issue is the polarity of the permanent magnet and the coils, which must have not been set properly.

4.9 Conclusion

The permanent magnet fault current limiter is a passive device as it does not require any external source to perform its function. The design and analysis of such devices is challenging due to the saturation of the magnetic circuit. The Neodymium Iron Boron N_dF_eB magnet can provide an adequate magnetic field to saturate the core of the PMFCL device in steady state condition. The analytical approach to estimate the magnetic circuit parameters is fall short of a realistic estimation of the operating current range. The (FEM) magneto static solver inductance-current profile is a useful approach in estimating the PMFCL device characteristics in transient condition. Despite the model magnetic circuit symmetry, there is a discrepancy

in the accuracy obtained from 2D and 3D design tool. The leakage flux should be taken into consideration for a better evaluation of the magneto static flux density in the core. Moreover, the device should have a few numbers of turns to minimise the voltage drop and losses during normal operating condition. The high number of turns has a significant effect on the performance of the PMFCL device. In addition, the model sweep distance should be considered in the both 2D and 3D modelling as they can have a major inconsistency on the results. Besides, the permanent magnet and coils polarity should be ensured. With respect to the transient simulation, the fault current in an alternative half cycle forces one of the iron cores to come out of saturation and consequently the magnetic circuit inductance increases rapidly to limit the fault current. The air-cored transient modelling is very useful because it gives information about the fault current without the use of the PMFCL device. Therefore, device has a fast response to the transient current. Besides its advantages such as easy to install and safe operation, it restores energy and returns it to the system should there is no interruption to the flow of load current.

References

[4.1] Liang Zou, et al. (2009). Study on the feasibility of developing high voltage and large capacity permanent-magnet-biased fault current limiter. Universities Power Engineering Conference (UPEC), 2009 Proceedings of the 44th International, 1-5.

[4.2] Magnet user manual by Infolytica, www.infolytica.com.

[4.3] Anastasis C. Polycarpou. (2006). Introduction to the finite element method in electromagnetics.

[4.4] Nimje, P., Kannan, C., & Amir, Q. Finite element modelling & experimental simulation of magnetic leakage flux from metal loss defects in steel pipelines.

[4.5] H. L. Toms, R. G. Colclaser and M. P. Krefta (2001). Two-dimensional finite element magnetic modeling for scalar hysteresis effects. *IEEE transactions on magnetics,* **37** (2), 982-988.

[4.6] Sarac, Vasilija. "(FEM) 2D and 3D design of transformer for core losses computation." *International Scientific Journal Industry 4.0* 2.3 (2017): 119-122.

[4.7] Liu, Hongshun, et al. "Comparative study on the static and dynamic characteristics of four types of PMFCLs for large capacity applications." *International Journal of Electrical Power & Energy Systems* 34.1 (2012): 47-56.

[4.8] 48531 EMS – Chapter 7. Magnetic Materials and Magnetic Circuit Analysis.

[4.9] J. R. Prigmore, J. A. Mendoza, & G. G. Karady. (2013). Comparison of four different types of ferromagnetic materials for fault current limiter applications. IEEE Transactions on Power Delivery, 28(3), 1491-1498.

[4.10] Liang Zou, Yuan Ma, Hong-shun Liu, Qing-min Li, & Shu-min Sun. (2008). Impact of saturation depth ratio of iron-core on the PMFCL. 2008 International Conference on Electrical Machines and Systems, pp. 4338-4343.

[4.11] Ali, Amer Mejbel. "Different Techniques for Calculating Apparent and Incremental Inductances using Finite Element Method." Iraqi Journal for Electrical & Electronic Engineering 11.2 (2015).

Chapter 5: - A prototype PMFCL

5.1 Introduction

In this chapter, experimental work is carried out on a prototype of a proposed design of permanent magnet fault current limiter. Prior to a large scale PMFCL implementation, the prototype is needed for developing the design, proof of concept of the proposed design techniques and improving ideas beforehand. The single phase 90V, 50HZ, square shape topology, benchtop prototype, is designed with 3D (FEM) [5.1], built and tested at the Electrical Laboratory of Sheffield Hallam University.

The aim of this work is to compare the numerical and experimental results to ensure the validity of the 3D FEM and demonstrate the current limiting capability of the PMFCL device. Furthermore, this activity aims to access the design of PMFCL to develop the ideas and explore solutions to enhance the PMFCL performance for mitigating the fault current in electrical distribution system.

An air-cored of the same size as the PMFCL device was constructed and tested to compare the outcome of having the device in service with the normal situation when there is no PMFCL. The air-cored and PMFCL prototype coils terminals (input/output) are identified at the assembly stage and left open so that the measuring devices can be connected, and different power circuit tests can be performed.

Two designs are involved, which are based on the AC windings connections for the same PMFCL device specifications, the named configuration 1 and 2, according to the AC coils magnetic flux direction with respect to the permanent magnets.

All the simulated and experimental results were compared with each other adequately to demonstrate the effect of the PMFCL AC coils configurations on the performance of the PMFCL device.

The PMFCL model with the same design specifications was simulated at different AC coil length to demonstrate the effect of AC coil length on the performance of the PMFCL device with fixed number of turns.

5.2 The prototype Design specifications

The 189 mm square shape prototype incorporated four PMs of a permanent magnet type neodymium iron boron grade 28/32, two M36 electrical steel cores of 4 mm thickness are placed between the magnets, and four AC copper coils wound around the 5 mm insulating bobbin and the cores. The length and height of each coil is equal to 99 and 49 mm respectively. Each coil consists of 210 turns, which is the maximum number of turns that can be wound around the core (satisfies the lab requirements) and they are arranged in 5 layers of 42 turns. The AC coils are connected in series and are inserted into the AC line in series with the load. The mmf-flux operating point of the cores is established by the permanent magnets. The magnets are positioned in the corner between the two cores and they are placed in alternate polarity such that each two opposite magnets are magnetized in the same direction, (magnets 1 and 3) and (magnets 2 and 4), as shown in Figure 5-1. The assembly of the PM poles that they must be placed in alternate polarities. Should one place the first pole with North Pole up, going clockwise, the next one will be South Pole up, then North up and last one will be South Pole up. The polarity of Magnet No 1 (the upper left) is (0, 0, 1) whereas magnet 2 polarity is (0, 0, -1). The polarity of magnet No 3 is as for magnet 1 and the polarity for magnet 4 is as for magnet 2. This means that the opposite magnets have the same polarity. The direction (0, 0, 1) indicates the direction in (X, Y, Z). The configuration 1 is denoted by dot whereas configuration 2 indicates by cross. The details are given in Table 5-1

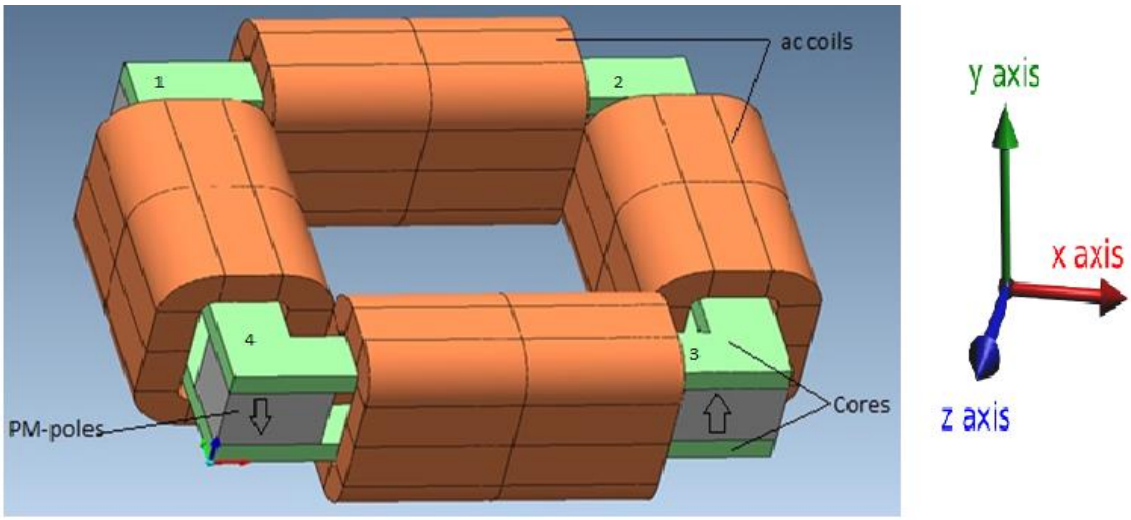

Figure 5-1 PMFCL prototype schematic diagram

Figure 5-2 and Figure 5-3 show the PMFCL type for AC coils winding configuration 1 and 2.

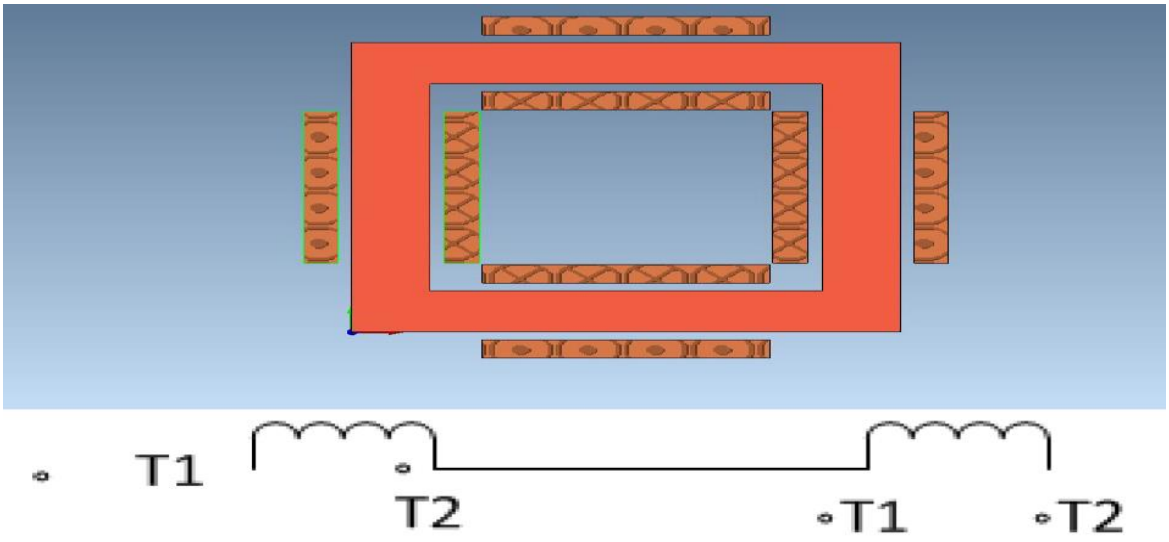

Figure 5-2 AC coil configuration 1 , 3D(FEM) design

The configuration 1 design has the outside windings of the four AC coils with the same polarity as shown in Figure 5-2 whereas the configuration 2 design has its AC coils winding configuration in dots and crosses in alternate fashion as in Figure 5-3. The novel idea of such design is that in the case of " configuration 1 design" the PMFCL operates two opposite sides of the upper core and two sides of the lower core are back to magnetisation state. While in the " configuration design 2" the PMFCL operates either the whole upper core or the whole lower core is back to magnetisation state depending on the ac cycle. Hence each configuration offers different characteristics in terms of operating current and inductance values. The PMFCL is a variable-inductance iron-core reactor that has the impedance of an air-core reactor under normal grid conditions and very high impedance during fault events [5.2], [5.3]. The change of the impedance from a low to high value depends on the required design parameters of the electrical network that is operated on. When the current increases beyond its permissible value during a fluty condition, the rapid increase in the impedance of the device produces the limiting effect [5.2]- [5.4]. During a fault event the rising current in the AC coil generates a magnetic field, which drives the core out of the saturation state, leading to increased permeability of the core section under the coil and hence increased impedance and limited fault current [5.5]. The magnetic field or the induction along the core is time and spatial dependent [5.6].

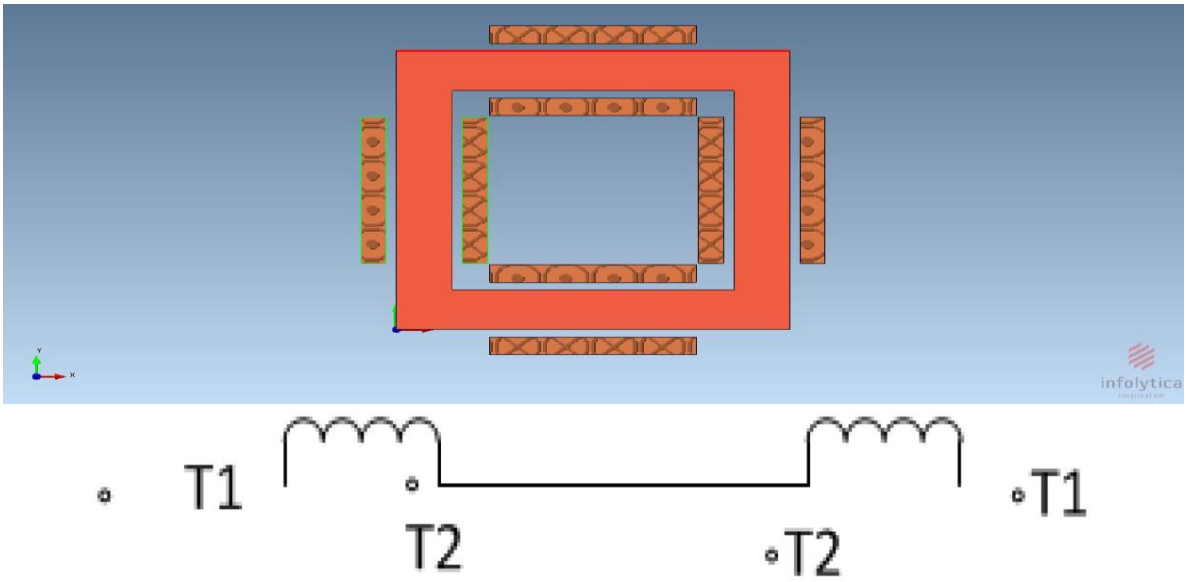

Figure 5-3 AC coil configuration 2, 3D(FEM) design

The design specifications of the prototype PMFCL is as detailed in Table 1.

Table 5- 1 The design specifications of the 90V PMFCL prototype

Parameter	**Type or value**	**Parameter**	**Type or value**
Iron core material	MR36	Fault duration	25 cycles
Iron core size	(189 x 27 x 4) mm	Recovery time	Instantaneous
Permanent Magnet type	N_d-F_e-B (N52)	Fault type	Single line to ground
Permanent Magnet size	(30 x 30 x 30) mm	Configuration 1 design PMFCL calculated/measured currents	37A/39A
A.C coils configuration	With/ opposite	Configuration 2 design PMFCL calculated/measured currents	45A/49A
Supply voltage	90V $_{RMS}$, 50 Hz	AC coil length along the core	99 mm
Input resistance	0.1 Ω	Stray resistance	40 Ω
A.C coils No of turns	210	Maximum load current	2.24A_{rms}

5.3 Experimental set-up

The prototype practical electrical circuit set-up was based on the PMFCL model design specifications given in Table 5-1.

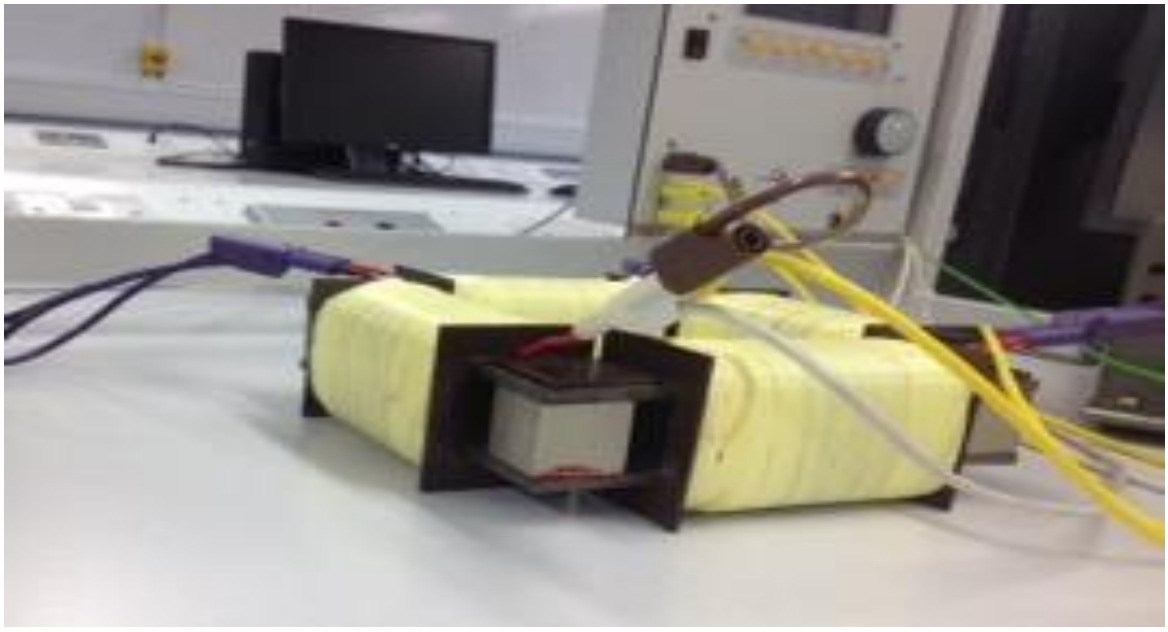

Figure 5-4 PMFCL prototype experimental wiring diagram

Figure 5-4 shows the PMFCL experimental wiring diagram where it is connected to the measuring instruments.

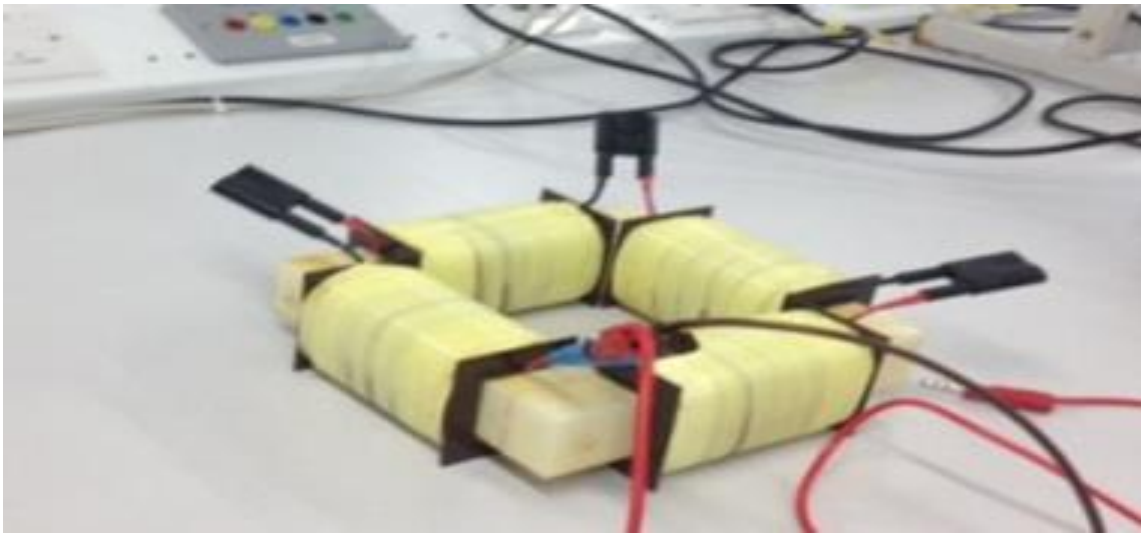

Figure 5-5 Air-cored PMFCL prototype experimental set-up

The air-cored PMFCL was connected in two design configurations to obtain the transient air-cored current to evaluate the performance of the PMFCL. The total resistance and inductance

for configuration 1 design air-core PMFCL was 1.5 Ω and 3.97 mH whereas the values for the configuration 2 design air-core PMFCL were 1.324 Ω and 3.1 mH .

The practical circuit diagram, as shown in Figure 5-6, consists of the Variac, 3.3KVA, which is powered by 240V, 50 Hz, connected to the PMFCL and a load resistance of 40 Ω in parallel with a switch. The practical work was performed on the two types of AC coils configurations, the named as " configuration 1 design" and " configuration 2 design", to obtain the measured steady state current against inductance and in addition to the transient current values.

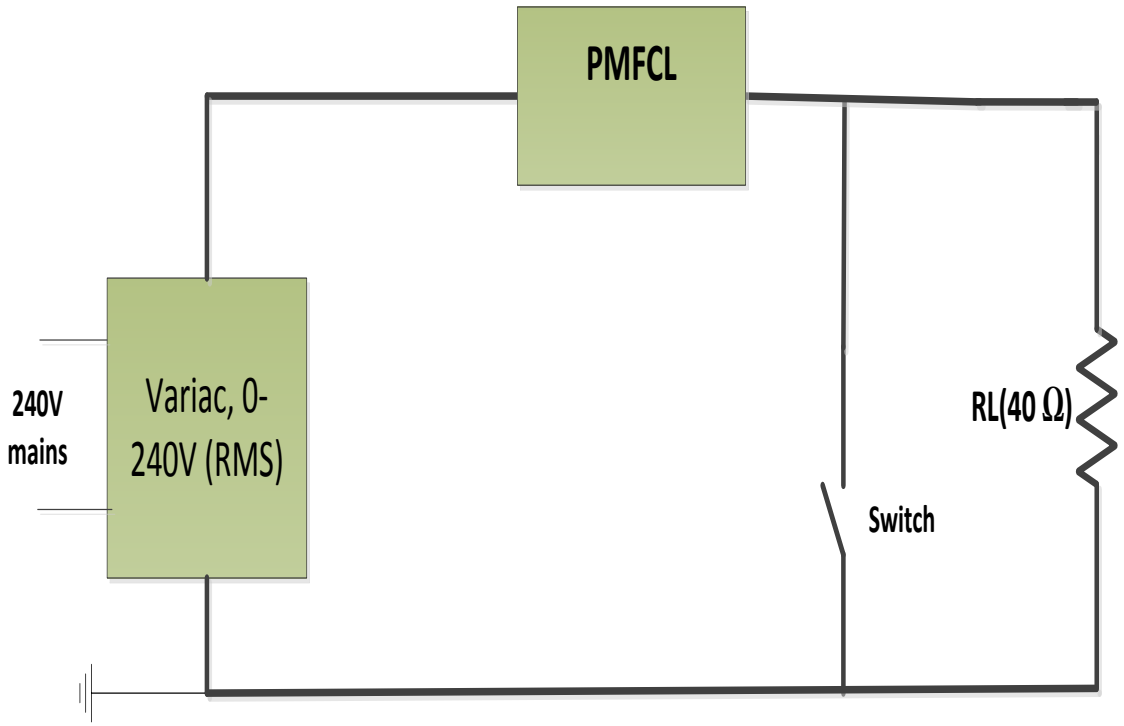

Figure 5-6 Experimental circuit set up

The PMFCL resistance and inductance per coil was measured individually by the RLC bridge instrument at 50 HZ and found to be 318 mΩ and 1. 65 mH. The total resistance and inductance for the low capacity configuration named "configuration 1" is 1.18 Ω and 7.33 mH, whereas the total resistance and inductance for the higher capacity (current rating) configuration, configuration 2 is 1.12 Ω and 6. 06 mH respectively.

The sequence of prototyping work was carried out according to the following steps:

- Ensure the limiter cores are in full saturation ($2T^{+}$) at zero AC current and the permanent magnet is capable to withstand the maximum fault current.

- Carry out 3D (FEM) modelling to evaluate the performance of the device under test to calculate the minimum and maximum operating current, the minimum current was calculated to be 2.24A and the maximum current was found to be 37 A / 45 A for design configuration 1 and 2 respectively.
- Ensure that the equipment under test is housed in a protective box.
- Choose the appropriate cables in terms of current rating for connecting the equipment with the supply voltage.
- Ensure that the equipment is properly earthed.
- Ensure that the heat generated does not affect the circuit components.
- Choose a spot in the lab close to the emergency switch.
- Carry out no load test of the variac to ensure the proper supply voltage.
- Take an off- line measurement of the PMFCL device under test to establish the load values.
- Ensure that the measuring instruments are calibrated for accurate results.

The total resistance and inductance for the four coils of the PMFCL device were measured by the RLC bridge instrument at 50 HZ. The low capacity configuration named " configuration 1" total resistance and inductance were 1.18 Ω and 9.5 mH, whereas the total resistance and inductance for the higher capacity (current rating), " configuration 2", were 1.12 Ω and 7.33 mH respectively.

5.4 Measured and calculated inductance/current profile

The inductance- current profile for the model and PMFCL prototype was obtained to validate the modelling method and to evaluate the device inductance in the limiting and non-limiting state and hence to determine the operating current values. This means to estimate the current limitation in short circuit situation.

The circuit shown in Figure 5-6 was wired up with the required measuring instruments for the current, voltage, power and power factor and without using the switch and the load (RL). The voltage was gradually increased through the variac (0-240) V_{RMS}. The current was monitored with the change in voltage and the inductance/current profile for the two design types of the prototype PMFCL was plotted.

5.4.1 "Configuration 1" PMFCL inductance-current profile

In this type, the neighbouring terminals of the coils are connected with each other as indicated previously in Figure 5-2. The current dependant inductance L (I) values obtained by 3D FEM magneto static solver using flux linkage method were thoroughly checked. The steady state modelling using the 3D (FEM) magneto static solver aimed to investigate the characteristics of the PMFCL and predict the fault current limitation at which the device activates in the abnormal condition i.e. fault condition. Figure 5-7 shows the activation of the PMFCL device at the predicted limited fault current using magneto static solver. The figure also shows the values of flux density distribution along the cores and it is almost 2.1 T.

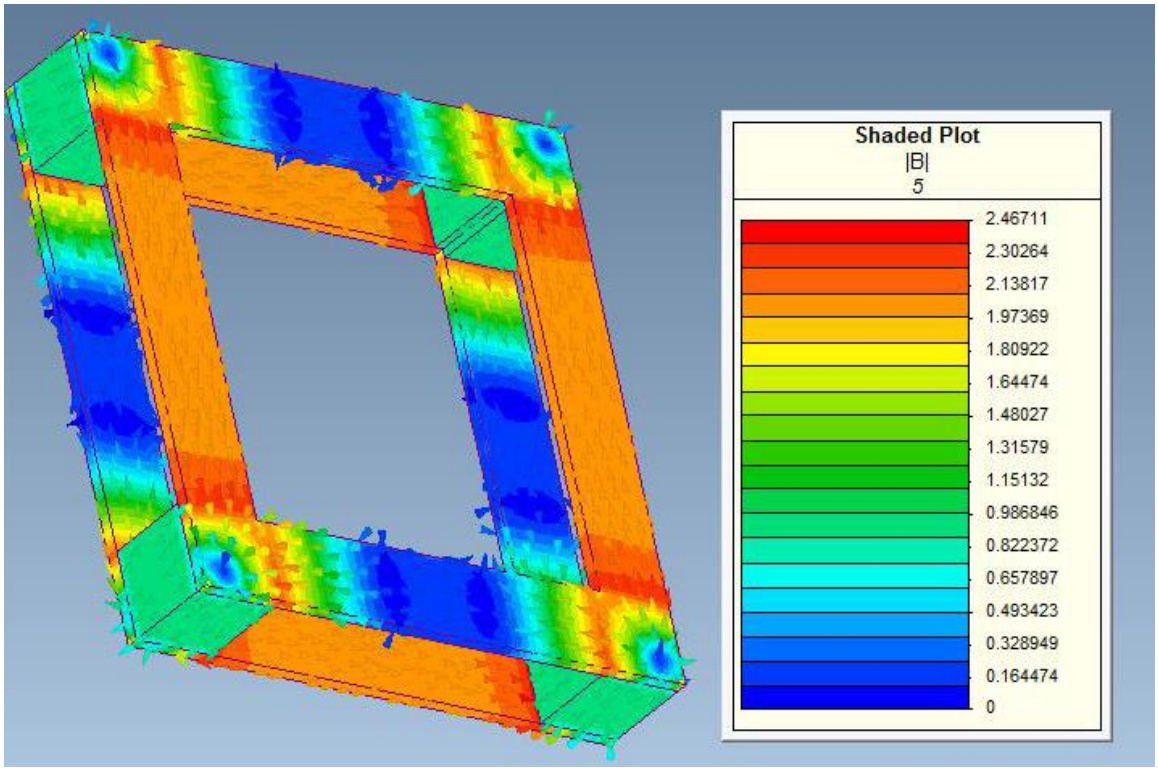

Figure 5-7 The 3D FEM PMFCL activation at the occurrence of the predicted fault current

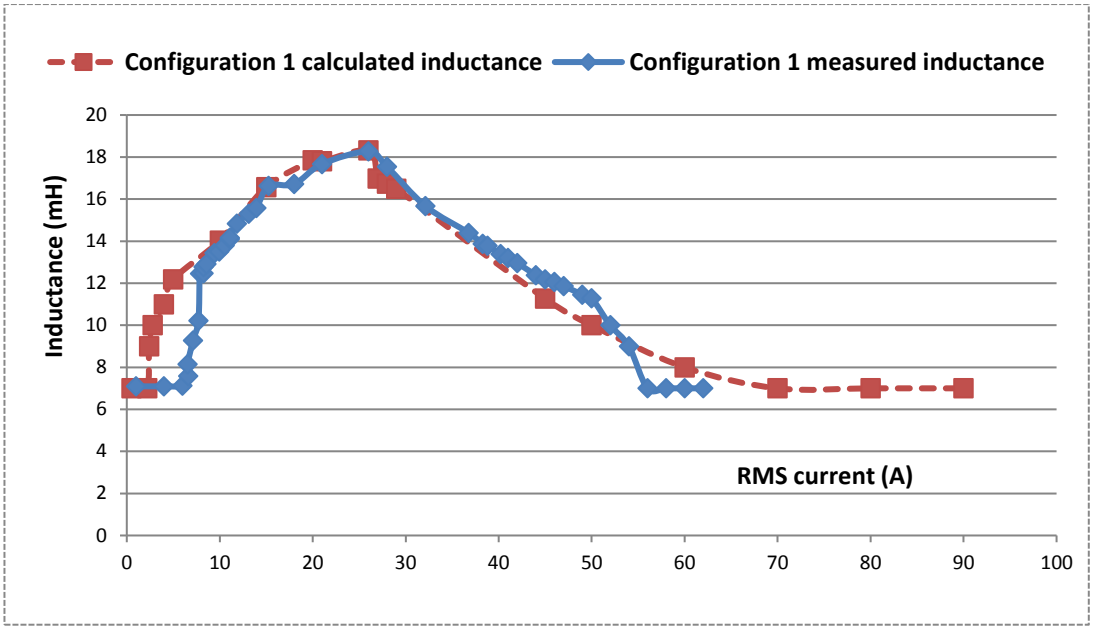

Figure 5-8 Calculated and measured inductance/current profile for configuration 1

Figure 5-8 shows inductance/current calculated and measured values for configuration 1(the flux of the magnets and AC current are in phase). The figure shows a fast increase in the inductance of the PMFCL device from the calculated and measured inclusion inductance of 7.0 mH up to the maximum calculated and measured inductance of 18.3 mH and 18.37 mH respectively. The both the calculated inclusion and maximum inductance for the designed model is almost the same as the laboratory prototype measurement.

The inductance value error percentage = [(18.37– 18.3)/18.3] * 100 = 0.38%

This means that the prototype is a replica of the designed model. Configuration 1 design has therefore fault to normal impedance ratio of 2.6. The figure also indicates that the maximum value of the inductance occurs at steady state current of 26 A_{rms}. This implies that the device will limit the transient fault current to or near the value of 26 $\sqrt{2}$ A.

5.4.2 "Configuration 2" PMFCL inductance-current profile

Configuration 2 design PMFCL has its AC coils connected as previously shown in Figure 5-2. The same PMFCL model specifications given in Table 5-1 has its AC coils configuration changed so that the magnetic flux produced by the AC current is in opposite direction to the permanent magnet's. The model was simulated by 3D FEM tool and later its replica was connected in the laboratory to 90V, 50Hz. The prototype was connected to the mains through the variac and the laboratory measured inductance vs current was obtained and compared with the calculated values. Figure 5-9 shows the inclusion calculated and

measured inductance value of 6 mH while the maximum calculated and measured inductance is 11.3 mH. The nominal inductance at zero AC current is limited by the air inductance whereas the maximum inductance is dependent on the PMFCL design specifications.

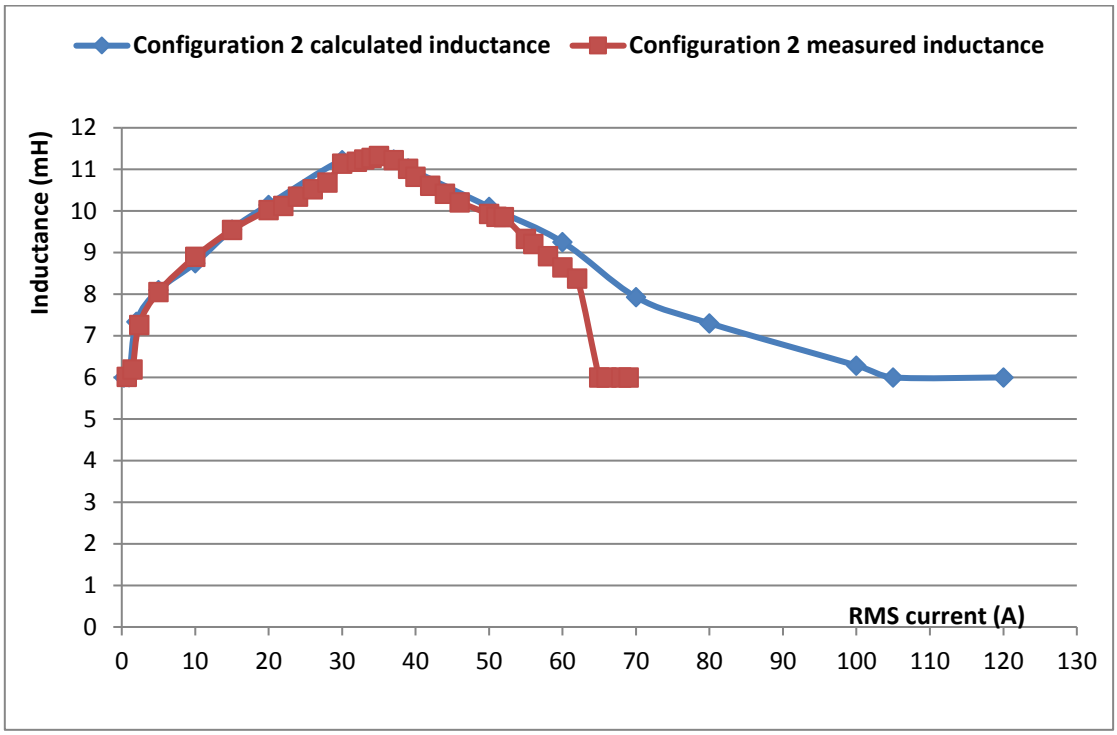

Figure 5-9 Calculated and measured inductance/current profile for configuration 2

Figure 5-9 illustrates that the inclusion and maximum calculated inductances are 6 mH and 11.3 mH respectively. The maximum measured inductance is nearly the same as the calculated inductance with a value of 11.36 mH. Each of the calculated and measured inductance arrives at its peak value at steady state current of 35 A.

The inductance value error percentage = [(11.36 – 11.3)/11.3] * 100 = 0.53%

configuration 2 design PMFCL device therefore has impedance ratio of 1.9 from normal to abnormal state according to calculated and measured results. The device should limit the actual fault current to or approximately equal to 35 √2 A.

5.5 PMFCL calculated and measured transient currents

The PMFCL transient modelling was investigated both using simulations and a laboratory scale prototype. The PMFCL prototype and an air-cored of similar specifications as the limiter

device were modelled at 90V, 50Hz to examine the performance of the device. The work involves three essential tasks.

1. To validate the time effective 3D (FEM) magneto static inductance/current approach in predicting the device fault current limitation.
2. To compare the two PMFCL designs calculated and measured limited transient fault currents.
3. To evaluate the two designs fault current limiting capability.

The device was simulated using 3D (FEM) time-step solver. The modelling circuit parameters for a quarter of the model are as shown in Figure 5-10.

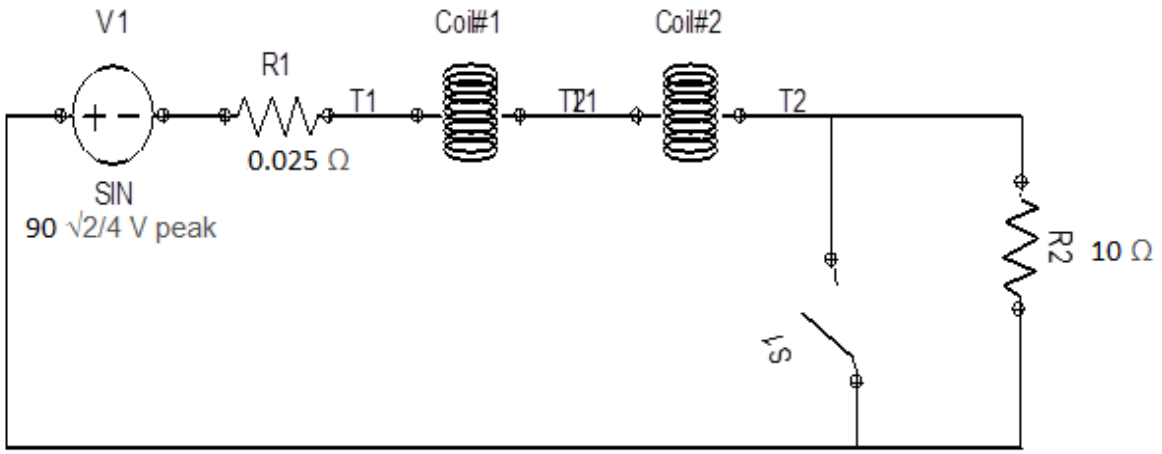

Figure 5-10 Transient circuit 3D (FEM) simulation for a quarter of the model

The above circuit was used for the simulation of the two PMFCL and the air-cored designs. The value of V1 was (90 √2)/4 V_{peak} and each coil has 55 turns. The input and load resistances were 0.025 Ω and 10 Ω respectively. The switch S1 was closed to initiate the fault at 40 mS and the simulation end time was 80 m.S.

The transient measured fault currents for the two PMFCL designs were obtained using the practical circuit shown in Figure 5-11 and Figure 5-12 where the device was installed inside a protective steel box. The oscilloscope was connected to the ammeter probe and set to be current triggered. Then the circuit input voltage was increased via the variac till it reached 90V where the RMS load current through the stray resistance (R2) was 2.24A. At 40m.s the switch was closed. The oscilloscope captured the transient current waveforms for 10 cycles.

Then the data was exported to the computer for evaluation and the measured transient results were compared with the calculated values. The calculated and measured transient currents were lastly compared with the air-cored PMFCL to evaluate the influence of the device on fault current reduction.

The figure below shows the connection of the prototype PMFCL device inside the protective box.

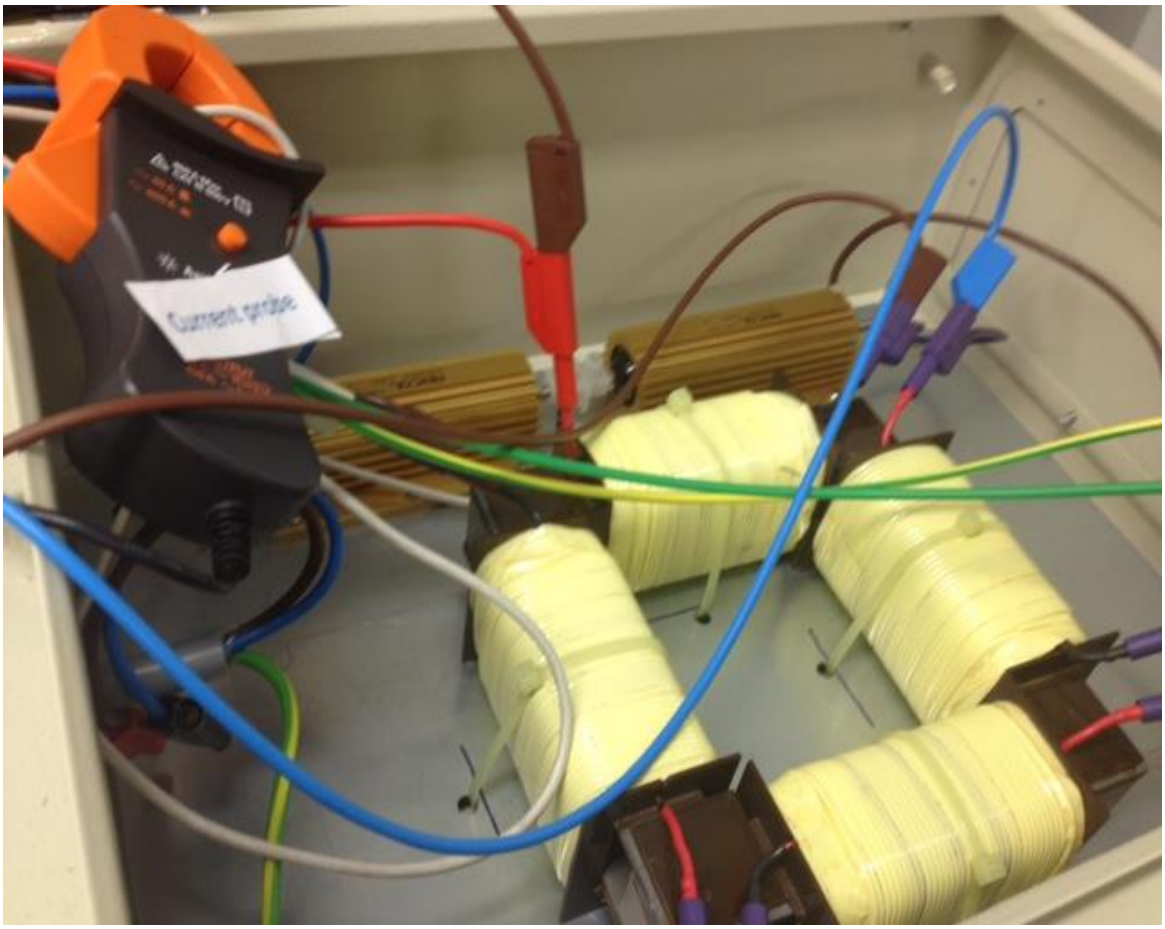

Figure 5-11 The connection of PMFCL inside the protective box

Figure 5-12 shows the PMFCL transient circuit wiring diagram where it is connected to the variac, oscilloscope, a switch and measuring instruments.

Figure 5-12 The transient circuit wiring up

5.5.1 "configuration 1" PMFCL calculated and measured transient currents

Configuration 1 design PMFCL and its air-cored were simulated using 3D(FEM) time-step solver and connected in the Lab. The simulation and measured results are as shown in Figure 5-13 and 5-14 respectively.

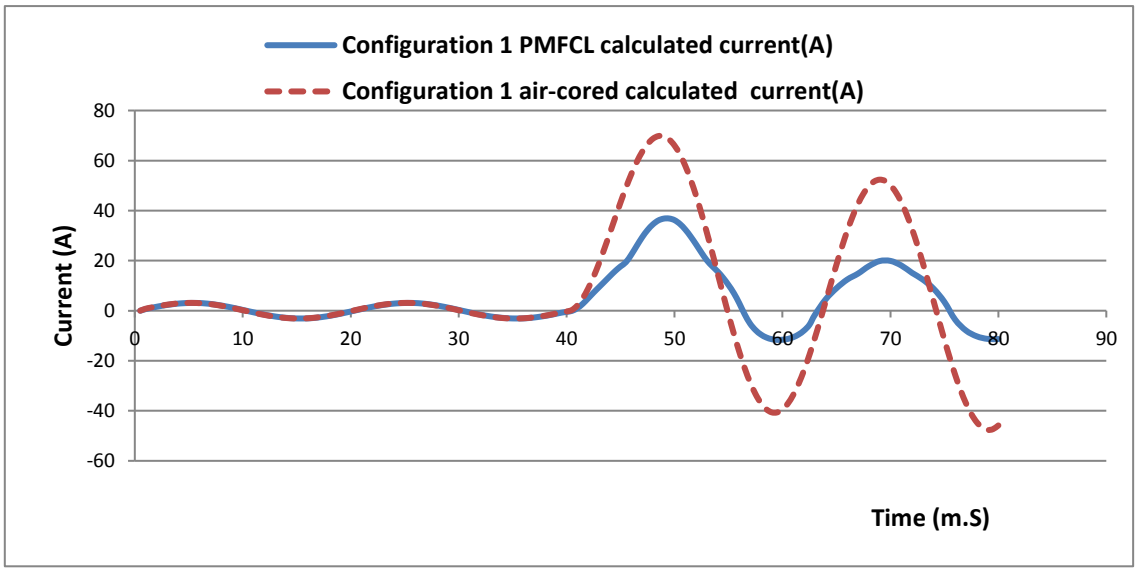

Figure 5-13 Cconfiguration 1calculated transient current

The above figure shows that the device 3D (FEM) calculated limited fault current was 37 A.

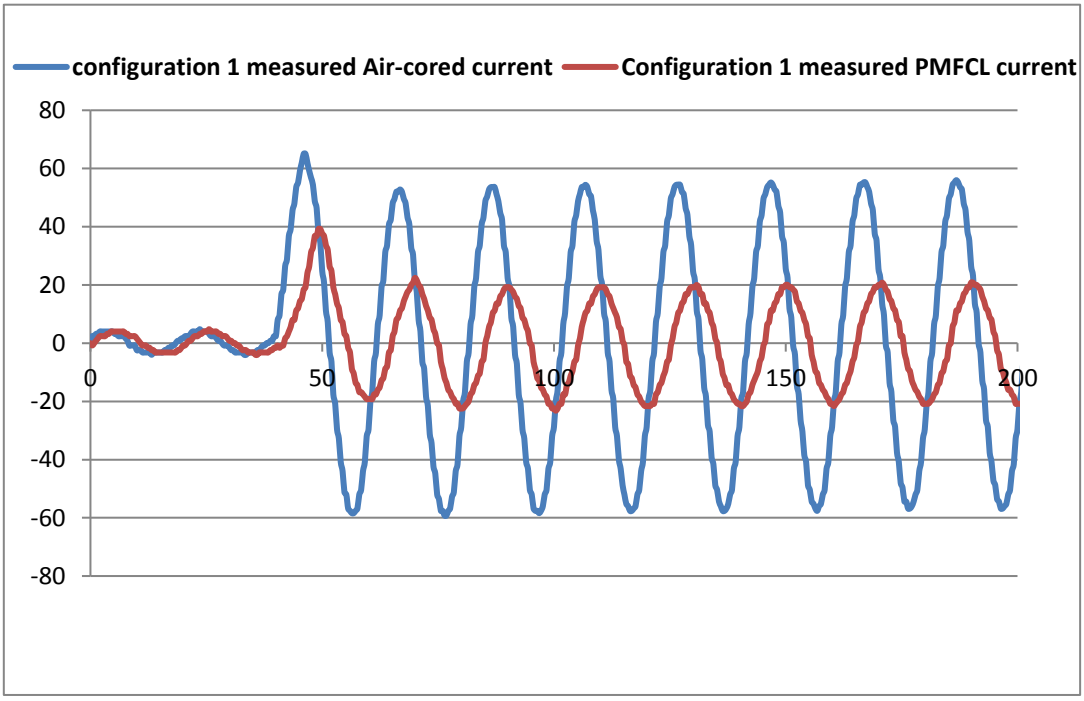

Figure 5-14 Configuration 1 measured transient current

Figure 5-14 shows that the Lab measured fault current was 39 A. The calculated and measured fault current without the PMFC is the same as the both the Figures 5-13 and 5-14 show that

the first peak air-cored current was 65A. This means the device fault current limiting capability according to the 3D FEM simulation and lab measurements are 43 % and 40 % respectively.

5.5.2 "Configuration 2" PMFCL calculated and measured transient currents

The opposite design PMFCL was simulated and the prototype was connected in the Lab to obtain the practical results.

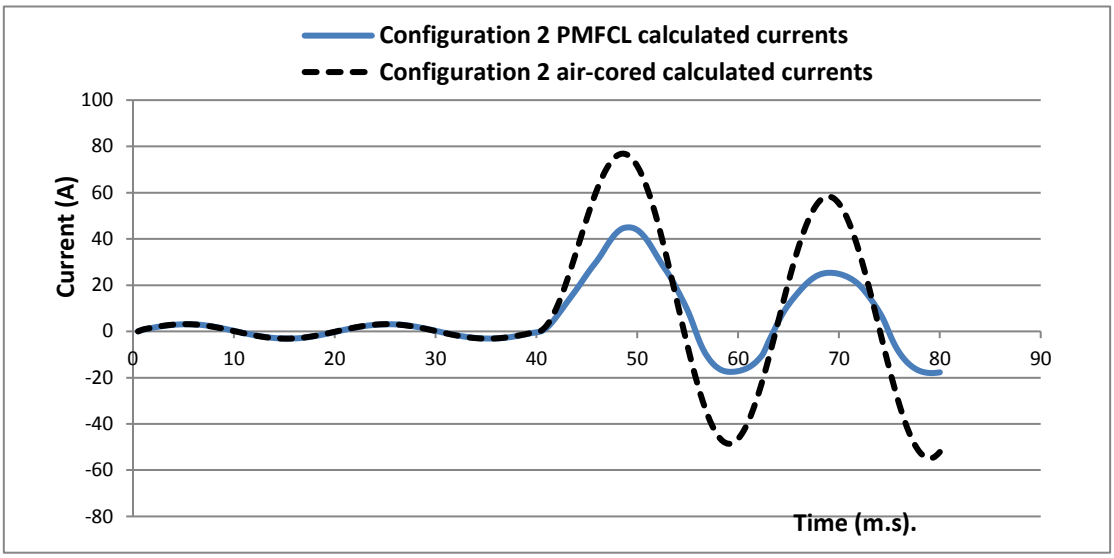

Figure 5-15 Configuration 2 calculated transient current

Figure 5-15 shows that the PMFCL calculated 3D (FEM) transient current was 45 A. In contrast, the PMFCL measured limited fault current was 49A as illustrated by Figure 5-16.

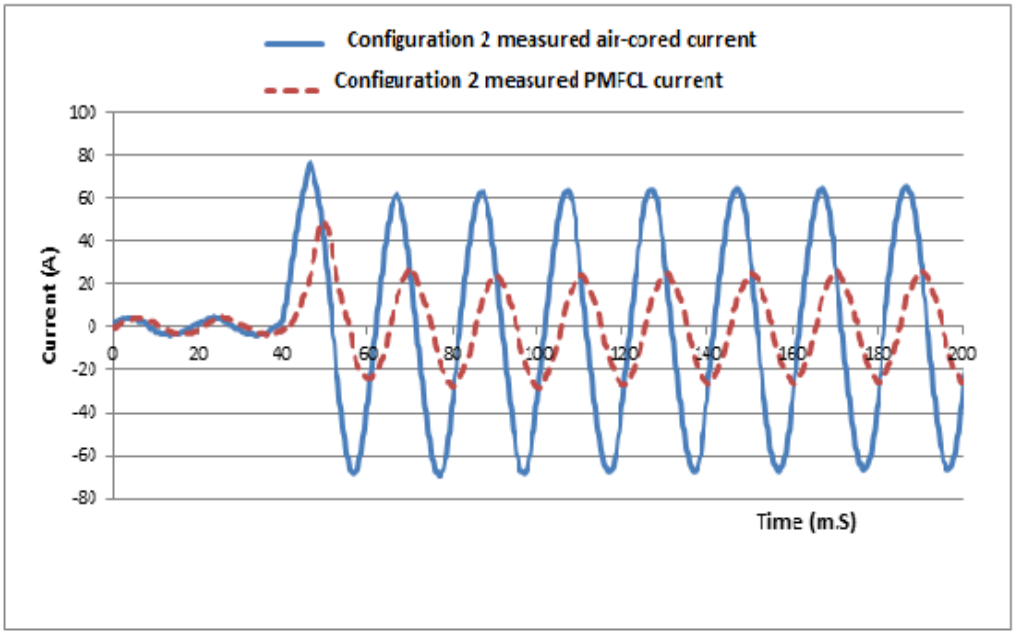

Figure 5-16 Configuration 2 measured transient current

The air-cored transient current for the opposite design was 77 A as indicated by Figure 5-15 and Figure 5-16. The figure shows a phase angle shift due to the different values of the air-cored and PMFCL inductance values. In comparison between the numerical and measured results, the device has fault current limiting capability of 41.5 % and 36% according to the simulation and lab measurement respectively.

The transient current values obtained for the both configuration 1 and 2 design validate the results obtained previously using the steady state inductance/current profiles.

The influence of the fault current on the PMFCL operation during the fault has been predicted by the time-saving technique and lengthy computation process, as shown in Figure 5-17 where the core was driven out of saturation.

Figure 5-17 expresses the prediction of the device activation and flux density variation along the core at the expected fault current limitation using the quick solution of the (FEM) magneto static solver inductance/current approach. The figure also confirms the response of the device at the expected fault current limitation using the lengthy computation process of the (FEM) transient time-step solver.

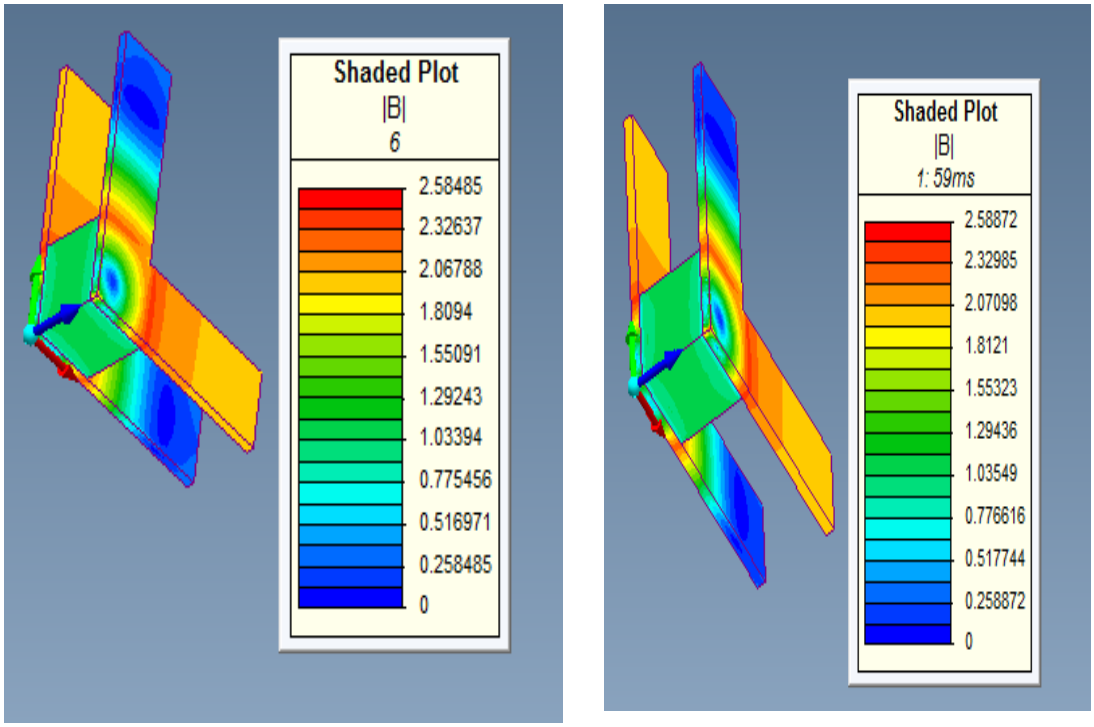

Figure 5-17 Prediction of the device activation and flux density variation using time-saving technique and lengthy process step-up solver

The device has the same expected reaction to the fault current with almost the same flux density distributed along the cores with either using the short or long-time solution method.

5.6 The effect of AC coils length on the performance of the PMFCL device.

The influence of coil length mounted at the centre of the core for the prototype with fixed number of turns was utilized through 3D (FEM). Inductance current profiles at 39 mm and 69 mm AC coil length were plotted for the two types of the model and compared with the calculated inductance dependant current L (I) at 99 mm. The lowest value of inductance is at zero AC current whereas the maximum value is at maximum permeability at which the core magnetization is the least value.

Figure 5-18 depicts the inductance/current profiles for configuration 1 PMFCL. It demonstrates that the 39 mm AC coil length along the core offers the highest inductance compared with the 69 mm and 99 mm ones. This means that the shortest coil length has its core with the weakest saturation extent and core can easily get desaturated. The figure also illustrates that the 99 mm coil length along the core exhibits a lower inclusion and fault inductance of 7 mH and 18.3mH respectively, compared with 39 mm and 69 mm, and hence

it has an impedance ratio of 2.6.This implies that the core has the highest saturation extent at 99 mm coil length at which the flux linkage between the windings makes the mutual inductance low and as a result the total inductance is reduced.

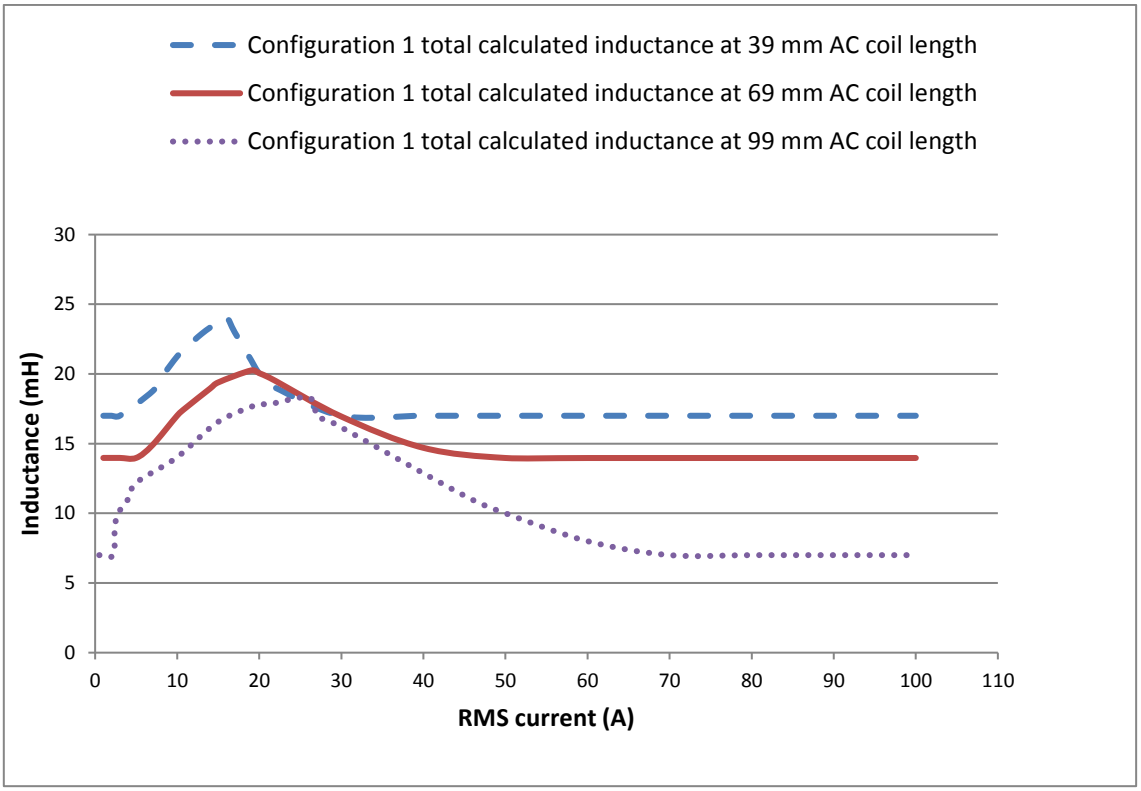

Figure 5-18 Configuration 1 inductance current profiles at 39 mm, 69 mm and 99 mm coil length

The low nominal inductance for the longer coil is attributed to the higher saturation for the core under the coil regions and the maximum inductance limits the extreme fault current. Therefore, the effective coil length is the 99 mm, which has steep increase and a higher abnormal to nominal impedance ratio. The calculated inclusion and fault inductance for the with design models at different AC coil length along the core is illustrated in Table 5-2.

Table 5- 2 gives the values of configuration 1 inclusion and maximum inductance for different coil length

Table 5- 2 configuration 1 inclusion and maximum inductance for different coil length

Type of PMFCL	Inclusion inductance (mH)	Maximum inductance (mH)	Normal/abnormal inductance ratio
39 mm coil length	17	24	1.41
69 mm coil length	13.98	20.3	1.45
99 mm coil length (calculated)	7	18.3	2.6

Figure 5.19 refers to configuration 2 inductance current profiles for three different coil length mounted at the centre of the core.

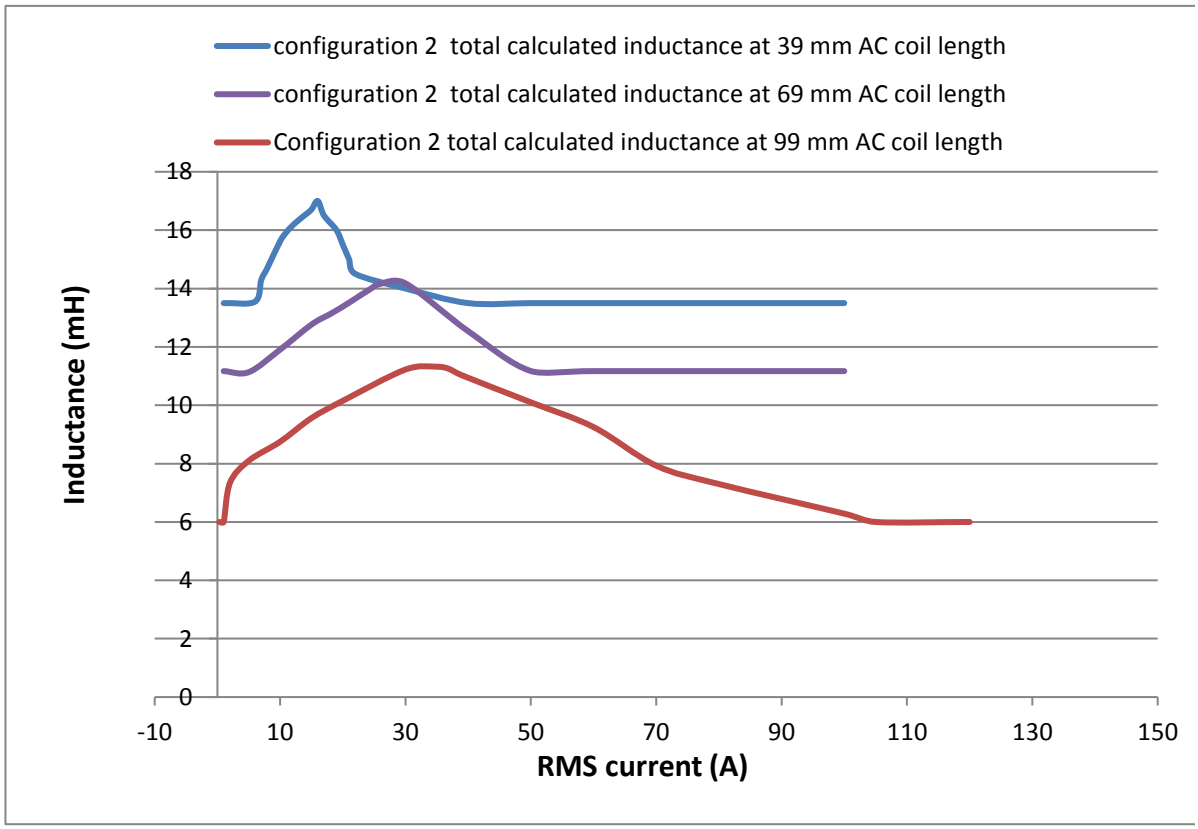

Figure 5-19 configuration 2 inductance current profiles at 39 mm, 69 mm, 99 mm coil length

The 3D (FEM) simulation for opposite type PMFCL at different coil length mounted at the centre of the core can clearly indicate the inductance/current profiles at 39 mm, 69 mm and

99 mm coil length along the core. Although the highest inductance value is for the coil length of 39 mm, this value is less than the previous type least inductance. The graph for the opposite type shows that the 99 mm coil length has low nominal and fault inductance in comparison to the 39 mm and 69 mm. Thus, the device with 99 mm coil length has a lower voltage drop in the normal steady state operation. In abnormal state, the 69 mm coil length has a maximum inductance of 14.06 mH. On the other hand, the 39 mm coil incorporates with the highest inductance value of 17.03 mH. Therefore, the most suitable coil length is the 99 mm coil length as it has a low inductance value in the normal and abnormal system operation. This makes the longer coil more convenient in the use with the grid for large capacity applications.

Table 5-3 illustrates the inclusion and maximum inductance for configuration 2 at different AC coil length along the core.

Table 5- 3 configuration 2 inclusion and maximum inductance for different coil

Type of PMFCL	**Inclusion inductance (mH)**	**Maximum inductance (mH)**	**Normal/abnormal inductance ratio**
39 mm coil length	13.88	17.03	1.23
69 mm coil length	11.13	14.17	1.27
99 mm coil length (calculated)	6	11.39	1.9

The longer the coil along its core the larger the normal to fault impedance ratio. Figure 5-19 and Table 5-3 correlated that the highest impedance ratio was achieved by the designed PMFCL with the longest AC coil length along the core, which means that the prototype PMFCL has less voltage drop in normal and abnormal power system operation.

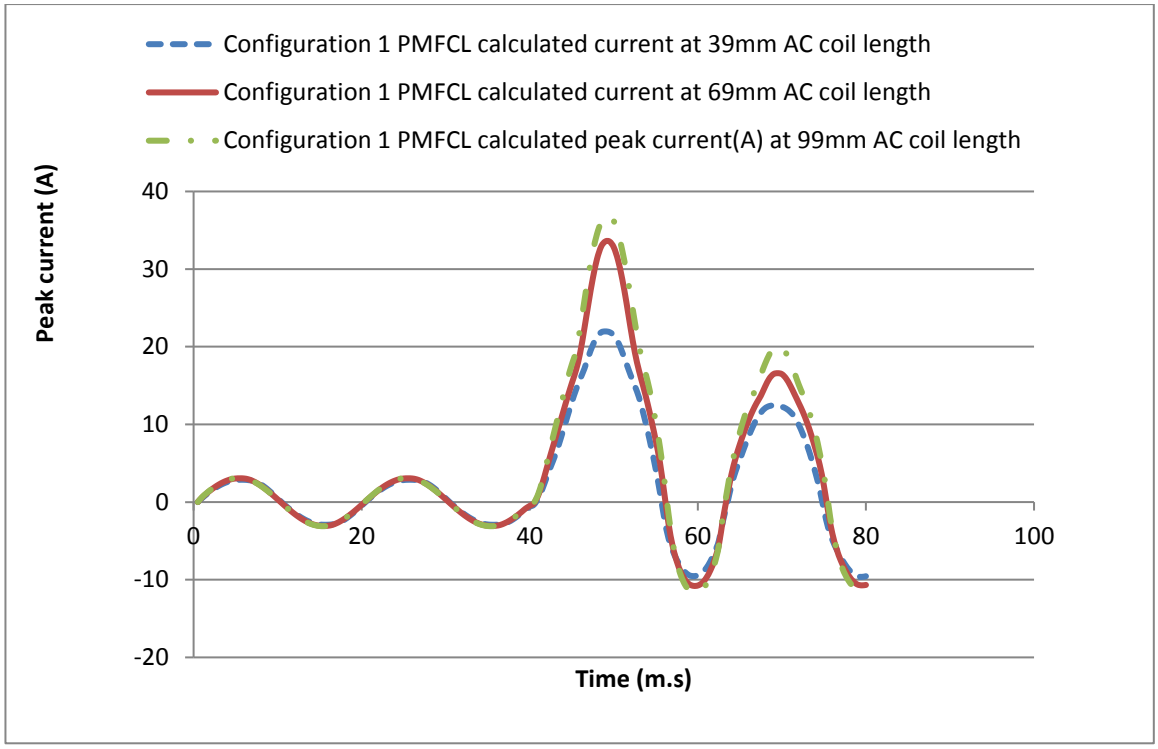

Figure 5-20 Configuration 1 transient current simulations at 39, 69 and 99 coil length

The limited fault current for the 39 mm, 69 mm and 99 mm AC coil length is as shown in Figure 5-20. Clearly, the limited fault current is dependent on the length of the coil as the longer coil along the core offers more contribution to the fault current limitation. This is due to the high magnetic field, which drives the core out of saturation during the fault event. The influence of the coil length along the core on the fault current for the with design is illustrated in Tables 5-4.

Table 5- 4 Configuration 1 transient current for different coil length

Type of PMFCL	PMFCL first peak transient current (A)	Air-cored transient current (A)	percentage of PMFCL transient capability
39 mm coil length	22	30	26%
69 mm coil length	27	41	34%
99 mm coil length (calculated)	37	60	48%

The opposite type for the same designed model has been modelled at different AC coil length along the core using 3D (FEM) time-step solver. The calculated and measure prospective fault current for the 99 mm designed model and its similar prototype were taken as a reference point to compare the influence of the coil length along the core on the fault current limitation.

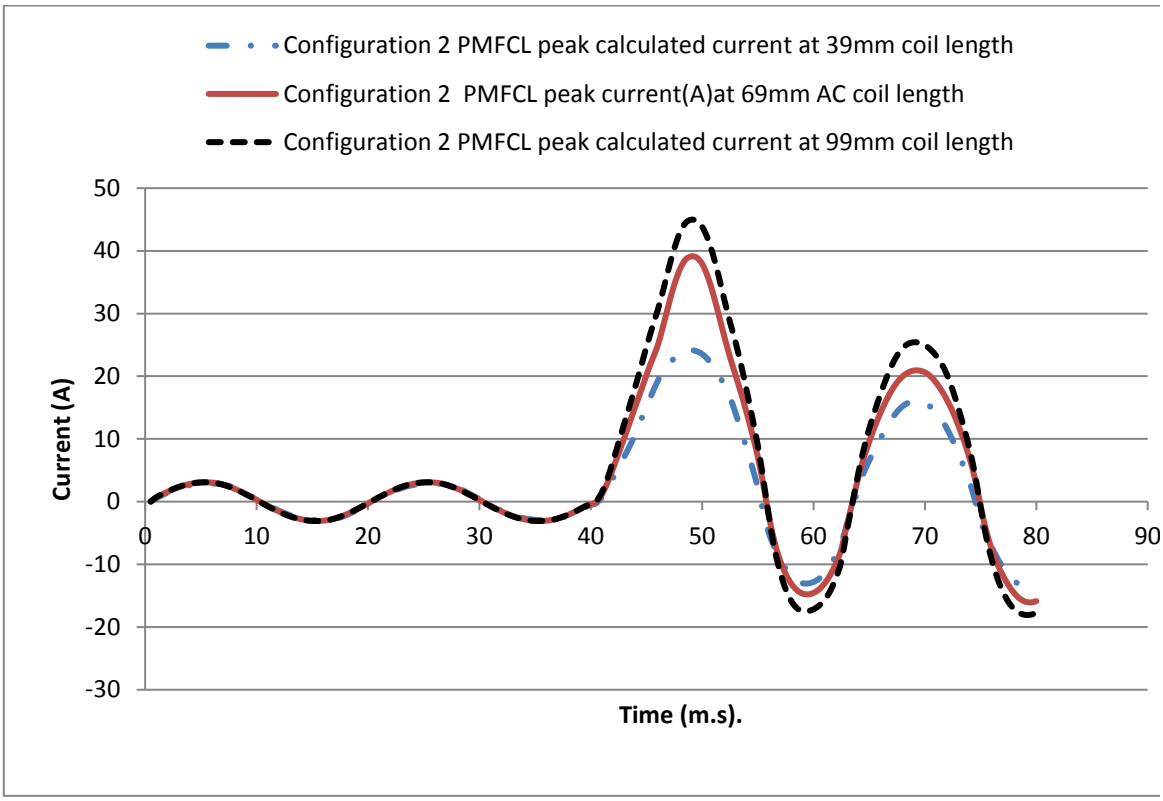

Figure 5-21 Configuration 2 transient current simulations at 39 mm, 69 mm and 99 mm coil length

The effective core length for the higher current rating design is the 99 mm as it has a flexible operation from the normal state where the load current is 2.2 A_{rms} to the maximum limited fault current of 45 A according to 3D (FEM) and 49 A with respect to the laboratory measurement.

Table 5- 5 Configuration 2 transient current for different coil length

Type of PMFCL	PMFCL first peak transient current (A)	Air-cored transient current (A)	percentage of PMFCL transient capability
39 mm coil length	24	35	31%
69 mm coil length	39	58	33%
99 mm coil length (calculated)	45	76.8	41%

5.7 Conclusion

The small-scale model of PMFCL was designed using 3D (FEM), constructed and tested. The laboratory scale prototype has been tested at the both the steady and transient state conditions. The steady state inductance/current profile for both types of the device show that configuration 2 design has less inclusion and fault impedance compared with configuration1 and hence can be used for large capacity (higher current rating) applications.

The PMFCL model simulation results were compared with the experimental results to investigate the effect of coil winding configuration on the performance of the device. The outcome from the investigation deduced that the coil winding configuration plays an important role in relation to the normal and maximum current in the power circuit and should be considered in the design of the device. However, there are no published studies have been reported regarding the effect of AC coils configuration on the performance of the fault current limiter device.

The influence of coil length on the performance of the PMFCL was also verified. The calculated results for the candidate prototype with 99 mm coil length were taken as a reference and compared with the simulated results obtained using 3DFEM at 39 mm and 69mm, with fixed number of turns. The key findings from the steady and transient results show that the 99 mm coil is the more efficient device as it offers higher percentage of fault current limitation and a low inductance in the normal and faulted state operation. Hence, the coil length along the core is an important parameter that should be considered in the design of the PMFCL device. The designed prototype modelling and experimental results confirm the device principle of operation.

References

[5.1] Magnet user manual by Infolytica, www.infolytica.com.

[5.2] M. Mordadi-Bidgoli and H. Heydari (2014). Comprehensive (FEM) analysis for saturable core fault current limiters in distribution network. *2014 22nd iranian conference on electrical engineering (ICEE),* 665-670.

[5.3] J. H. Teng and C. N. Lu (2007). Optimum Fault Current Limiter Placement. In: *2007 international conference on intelligent systems applications to power systems,* 1-6.

[5.4] Y. Zhang and R. A. Dougal (2012). State of the art of Fault Current Limiters and their applications in smart grid. *2012 IEEE power and energy society general meeting,* 1-6.

[5.5] Y. Nikulshin *et al*., "Saturated Core Fault Current Limiters in a Live Grid," in *IEEE Transactions on Applied Superconductivity*, vol. 26, no. 3, pp. 1-4, April 2016.

[5.6] Y. Nikulshin, A. Friedman, Y. Wolfus, V. Rozenshtein and Y. Yeshurun, "Dynamic Desaturation Process in Saturated Cores Fault Current Limiters," IEEE Transactions on Applied Superconductivity, vol. 22, no. 3, pp. 5601704-5601704, June 2012.2

[5.7] Liang Zou, et al. (2009). Study on the feasibility of developing high voltage and large capacity permanent-magnet-biased fault current limiter. Universities Power Engineering Conference (UPEC), 2009 Proceedings of the 44th International, 1-5.

Chapter 6: - Design of low and medium voltage PMFCL

6.1- Introduction

The previous chapter presented the design and testing of the small-scale prototype PMFCL. The experimental results verified that the PMFCL operated according to the proposed design methodology. The development of the PMFCL for better performance depends greatly on the design topology and the state of the art soft and hard magnetic materials [6.1]. This chapter covers two designs of PMFCL, design 1 is for 11 kV power grid and design 2 is for low voltage applications. The low and distribution voltage level models are designed and analysed using 3D (FEM) [6.2]- [6.5].

The work in this chapter commenced with the design and modelling of the 11 kV PMFCL for the power grid. The distribution voltage level PMFCL model is chosen to match the commercial small scale square sided shape, which was covered in last chapter. The classical analytical approach based on reluctance calculations of the magnetic circuit reported in [6.1] did not produce an accurate estimation of the main geometry. Also, the 2D numerical (FEM) approach was insufficient, this is due to flux distribution in which the PMs flux direction is orthogonal to the AC flux in the core. The grid full scale 11 kV PMFCL model specifications are given in section 6.2. The model design method and steady state modelling are given in Section 6.3. Section 6.4 gives the dynamic modelling of the PMFCL and presents the time-step 3D FEM transient results. The device cost evaluation is given in section 6.5.

The low voltage 277 V PMFCL is a toroidal-shaped topology using samarium cobalt. The design lent itself towards the electrical power requirement for the promising renewable energy. The toroidal model PMFCL can be used for an individual renewable source of energy such as the solar or wind power farms or for the future wind-photovoltaic (wind-PV) power generation step up transformer [6.6], [6.7]. The low voltage PMFCL topology and operating principle are given in section 6.6. The PMFCL model steady and transient results are given in section 6.7.

The capability of the samarium cobalt magnet to withstand excessive fault currents has been evaluated in section 6.8. Section 6.9 presents the cost evaluation of design 2.

The power grid PMFCL can be positioned at different locations in the electrical power distribution system, it can be installed in series with a generator, busbar or feeder. However, a relationship between fault current limiters and protection schemes should be established.

It is essential that the PMFCL's installation does not cause an adverse effect to the functionality of the power system protection, power quality and power system stability. The functional requirements imposed on an FCL can vary for the different FCL positions [6.8], [6.9]. This is presented in Section 6.10. The utmost importance aspect of device's installation is to check whether the device principle of operation affects the protective relays so that proper operation of the protection relays is insured. This is introduced in section 6.11. The PMFCL device reduces the fault current in the first half cycle to a permissible value that a circuit breaker can endure. The main or backup protective relay detects the fault and sends a trip signal to the circuit breaker to immediately isolate the fault from the power source [6.10]-[6.17]. The circuit breakers must be ensured that their operation during a fault is not affected by the supplement of the PMFCL device. Section 6.12 discussed the interaction between the device and the CBs [6.18]- [6.22].

Besides the merit of the PMFC's principle of operation, the economical factor must be considered. It is very important to check whether there is a compromise between the device's operation in the power system and its total cost.

6.2 Design 1, the medium voltage PMFCL model specifications

The power grid PMFCL is chosen to match the 90 V prototype, which was designed and analysed in last chapter. The proposed design offers the followings merits: -

(i) High efficiency due to PM excitations.

(ii) Low magnetic core losses due to core static saturation.

(iii) Instant response to short circuit current due to inherent permeability feature of the core.

(iv) Flexibility in determining the operating current range by reconfiguration of AC coils number of turns.

(v) Low maintenance cost. For 3-phase design a stackable of three devices with high degree of magnetic coupling could be achieved.

Table 6-1 details the full-scale model dimensions and type of materials used.

Table 6- 1 The 11 kV PMFCL design specifications

Parameter	Type or value	Parameter	Type or value
Iron core material	MR36	Coil winding resistance	0.04 Ω
Core material relative permeability at saturation level	57	Magnet coercivity	$H_c = 8.68 \times 10^5 \frac{A}{m}$
Iron core size	(3 x 0.3 x 0.008) m^3	Frequency	50Hz
Permanent Magnet type	N_d-F_e-B (N52)	A.C coils No of turns	100
Remanence, B_r	1.22 T (Tesla)	PMFCL first cycle limited fault current for configuration1 and 2	1700/1900 A
Permanent Magnet size	(1.7 x 0.3 x 1) m^3	Supply voltage	11kV/√3 RMS
A.C coils cross sectional area	(1.026 x 0.31) m^2	AC coil length along the core	0.5 m
Maximum load current	525 A_{rms}	Input resistance	0.528 Ω
Configuration 1 and 2 air-cored fault current	(3018/3410) A	Stray resistance	12.1 Ω

6.3 Design method and steady state modelling

A great deal of emphasis was placed on ensuring enough magnetic saturation of the core. The geometrical dimensions of the PMs and the cores could be determined. As well as, the interaction of the PMs and the AC flux could be investigated to ensure core saturations, the AC current operating range and the PM demagnetization state could be evaluated. The 3D magneto static solver was utilized; Figure (6-1) shows the flux distribution in the core due to PMs flux only.

The initial estimate of the PMFCL design parameters is obtained using an analytical approach. The flux density in the core was analytically calculated prior to performing the (FEM) numerical approach. The required mathematical equations were covered in Chapter four nevertheless they did not give a precise indication regarding the design of the PMFCL. The flux density calculated analytically is completely different from the one obtained from the numerically calculated. For example, the iron core flux density was calculated using the analytical approach and was found to be 3.77 T, which is unrealistic. It is also the use of 2D

(FEM) is not realistic due to the flux distribution of the proposed model. Hence, the 3D (FEM) is used to develop the proposed design.

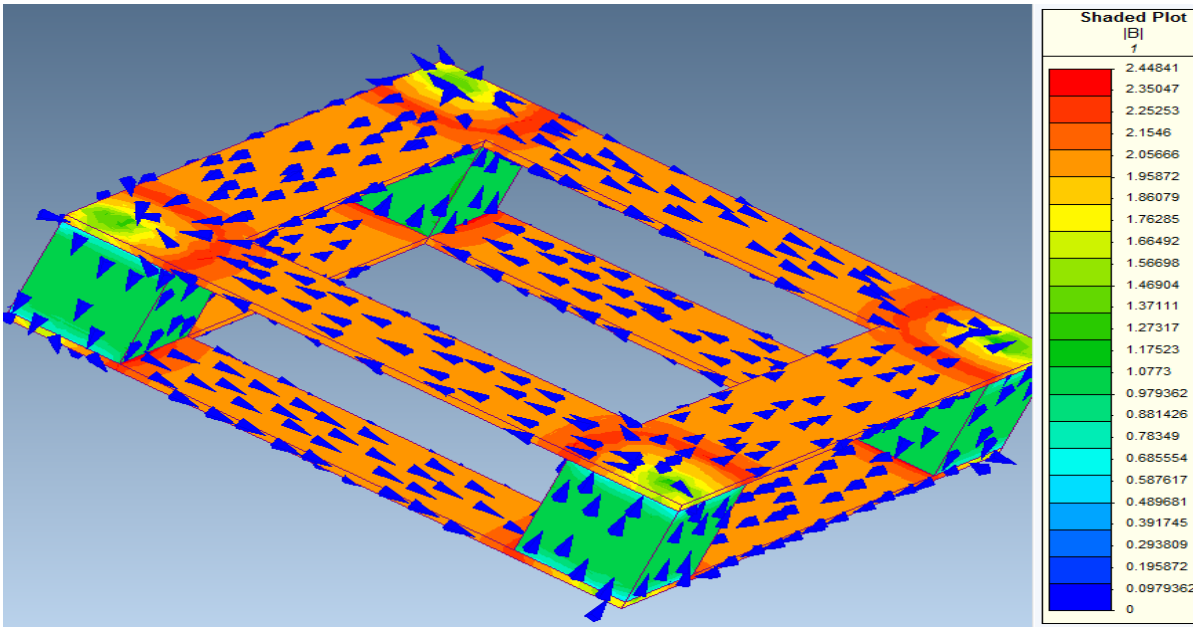

Figure 6-1 Flux distribution in complete model and the flux density values |B| at no excitation

Figure 6-1 shows the magneto static flux density distribution along the cores in a complete model at zero AC current. The model designs (configuration 1 and 2) characteristics are obtained using 3D (FEM) magneto static solver by means of the inductance / current approach. The steady state obtained RMS current is the predicted limited fault current during abnormal condition.

The advantageous inductance/current profiles for 11 kV PMFCL, configuration 1 and 2, are illustrated by Figure 6-2.

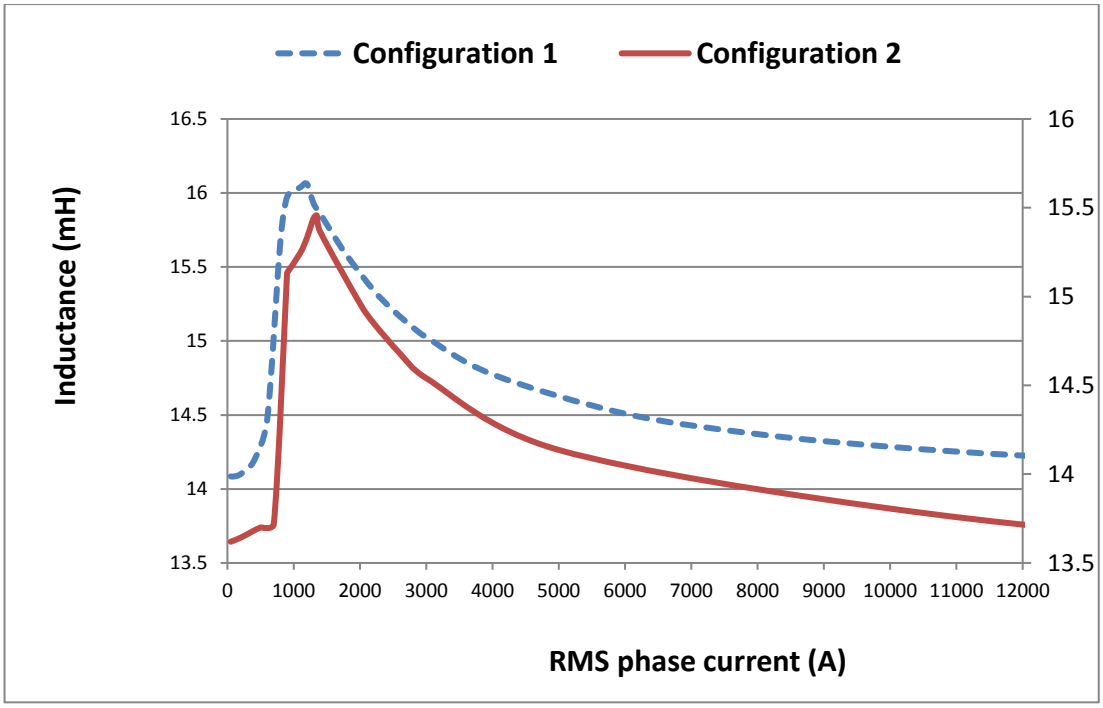

Figure 6-2 Configuration 1 and 2, 11 kV PMFCL inductance-current profile

As it can be seen from the figure that the inductance for the configuration 2 design model increases from its nominal value of 13.6 mH until it reaches its maximum value of 15.46 mH, which is corresponding to the maximum RMS current of 1350 A. The calculated limited transient current will be obtained by the 3D (FEM) time step solver, which is predicted to be almost equal to 1350 *√2 A.

Configuration 1 design on the other hand has an inclusion inductance of 14.08 mH and a maximum inductance of 16.06 mH at a corresponding current value of 1200 A_{rms}, as shown in Figure 6-2. This means that the peak fault current is predicted to be 1200 * √2. A.

Although there has been a small difference of inductance between the two designs, Configuration 2 offers a higher current rating of 1.13 %. However, the discrepancy between the two design characteristics will be more oblivious with the increased number of turns as previously stated in chapter four.

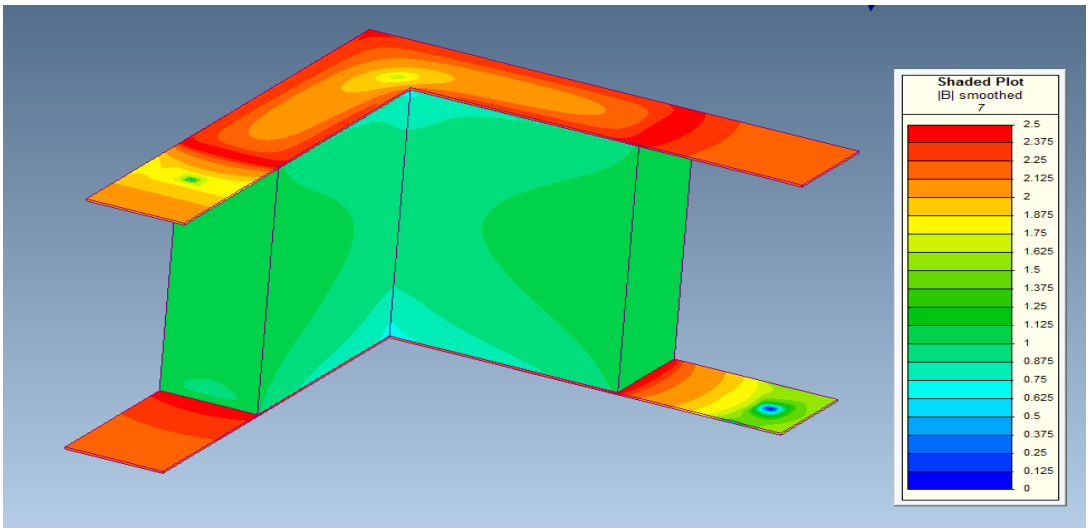

Figure 6-3 FEM magneto static model at fault current limitation

The magneto static solver shows at the expected fault current limitation that a part of the core becomes desaturated.

6.4 Dynamic modelling of the PMFCL

The transient FEM solver was used to model the dynamic response of the PMFCL. The PMFCL model and an air-cored of similar specifications were modelled to investigate the performance of the device. The system voltage was 11/4√3 kV_{RMS}, 50 Hz, (R1) and (R2) were 0.15 Ω and 3.026 Ω respectively. The normal load current in (R2) was 525 A_{RMS}. The model of the PMFCL is coupled to electrical circuit model as shown in Figure 6-4 where the performance of the device was assessed. The fault was initiated by closing the switch (S1) across the load resistance (R2) at the time of 40 Milliseconds.

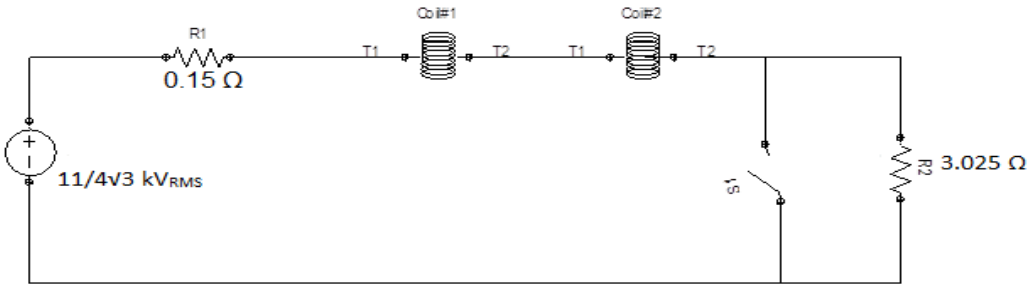

Figure 6-4 Transient circuit for a quarter of 11 kV mode

Figure 6-5 indicates that the core lost its saturation in the half cycle of the fault current. When one of the cores completely desaturates due to the high fault current, its inductance increases, and the fault current is reduced by the rushed impedance of the device.

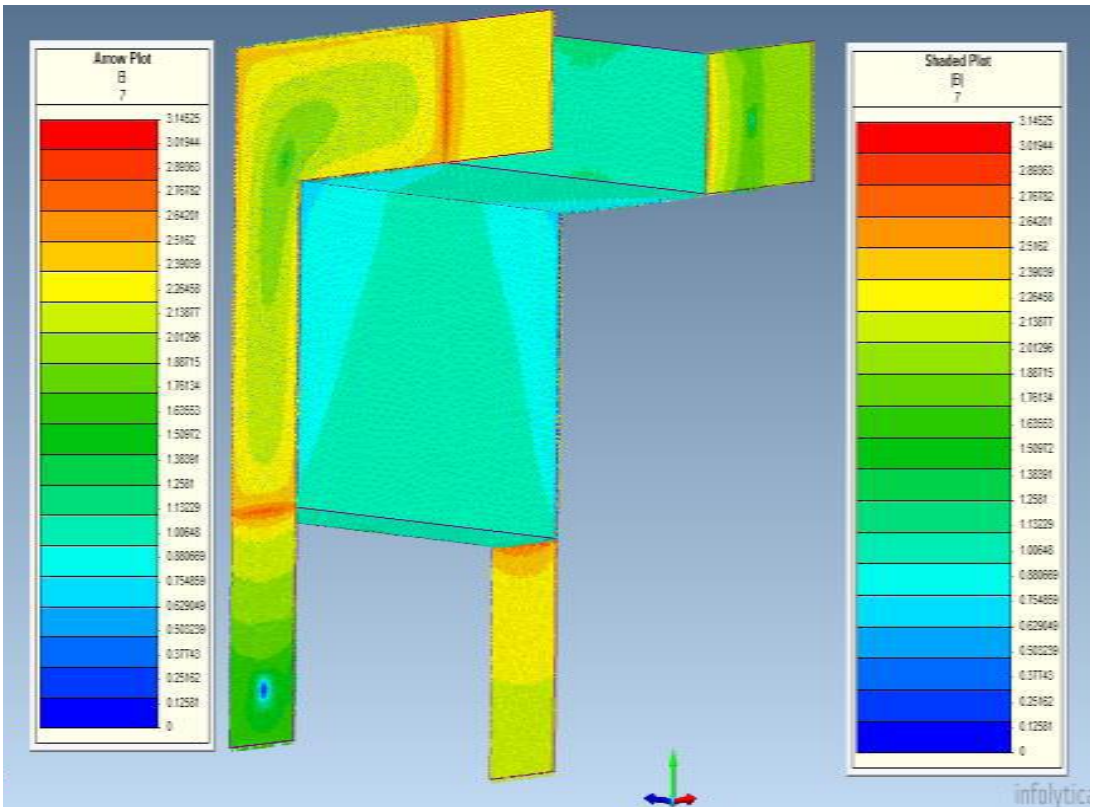

Figure 6-5 PMFCL at fault condition

The air-cored PMFCL of similar specifications as the PMFCL device was modelled to compare the value of the fault current due to the presence of the device with the normal case, with no device in the circuit.

The actual peak fault current is 14.974 kA, which is calculated by dividing the transient circuit input voltage by the resistance (R1) (Figure 6-4).

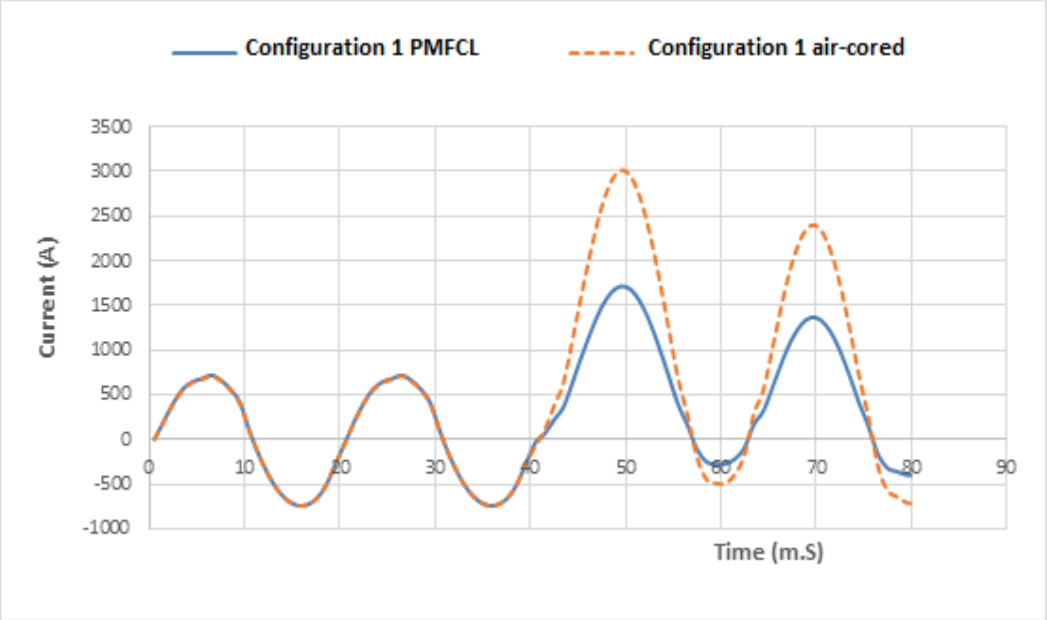

Figure 6-6 Configuration 1 PMFCL and air-cored transient current simulation

Prior to the fault inception the load current was 525*√2 A. On the fault occurrence, the air-cored fault current rushed to 3018 A. However, the power grid PMFCL reduced the fault current to 1700 A. Thus, the 11 kV PMFCL device has a fault current limitation capability of almost 44%.

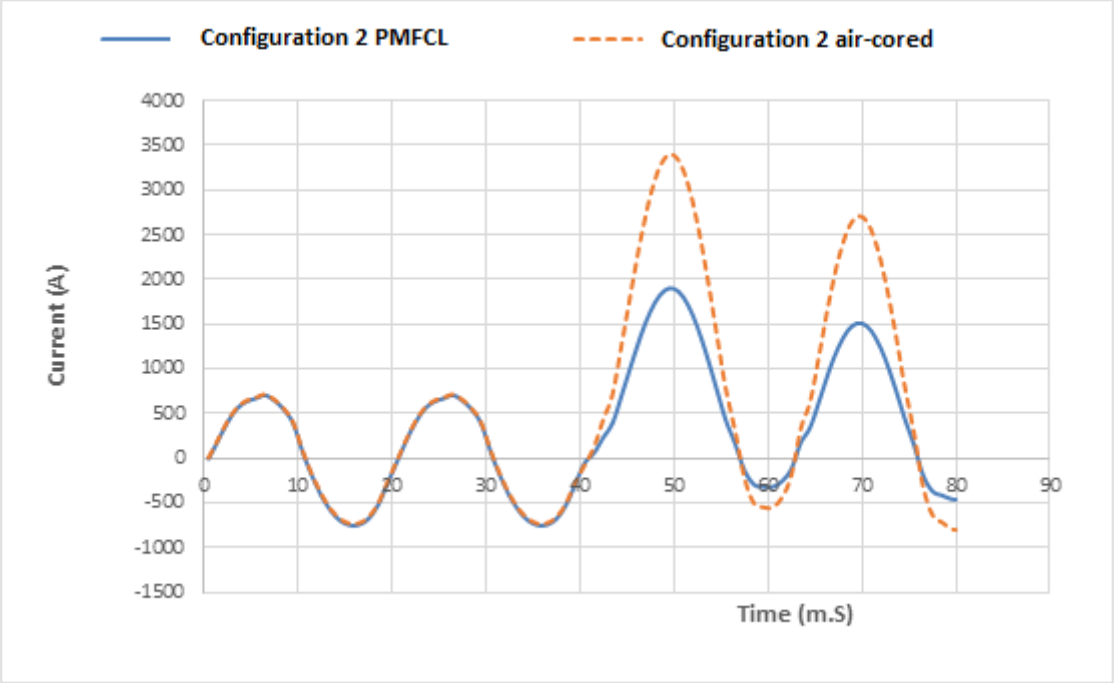

Figure 6-7 Configuration 2 PMFCL and air-cored transient current simulation

Figure 6-7 displays the fault current for configuration 2 air-cored and PMFCL. The air-cored fault current was 3410 A. However, the device reduced the current to 1900 A with fault current limiting capability of 44%. Thus, the two devices have got almost the same fault current reduction capability. Hence, the reduction to the fault has been achieved without using any external source.

The neodymium magnets have been checked for demagnetization at the occurrence of fault current. Figure 6-8 indicates that the demagnetization proximity is below zero, which means that the magnet has enough strength and capability to perform its function without losing its characteristics.

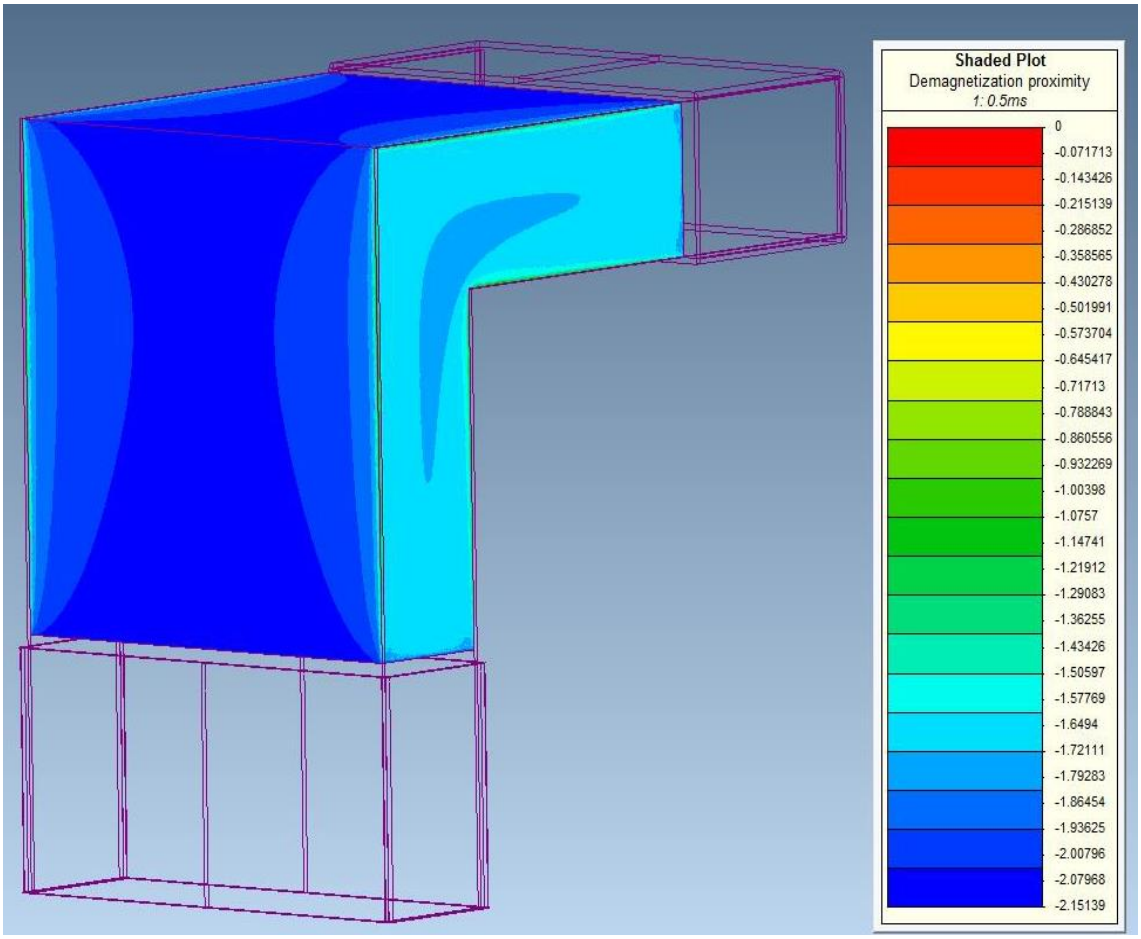

Figure 6-8 Design 1 PMFCL demagnetization proximity during the fault

6.5 Cost of design 1, the power grid PMFCL

The total cost of the PMFCL device incorporates the initial [6.23] - [6.25] and the operational cost. The PMFCL initial cost is evaluated by calculating the cost of the core, magnets and windings materials, as shown in Table 6-2.

The energy cost includes the core (eddy current and hysteresis losses) and the copper losses cost for the device life expectancy. The life expectancy for the device is expected to be at least 40 years in comparison to power transformer, which have properly maintained and reached in service for almost 60 years [6.26]. The eddy current loss is very small due to the core lamination, the hysteresis losses has no effect since the device operates in saturation region and hence the core losses are neglected.

Table 6- 2 Power grid PMFCL initial cost

Material	**Volume (m^3)**	**Total volume (m^3)**	**Specific density (tone/m^3)**	**Total weight (Tone)**	**Price per tones (GBP)**	**Price (GBP)**
PM (NdFeB)	1.7× 0.3×1=0.51	0.51×4 = 2.04	7.6	2.04×7.6=15.5	25000	387600
Electrical steel (M36)	(3^2-2.4^2)×0.008 = 0.026	0.026×2=0.05	7.85	0.052×7.85= 0.4068	1200	488.2
Copper coils	0.95×0.31× 0.45=0.133	0.133 × 4=0.53	8.94	0.53×8.94=4.74	8000	37912.8
PMFCL device total initial cost						426001

The operational cost was calculated over a period of 40 years. The load current is 525 A_{RMS}, the coil winding resistance is 0.04 Ω and the cost of a kilowatt hour (kWh) at present is 14.37 pence [6.27]. The operational cost is calculated as,

$$\frac{Il^2 * 4(R_{AC\,coil})}{1000} * 40 * 8760 * \frac{14.37}{100} = \frac{525^2 * 4(0.04)}{1000} * 75528.72 = £555136$$

The device total cost is £426001.1 + £555136 = £981137

6.6 Design 2, the low voltage PMFCL, topology and operating principle

Figure 6-9 shows a 3D sketch of design 2, toroidal shape PMFCL topology. The model topology consists of two samarium cobalt magnets, mild steel inter-pole, a toroidal steel core (MR36) and 3 pair copper coils mounted around the core. The inter-pole (steel 1010) is positioned between two high energy rare earth rectangular shaped samarium cobalt magnets, type SmCo5, to provides excitation for the M36 grain oriented electrical steel core. A 3 pair, 6 copper coils, 10 turns each, wound around the toroidal core.

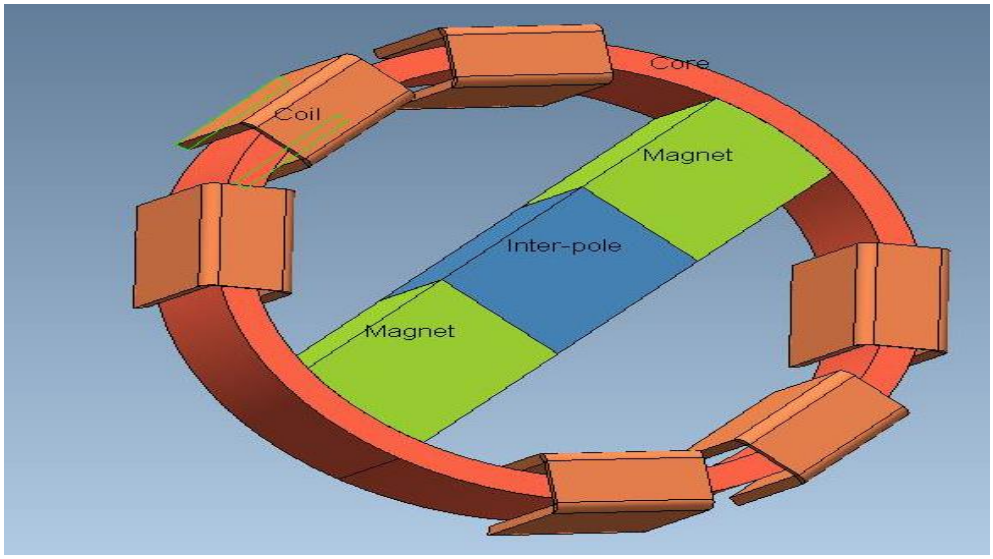

Figure 6-9 Design 2 toroidal shape topology

The toroidal shape electrical steel core has better magnetic properties and performance over other shapes as there is no corners and no air gaps exist. Due to its symmetry, little magnetic flux escapes outside the core. Furthermore, the coil winding resistance is low due to a shorter turn length around the core. The toroidal core topology with large inner diameter and small build up core incorporates low operating losses and cost. In addition, it is more compact, easy to install and lighter [6.28]. The PMFCL principle of operation is the same as previously discussed in chapter five.

The analytical flux density in the core was derived using the following equation: -

$$2H_c l_m - 2\phi_m R_m - \phi_{ms} R_{ms} - \phi_e R_e + 6\,ni = 0 \qquad (6.1\})$$

Where the subscripts (m), (ms) and e stand for the magnet, mild steel inter-pole and the core. The magnets and the AC coils have the same polarity such that in every half cycle of the AC current 3 coils on one side of the core material ring act against the magnets' field. Hence, the flux density in one half of the core can be calculated as

$$2H_c l_m - 2\phi_m R_m - \phi_s R_s - \frac{\phi_e}{2} R_e + 3\,ni = 0 \qquad (6.2)$$

$$2H_c l_m - 2\phi_m R_m = \phi_s R_s + \frac{\phi_e}{2} R_e + 3\,ni \qquad (6.3)$$

The magnetic flux supplied by the magnets in each half ring of the core is the same, (ϕe), (ϕm) and (ϕs) are the same. The core flux density therefore can be calculated from equation 6.4.

$$\phi_e = \frac{H_c\ l_m + 1.5\ ni}{R_m + 0.5\ R_s + 0.25\ R_e} \qquad (6.4)$$

The preliminary design stage was carried out using the analytical approach, which gives an initial prospect regarding the model parameters due to its limitation in solving non-linear

magnetic flux equations. It has been shown previously in chapter four that the analytical approach did not give a precise value of the flux density in the core and hence the model final design specifications are established using the 3D (FEM)

The model main dimensions and specifications are given in Table 6-3.

Table 6- 3 Design 2 specifications

Magnetic material	Magnetic parameters	Topology parameters
samarium cobalt (Sm2Co17)	Intrinsic coercivity, $H_c^- = 7.36 \times 10^5 \frac{A}{m}$ Remanence, B_r = 1.12 T Permeability, $\mu_m = 1.7 \times 10^{-6}\, H/m$	Length (L_m) =0.3 m, cross sectional area (S_m) = 0.3* 0.22= 0.066m^2
Core Electrical steel M36	Relative permeability (μ_r) =57	Inner diameter = 0.9 m, outside diameter = 1 m. Cross sectional area (S_m) = 0.15 m^2
Mild steel (1010) Inter-pole	Relative permeability (μ_r) = 49	Length (L_m) =0.3 m, cross sectional area (S_m) = 0.3* 0.22= 0.066m^2
Magnetic material depth	0.36 m	
Number of coils	6	
Number of turns per coil	10	
Winding resistance per coil	1× 10^{-4} Ω	
Operating single phase Voltage	277 V	
Frequency	50 HZ	
Normal load current	1000A$_{RMS}$	
Peak prospective fault current	11.520 kA	
Air-cored prospective fault current	11 kA	
First cycle peak limited fault current	4240 A	

6.7 The low voltage PMFCL (Design 2) modelling results.

Once the model geometry has been created, the 3D (FEM) simulation is developed by assigning the materials for the magnet, core, inter-pole and the coils. A proper mesh refinement especially for the core and coils were made for the sake of accurate modelling results. The model was checked for the core full saturation extent at zero AC current to ensure the biasing capability of the samarium magnet so that the device can operate correctly and

efficiently in the both steady and transient state conditions. The default magneto static solver is used to show the magneto static flux density core saturation at zero AC current. A current density was distributed uniformly in the conductor region and the calculation of the steady state inductance was established by the non-linear magneto static solver.

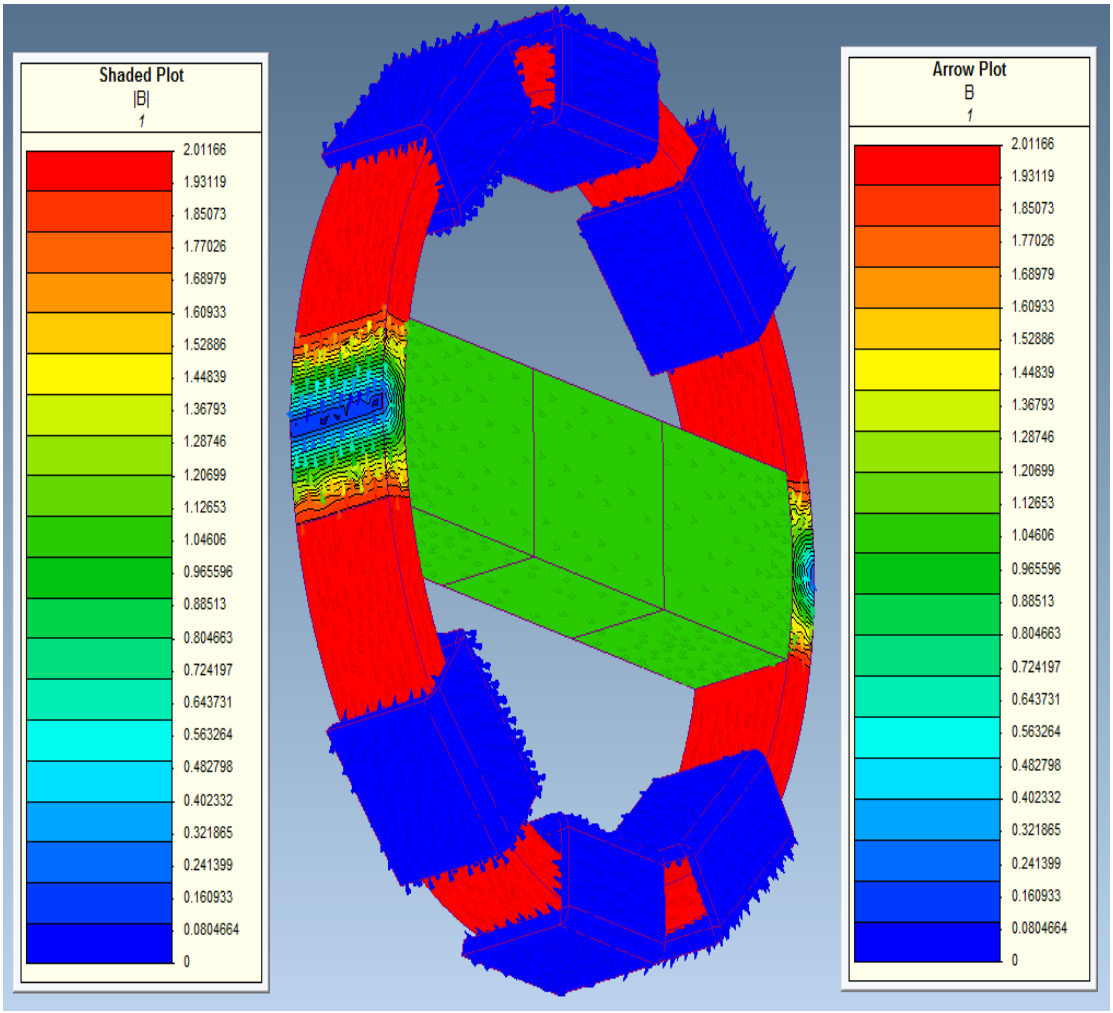

Figure 6-10 Design 2 magneto static flux density distribution at zero AC current

The inductance/ current profile was obtained by the 3D (FEM) magneto static solver using the flux linkage method. The peak value of the inductance gives the expected maximum transient current that the PMFCL is designed for. The inductance/current profile is given in Figure 6-11. The figure indicates that an inductance of 310 µH at a coincide current of 3000A_{rms}. This implies that the device limited fault current is expected to be close to or equal the maximum of the obtained RMS value, which is 4242 A.

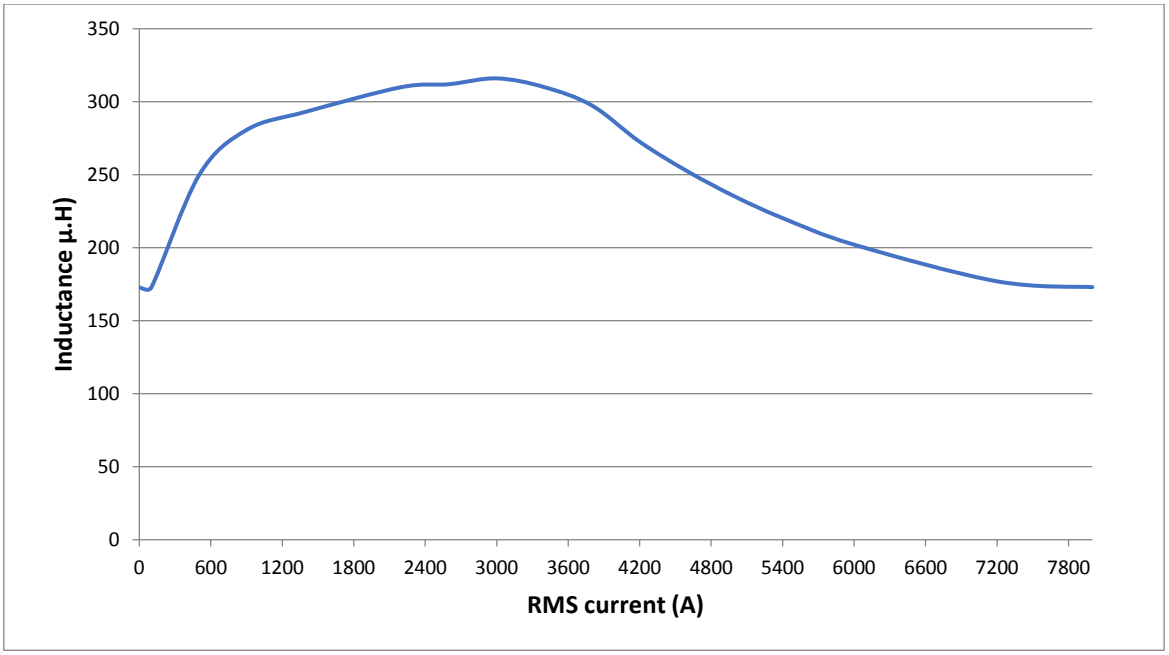

Figure 6-11 Design 2 inductance/current profile

Figure 6-12 shows that at the expected fault current limitation, a half of the core becomes desaturated and it offers an adequate fault impedance to limit the fault current whereas the other half of the core remains in saturation state.

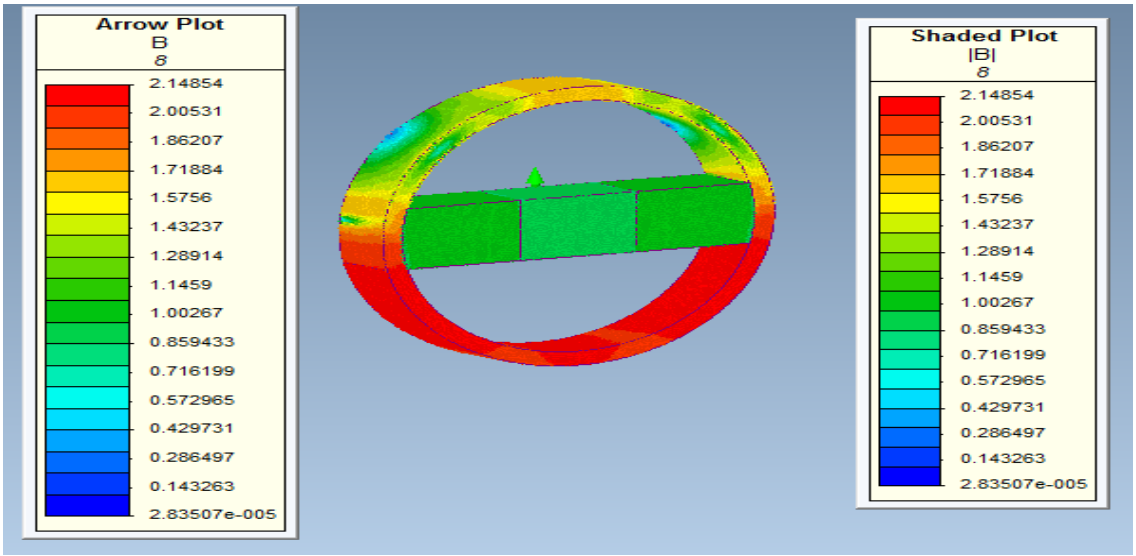

Figure 6-12 FEM magneto static model at fault current of 3000 Arms

The 3D (FEM) transient solver was used to simulate the fault current operation. Based on the results obtained from the 3D magneto static models, the parameters of the 3D (FEM) time-

step solver were obtained for example the maximum current values obtained by the inductance/current approach. The coupled electrical circuit to the transient (FEM) model is shown in Figure 6-13.

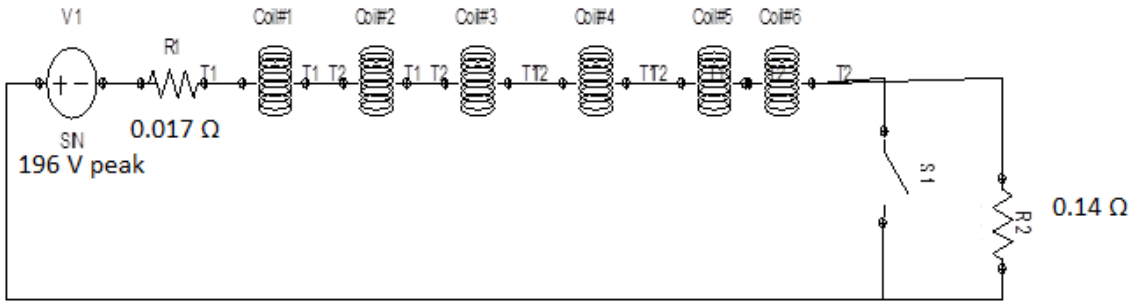

Figure 6-13 Electrical circuit of a half of the design

The circuit contain a single-phase voltage source, an input resistance of 0.017 Ω and a stray resistance of 0.14 Ω. The electrical circuit and the PMFCL (FEM) model are coupled by means of common nodes. The circuit normal load current was calculated to be 1000 A_{rms} up to 2 cycles, at 0.04 seconds the fault is initiated by closing the switch S1. The data for the PMFCL is compared with an air -cored of the same size as the PMFCL device. The transient current waveform in Figure 6-14 indicates that the low voltage PMFCL device limited peak fault current is 4242 A. The figure also illustrates the air-cored transient current of 11 kA; however, the peak fault current without any means of fault current limitation is 11.520 kA. This means the air-cored reactors have no considerable effect on the fault current limitation due to the low inductance value of the model toroidal geometry.

The PMFCL transient results validate the results obtained by the inductance/current profiles since the RMS value of the peak fault current gives the current values obtained by the Magneto static solver inductance/current profiles approach. In comparison between the device fault current limitation and the air-cored, the low voltage (Design 2) has a fault current limiting capability of almost 61 %.

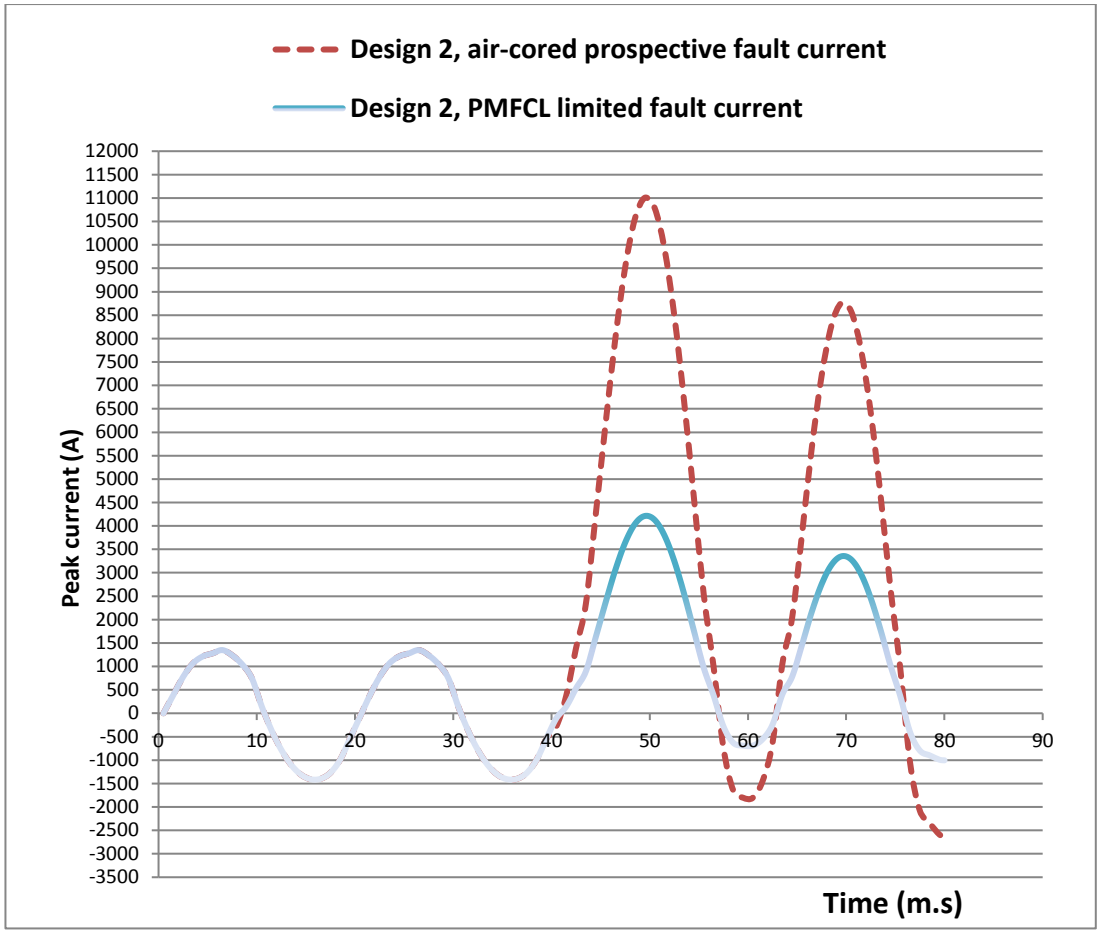

Figure 6-14 Design 2 transient results

6.8 Proximity to demagnetisation of samarium cobalt magnets

A post-processing solver was used to investigate the likelihood of demagnetisation of the samarium cobalt magnets. In this approach the knee of the samarium cobalt was defined to be 0T. (In fact, the knee for the real material lies just below this value in the third quadrant of the BH curve.) Figure 6.15 shows the demagnetisation state of the samarium cobalt magnet for a peak coil current of 4242A. A value below zero indicates no risk of demagnetisation in the magnet. The magnitude of the negative values in the figure indicates the degree of proximity away from the specified zero point of the knee of the BH curve.

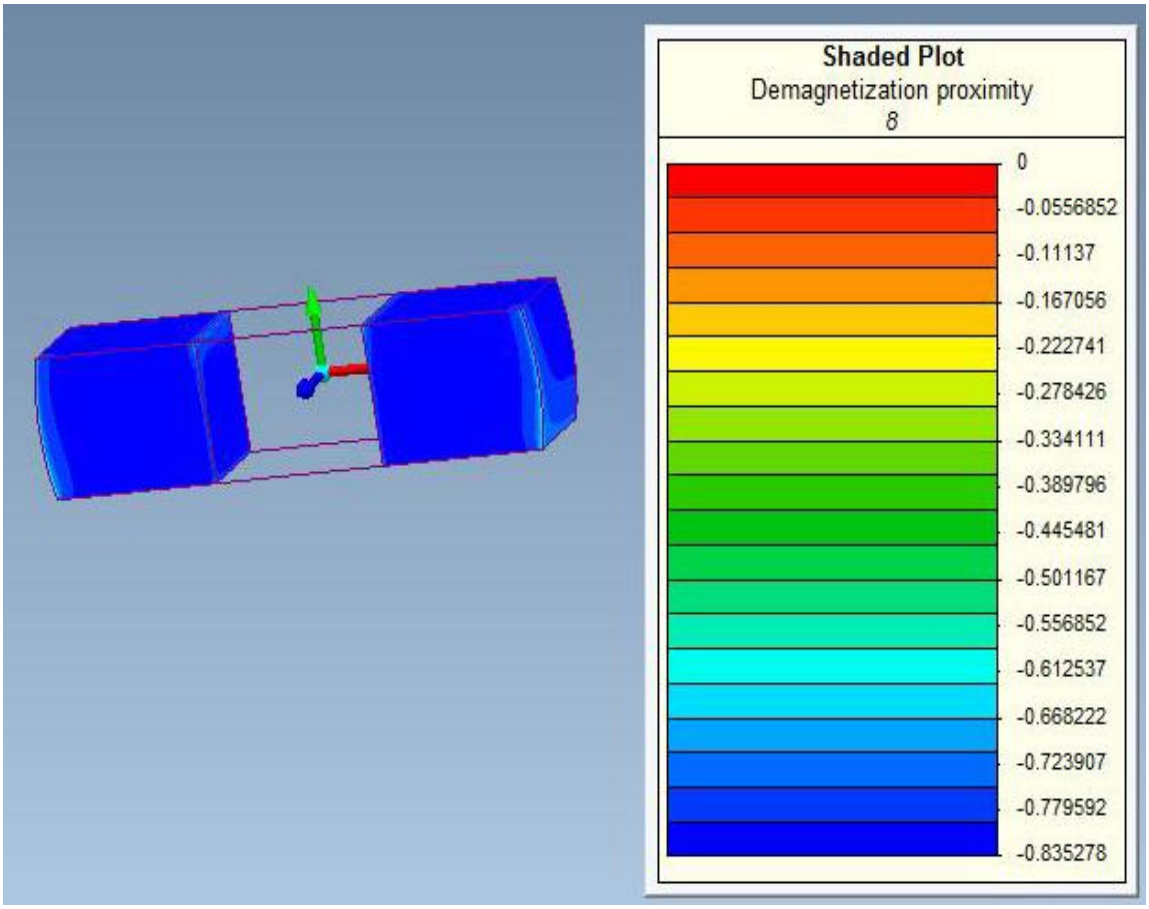

Figure 6-15 Design 2 demagnetization proximity at the peak fault current of 2545 A

6.9 Design 2, total cost evaluation

As previously discussed in section 6.5, the device total cost incorporates the total initial and operational cost. The initial cost [6.23]- [6.25] is the cost of the materials, as shown in Table 6.4.

The load current is 1000 A, the coil winding resistance is $1 \times 10^{-4}\ \Omega$, the number of coils =6, and the cost of a kilowatt hour (kwh) at present is 14.37 pence [6.27].

The operational cost is calculated as,

$[(1000)^2 \times 1 \times 10^{-4} \times 6 \times 40 \times 8760 \times 14.37]/10^5$ = £30211

Table 6- 4 Design 2, PMFCL initial cost

Material	Volume (m^3)	Total volume (m^3)	Specific density (tone/m^3)	Total weight (Tone)	Price per tones (GBP)	Price (GBP)
Sm2Co5	0.066 × 0.36= 0.02376	0.0238 × 2=0.04752	8.2	0.39032	15000	5854.8
Mild steel (1010)	0.066 × 0.36=0.02376	0.0238	7.85	0.18683	544	101.64
Electrical steel (M36)	0.15 × 0.36 =0.054	0.054	7.85	0.4239	1200	508.68
Copper coils	0.22 × 0.09 × 0.38 =0.007524	0.00524 × 6 =0.045	8.94	0.4	8000	3228.7
Design 2, PMFCL device total initial cost						9693.82

The total cost of design 2= £9693.82 +£30211 = £39904

6.10 Positioning of PMFCL in the power grid.

An important aspect that has a great effect on the capability of the PMFCL is the positioning of the device in the power grid. The fault current limiter device (FCL) in Figure 6-16 shows that the device can be installed at different locations of the power system network depending on its specifications. Thus, it has different effects on a faulted system.

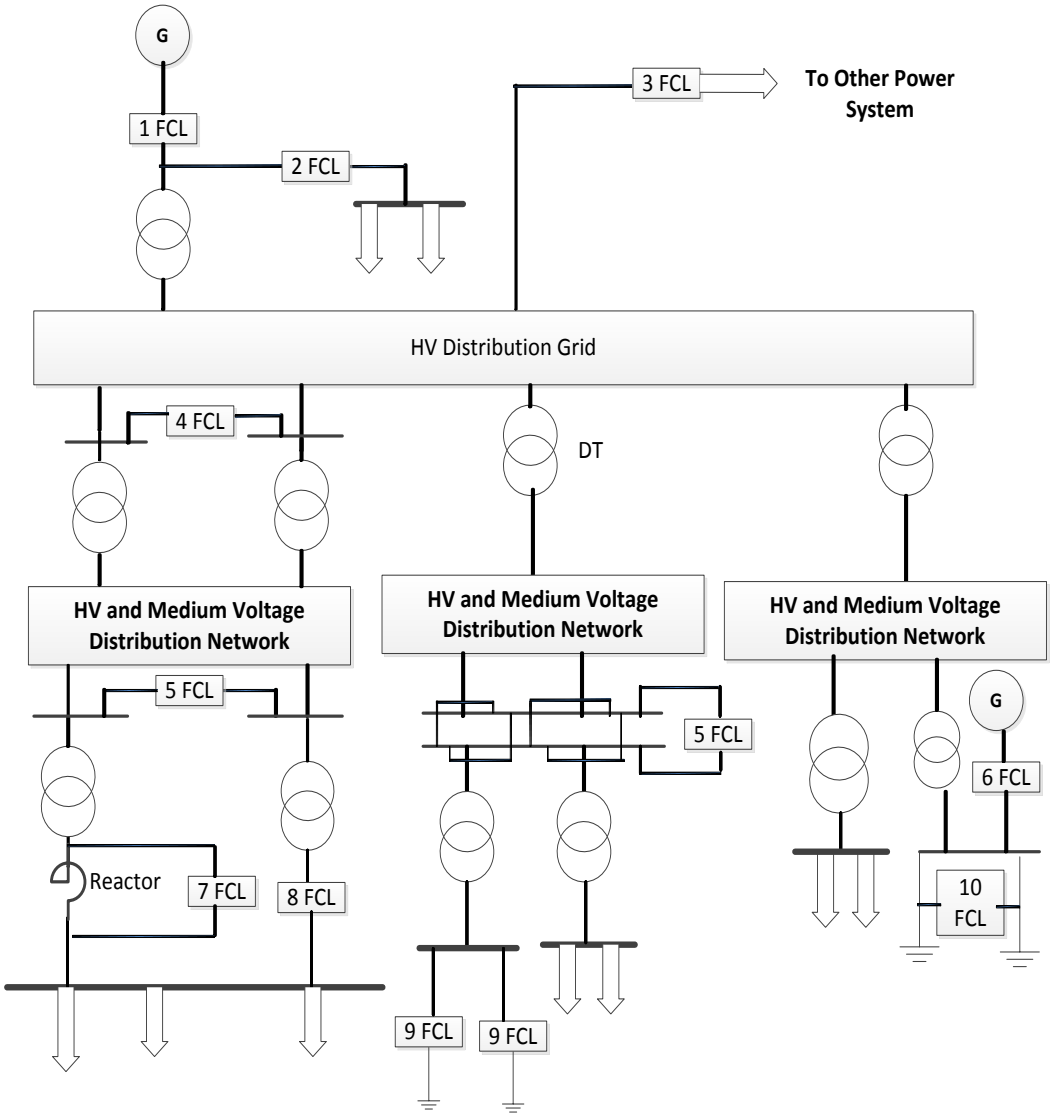

Figure 6-16 Positioning of FCLs

The FCL can be positioned at the power generation side (location 1) to reduce the maximum short-circuit current of the network. In location 2, it can protect the high voltage station transformer from the high short circuit current. The FCL is also, protects the equipment at the substation building, its main function is to prevent the short-circuit contribution of the substation auxiliary components. In location 3, the device is needed for connection with other power system via high voltage transmission lines. The FCL can be placed between power distribution networks to reduce the fault current from one electrical power distribution to the other, as indicated in location 4. The device can be used for the high or medium voltage bus bar coupling to enhance the reliability of the power system, as in location 5. In addition, the FCL is required for distribution generators, as in location 6, where the wind or gas turbine-

generator is protected by the device from the excessive fault current. The FCL is connected as a bypass switch across the series current limiting reactor, as in location 7, to minimise losses and voltage drop during normal steady state operation. Furthermore, the FCL can be installed in the transformer incoming feeder (location8) or outgoing feeder (location 9). It can also be used for low voltage bulbar coupling (location 10) [6.8], 6.9]. However, the design 1, PMFCL device is designed to be used with the indoor or outdoor 11 kV power grid whereas design 2 is proposed for renewable energy transformer protection.

6.11 Operation of power system with PMFCL device.

The PMFCLs must be integrated into the protection system design to ensure correct protection of the switchgear and to avoid any undesirable tripping. In existing power system, the PMFCL replaces the series reactor, though, it can be installed as a bypass switch to provide shunt path across the conventional existing reactor. The new system installation takes the presence of the device from the initial design stage to be a part of the protection system infrastructure. Protective relays in power systems are essential even if the PMFCL is present in operation. A power system will be generally not energized without a proper protection design and proper relays settings matched to the system configuration. The requirements of the protection system are reliability, stability, sensitivity, selectivity and timely. However, the PMFCL should not affect the protective relays operation. [6.8]- [6.17]. The both designs of the 11 kV PMFCL for the power grid, which specified in Table 6.1 can be installed in the power system network to mitigate the ground fault current provided that the system maximum short circuit current at the location does not exceed the device rating according to 3D FEM magneto static inductance-current profiles (6.5 kA_{RMS} and 7.5 kA_{RMS}) and time-step solvers (9.06 kA and 10.5 kA peak). The device can be installed at the low voltage side of the step-up transformer such as 11/66 kV, 11/220 kV…etc. However, it can be installed at the high voltage side to protect the step-down transformers, for example,
11 / 0.4 kV. Conversely, the low voltage device is proposed to be occupied with the existing wind turbine-generator transformer. The installation of the PMFCL device in the power system should reduce the power outages, work in harmony with the existing protective relays and improve the power system reliability. However, there are some issues that need to be addressed in advance.

The transformer magnetising inrush current might trigger the PMFCL in normal steady state operation. The device should not affect the system normal operation and should only operate to mitigate the actual fault current.

The device should not affect the protective relays discrimination and co-ordination.

A proper operation of the protective relays should be insured. The operation of the PMFCL device might affect the overcurrent relay; the relays might fail to detect the fault current due to the fault current reduction once the PMFCL device has operated.

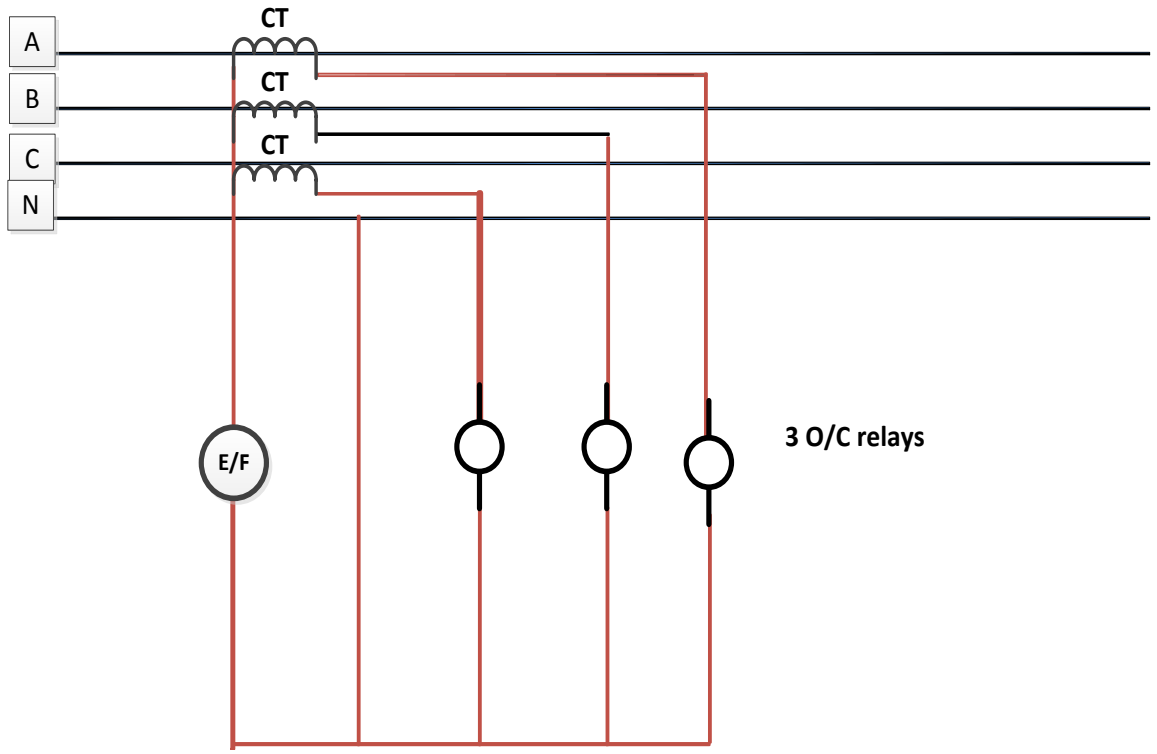

Figure 6-17 Overcurrent (O/C) and earth fault (E/F) relays protection

The distance relay is the main protection for the transmission lines, however, its operation should not be affected by the PMFCL device. The distance relay should properly trip the breaker for faults within 80% of the length of the transmission line.

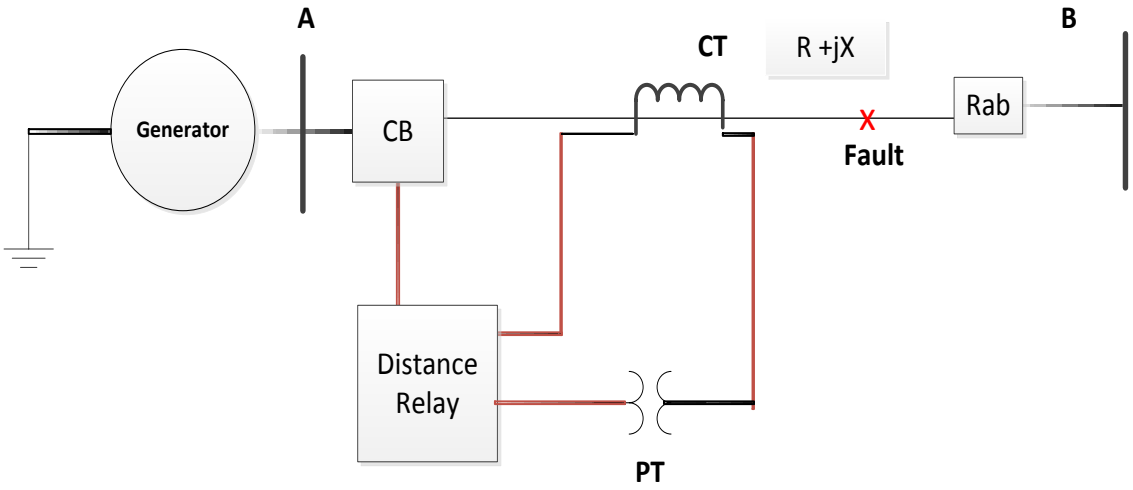

Figure 6-18 Distance relay protection

The distance relay in Figure 6-18 protects the line between the substation A and B. The relay receives information regarding the line via the current transformer (CT) and the voltage transformer (VT). The relay operates if the line impedance falls below the relay impedance value. However, the PMFCL will add additional impedance to the transmission line, which affects the distance relay operation in comparing between its impedance with the line's.

The operation of generator or transformer differential relay should not operate on external fault. The differential relay should operate for a fault inside the transformer, generator or on the bus bar. Besides that, the differential relay operates to provide backup protection if other protective relays fail to operate.

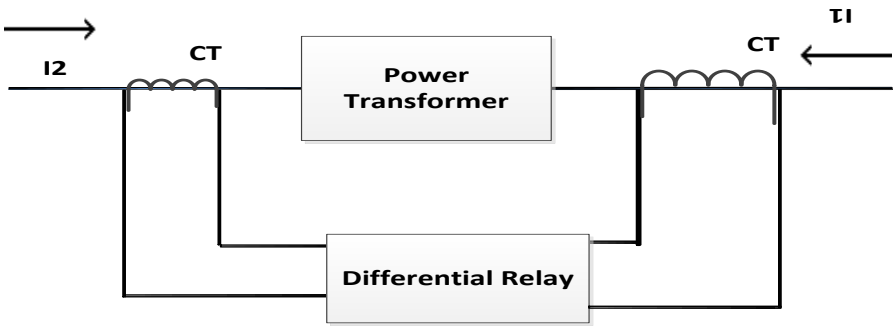

Figure 6-19 Power transformer differential Protection

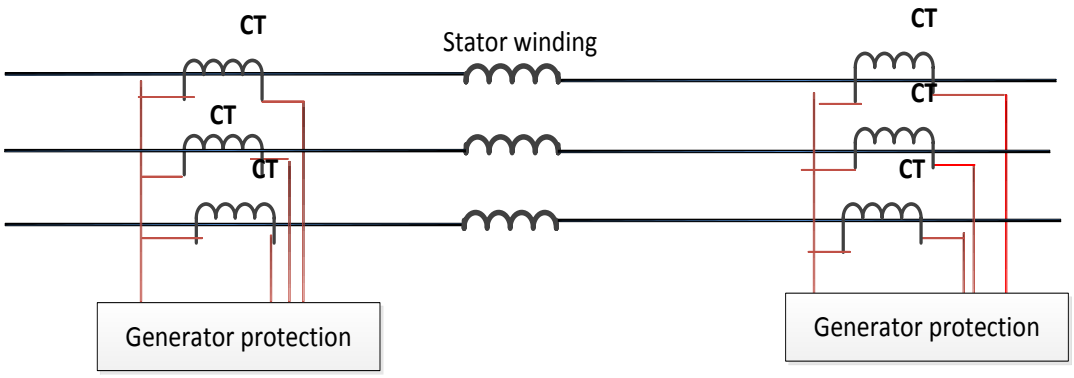

Figure 6-20 Generator differential

Hence, the protective relays settings are required to be re-settled prior to installing the PMFCL device.

Another issue that need to be studied is the saturation of the existing current transformer (CT) due to the PMFCL asymmetrical fault current. The size of the core is directly proportional to the maximum expected peak of the fault current. At the instant of fault, the unbalanced fault current lowers the range of the flux density in the core due to the presence of the PMFCL device. This is beneficial for the new system to account for CTs with small-sized cores. Though, it is a problem to the existing system as the existing current transformers will saturate during fault current limitation. When the core of the CT gets saturated, its inductance drops dramatically. Consequently, the secondary circuit coupled by the saturated core is highly distorted. The harmonic content in the CT secondary current affects the protective relays operation. The distorted information supplied by the CT affects the relays operation in distinguishing between the normal and abnormal condition and can cause trip delay to the overcurrent relay. If the signal supplied by the CT during a fault is distorted by saturation, the RMS values calculated by the protection device will be lower than the RMS values of the actual fault current This can cause protection device trip delay. When designing a CT for the PMFCL's installation. It is essential to ensure that it will not get saturated by the large asymmetrical faults [6.15], [6.16]. The replacement of the existing current transformers with new designed CTs may involve lack of system reliability during long period of shutdowns.

Another concern with the PMFCL device installation in the power grid is the effect of lightning overvoltage on the device performance, which must be taken into consideration. The device

should be subjected to high impulse voltage test in the laboratory to ensure its capability to withstand high voltage insulation breakdown before being installed in the power grid.

6.12 PMFCL with circuit breakers

When the circuit breaker operates to clear the fault, the voltage that appears between the fixed and moving contacts of the circuit breaker after arc extinction during opening process is the transient recovery voltage (TRV). The peak of the TRV divided by the total time of the voltage oscillation is the rate of rise of recovery voltage (RRRV). The both the level of TRV and RRRV are key factors in determining whether the fault can be cleared successfully. For successful fault interruption, the breakdown voltage of the interrupting medium between the circuit breaker contacts must always exceed the recovery voltage. If the maximum value is above the breaker rating, the increasing TRV to the gap between breaker contacts will restrike the arc and breakdown the interrupting medium. In other circumstances, even when the TRV peak is within the breaker rating, current rising could occur because the interrupting medium is not yet a good insulator and it may still have a relatively high conductance. If TRV has a high rate of rise (RRRV) in those first few microseconds, it may re-establish a current flow enough to heat the arc column and restore conduction. However, the installing of PMFCL mitigates the fault current to a permissible value by instantaneously inserting an additional inductance. The best position of the PMFCL device is between the circuit breaker and the load (downstream). This can make the source-side voltage of PMFCL be low and can also ensure security of PMFCL device. The stored energy in the fault inductance increases the RRRV and hence increases the stresses on the circuit breaker. Therefore, the device should be provided with a parallel surge arrester between the line and ground to discharge the stored energy during fault interruption and consequently reduce the effect of RRRV on the circuit breaker. In normal operation the surge capacitor acts as an insulator and has no effect on the system operation. However, on the fault inception the RRRV closes the arrester for very short time expressed in a few microseconds to discharge the stored energy to ground [6.18]- [6.22].

Regarding the system voltage drop during a fault, the fault current greatly increases the voltage drop. The slump in system voltage during fault is a major concern to the power system operation. Voltage dip or voltage sag due to a fault on 11 kV power distribution transformer can affect the power system equipment such as the generator unit out of step and is the most crucial power quality concern. The voltage dip can operate the generator under voltage relay

(relay device number 27), which sends a signal to the related generator breaker to trip. However, the voltage sag can operate the reverse power relay (relay device number 32) which shuts down the turbine unit completely [6.29]. The installation of PMFCLs however, limits the short duration severe fault current to a value comparable to the normal steady state current and as a result reduces the voltage sags and improves the power quality and stability.

6.13 Conclusion

The PMFCL for the power grid distribution voltage level has been designed with M36 electrical steel core and neodymium permanent magnets. The squared-shape topology PMFCL model has been simulated into two designs with the same model specifications detailed in Table 6-1, configuration 1 and 2 (previously discussed in last chapter), to protect a 10 MVA, 11 kV substation transformer.

In addition, the low total cost and efficient PMFCL device proposed for the renewable energy generator-step up transformer has been designed using samarium cobalt magnets and M36 electrical steel. The device can be used with the existing wind, solar power transformer or for the future wind-photovoltaic (wind-PV) generator-step up transformer 480 V / 11 kV.

The current-inductance profiles for both design PMFCL model were obtained to predict the behaviour of the device in the faulted condition. The calculated RMS current using the time effective (FEM) magneto static inductance-current profile method agreed with the peak transient currents obtained by the time step solver. The PMFCL showed exceptionally low insertion impedance in normal steady state operation and a high fault impedance to significantly improve the fault current limiting capability in abnormal condition. The passive, dry type PMFCL limits the fault current in its first peak cycle and requires minimum maintenance. The current limitation capability for design 1 and 2 have been calculated in comparison with the air-cored current limiting reactor of similar specifications as the PMFCL devices and a useful reduction in the fault current has been achieved. Design 1 (configuration 1 and 2) has a fault current limiting capability of 44% whereas design 2 shows a significant reduction to the fault current with a limiting capability of 61%.

Both the power grid PMFCL (design 1) and the low voltage (design 2) show no risk of demagnetization and can withstand the dangerous fault current. The low voltage PMFCL (design 2) has better performance as the amount of magnetic flux escaping outside the core is very low.

The location of PMFCL is very important for effective fault current reduction and for successful operation of the PMFCL device. Design 1 can be installed at different positions in the power system network depending on its power rating whereas Design 2 PMFCL device should be located close to the renewable energy generator- step up transformer because of the voltage level. The PMFCLs for design 1 and 2 must be integrated into the protection system design to ensure correct protection of the switchgear and to avoid any undesirable tripping of the circuit breakers. The installation of the PMFCL reduces the voltage sag, increases the service life of the equipment and improves the power quality and system stability.

The two-design initial and energy cost have been evaluated. The full scale PMFCL for the power grid (design 1) is much more expensive whereas design 2 is cost-effective.

References

[6.1] Liang Zou, et al. (2009). Study on the feasibility of developing high voltage and large capacity permanent-magnet-biased fault current limiter. Universities Power Engineering Conference (UPEC), 2009 Proceedings of the 44th International, 1-5.

[6.2] Magnet user manual by Infolytica, www.infolytica.com.

[6.3] Wilson, P. R. (2015). Modelling the Non-Linear Behaviour of a Magnetic Fault Current Limiter. *Advanced Electromagnetics*, *4*(3), 1-7.

[6.4] D. Cvoric, S. W. H. de Haan and J. A. Ferreira (2009). Guidelines for 2D/3D FE transient modelling of inductive saturable-core Fault Current Limiters. *2009 international conference on electric power and energy conversion systems, (EPECS),* 1-6.

[6.5] Ali, Amer Mejbel. "Different Techniques for Calculating Apparent and Incremental Inductances using Finite Element Method." *Iraqi Journal for Electrical & Electronic Engineering* 11.2 (2015).

[6.6] [N. R. Nair and M. Ebenezer (2014). Operation and control of grid connected wind — PV hybrid system. *2014 international conference on advances in green energy (ICAGE),* 197-203.

[6.7] H. Wang, et al. (2012). Modelling and Equivalence of Integrated Power Generation System of Wind, Photovoltaic and Energy Storage. *2012 Asia-pacific power and energy engineering conference,* 1-7.

[6.8] H. Schmitt (2006). Fault current limiters report on the activities of CIGRE WG A3.16. In: *2006 IEEE power engineering society general meeting,* 5 pp.

[6.9] J. Cao, et al. (2017). A new type of fault current limiter. *2017 IEEE 2nd advanced information technology*, *electronic and automation control conference (IAEAC)*, 2300-2304.

[6.10] A. Escobar, et al. (2011). A methodology to coordinate solid-state fault current limiters with conventional protective devices. *2011 IEEE/PES power systems conference and exposition,* 1-6.

[6.11] I. K. You, et al. (2010). Study on Protection Coordination Between Protective Devices in a Power Distribution System With an SFCL. *IEEE transactions on applied superconductivity,* 20 (3), 1168-1171.

[6.12] T. Hazel, B. Leforgeais and E. Savary (2015). Operation of power systems incorporating fault current limiting devices. *2015 petroleum and chemical industry conference Europe (PCIC Europe),* 1-8.

[6.13] S. M. Blair, et al. (2009). Operational control and protection implications of fault current limitation in distribution networks. *2009 44th international universities power engineering conference (UPEC),* 1-5.

[6.14] B. Li, et al. (2014). Overcurrent Protection Coordination in a Power Distribution Network with the Active Superconductive Fault Current Limiter. *IEEE transactions on applied superconductivity,* 24 (5), 1-4.

[6.15] L. A. Kojovic (2002). Impact of current transformer saturation on overcurrent protection operation. *IEEE power engineering society summer meeting,* 1078-1083 vol.3.

[6.16] S. Orpe and N. K. C. Nair (2009). State of art of fault current limiters and their impact on overcurrent protection. *2009 IEEE power & energy society general meeting,* 1-5.

[6.17] A. Wright and C. Christopoulos. Electrical power system protection. Chapman and Hall, London; New York, 1st Ed., 1993.

[6.18] M. Szewczyk and S. Kulas (2007). Investigation on circuit breaker influence on transient recovery voltage. In: *2007 42nd international universities power engineering conference*, 1036-1043.

[6.19] W. Li, S. Dan and Y. Li (2010). Impact of Position of Fault Current Limiter on the Interrupting of Circuit Breaker. *2010 Asia-pacific power and energy engineering conference*, 1-4.

[6.20] H. J. Bahirat, et al. (2016). Impact on superconducting fault current limiters on circuit breaker capability. *2016 national power systems conference (NPSC)*, 1-6.

[6.21] M. R. Haghifam, A. Ghaderi and M. Abapour (2009). Enhancement circuit breaker reliability by using fault current limiter. *2009 IEEE power & energy society general meeting,* 1-5.

[6.22] W. V. S. Azevêdo, et al. (2010). Device to limit Transient Recovery Voltage. 2010 IEEE/PES transmission and distribution conference and exposition: Latin america (T&D-LA), 1-6.

[6.23] https://www.worldsteel.org/media/press-releases/2017/worldsteel

[6.24] https://www.alibaba.com/countrysearch/CN/copper-price-per-kg.html

[6.25] www.magnetsales.co.uk

[6.26] A. Jahromi, et al. (2009). An approach to power transformer asset management using health index. IEEE electrical insulation magazine, 25 (2), 20-34.

[6.27] https://www.ukpower.co.uk/home_energy/tariffs-per-unit-kwh

[6.28] W. Grimmond, A. J. Moses and P. C. Y. Ling (1989). Geometrical factors affecting magnetic properties of wound toroidal cores. *IEEE transactions on magnetics,* 25 (3), 2686-2693.

[6.29] http://apps.geindustrial.com/publibrary/checkout/GET-6497A?TNR=White

Chapter 7: -Conclusion and future work

7.1 Conclusion

The thesis started with background information on the soft and hard magnetic materials. Electrical steel M36 has been selected as an appropriate magnetic core material for the design approach. Neodymium Iron Boron (NdFeB) and samarium cobalt (SmCo5) are used as a permanent magnet; however, samarium cobalt magnet maintains a position as a material of choice for high coercivity applications at temperatures beyond which Ndf_eB is no longer feasible. The PM is the main source of excitation to keep the non-oriented silicon steel iron core in magnetic saturation state. During the normal operation of the device the saturated core offers low impedance to the grid and during the fault state the core inherently rushed to high impedance state that limits the high short circuit current.

A commercial Finite Element software (FEM) MagNet was used in the device modelling techniques from the commencement till the end of the final design.

An overview of the previous related work was researched and the gap in the field of study was identified. The main concern was on how to implement the PMFCL device for the power system. A recently reported PMFCL model in 2D (FEM) was verified and investigated. The preliminary design of the device was obtained by the analytical approach to estimate the length of the magnets and the core dimensions. A new design method, the inductance-current profile approach using the 3D (FEM) magneto static solver has been used to evaluate the device fault current limitation in abnormal condition. The proposed time-saving inductance-current profile method is a useful approach in determining the device operating range. The outcome from the (FEM) analysis proved that the published results were inconsistent. A critical analysis of the published results was carried out to establish the reasons for inconsistency. The existing 2-D and 3-D transient performance analysis prove that the model was unrealistic. One essential factor which had led to incorrect published results was the sweep distance, which should be considered not only in 3-D but also in 2-D voltage driven circuit modelling. Another important issue that must have led to the error in the previous published results is the permanent magnet and the limiter coils magnetic flux direction, which must be set properly. In verification of the 2D (FEM) with 3D (FEM), the 3D(FEM) magneto static solver indicates that this model can only work below the rated

capacity that it was initially designed for. The PMFCL 3D (FEM) transient solver is impossible to be performed as the model did not match the 10-kV system voltage operation. However, the investigated results provided knowledge and guidelines towards the enhancement of PMFCL design.

A 90 V prototype PMFCL has been constructed, built and tested at the Electrical laboratory of Sheffield Hallam University. The experimental work was combined with the simulation results to verify the analysis. The operational principle of the PMFCL has been verified. The experimental results validate the 3D (FEM) simulation results and hence the validity of the (FEM) approach in designing and analysing the performance of the PMFCL is demonstrated. Two designs configurations 3D(FEM) squared-shape topology for the same PMFCL porotype were simulated and tested. The measured and calculated results for the two configurations PMFCL design (configuration 1 and 2), show good steady state performance and as well as good current limiting capabilities.

The influence of coil length on the performance of the PMFCL was verified. The calculated results for the candidate prototype with 99 mm coil length were taken as a reference and compared with the simulated results obtained using 3D (FEM) at 39 mm and 69 mm, with fixed number of turns. The key findings from the steady and transient results indicate that the 99 mm coil is the more efficient device as it offers a low inductance in the normal and faulted state operation. Hence, the coil length along the core is an important parameter that should be considered in the design of the PMFCL device. The Prototype PMFCL provided a “learning experience” and built confidence in new technology design. Following the prototype experimental and modelling results were the design of medium and low voltage PMFCL.

The 11 kV PMFCL model (design 1), aimed to protect the power distribution transformer, was designed to match the square-shaped topology of the 90 V prototype.

The low voltage toroidal PMFCL (design 2) was proposed for the existing renewable energy step up transformer 480 V/11 kV.

The dry type PMFCL current-inductance profiles were obtained by 3D (FEM) magneto static solver to predict the behaviour of the devices in the abnormal condition. The calculated RMS current using the time saving inductance-current approach agreed with the peak transient currents obtained by the 3D (FEM) time-step solver. The current limitation capability has been calculated in comparison with the air-cored of similar specifications as the PMFCL device and a useful reduction in the fault current has been achieved. The simulation results proved that

the proposed PMFCL topologies (toroidal and square-shaped) can protect the renewable energy generator-transformer and real power grids from the fault current.

The toroidal PMFCL design topology fault current limitation was compared with the squared shape model. Although the both the devices limit the fault current in its first peak cycle, the toroidal device showed a significant fault current limitation due to negligible leakage flux outside its core. The fault current reduction by 61% using the toroidal core of design 2 is a magnificent achievement in the technology of the PMFCL in comparison to the devices reported in the literature.

Even though the SmCo5 and NdFeB magnets for the both the designs provide adequate magneto static core saturation and are extremely resistant to demagnetization by the magnetic field due to the fault current, the toroidal design is more efficient, compact and cost effective. Hence, design 2 is much preferable than design 1, it proposed to protect the renewable energy step-up transformer nevertheless it can protect the existing power distribution transformer when it is installed at its primary side.

The installation of the PMFCL in power systems is also addressed at the end of this thesis, where the following issues are considered: the positioning of PMFCL in power systems, the interaction between PMFCL and existing protective schemes, the interaction between PMFCL and circuit breakers (CBs) and the influence of the device on power quality and system stability. Since the PMFCL changes the system short-circuit impedance, the influence of the device on the protective relays is taken into consideration in this thesis.

The advantageous (fit and forget) device requires minimum maintenance, has benefits of a completely passive and autonomous system. The device requires no external power, back-up or control, and recovers automatically and instantaneously when the fault is cleared. The merit of the device is that it will reduce downtime during power system outages by mitigating the severe fault current in the first half cycle.

The installation of the PMFCL device will avoid a major revamp of the power system network. It will protect and extend the service life of the under rated grid equipment such as the circuit breakers and power transformers. During fault current limitation, The PMFCL is expected to reduce the stress imposed on CBs during opening action. However, the installation of device could increase the rate of rise of recovery voltage (RRRV) across CBs and cause their failure. Hence a surge capacitor is used in parallel connection with the PMFCL device to reduce the effect of RRRV.

7.2 Future Work

1- Permanent magnet materials performance and demagnetization due to high fault current and at a wide range of temperature should be investigated to build a magnetic properties database that could be of great benefit to the researchers of PMFCL.

2- A design improvement to FEM model to reduce the initial and operational cost for power grid square shaped topology PMFCL device is valuable. This could be achieved by using the cost-effective toroidal topology design in three- phase system.

3 - To install the PMFCL in housing enclosure for 11 kV substations indoor or outdoor use.

5- To wire up the PMFCL with circuit breaker power and control circuit and other protective devices.

6- To commission the device with distribution transformer, protective relays and CBs and check its correct operation.

Appendix

Appendix A

Some pictures of the experimental work

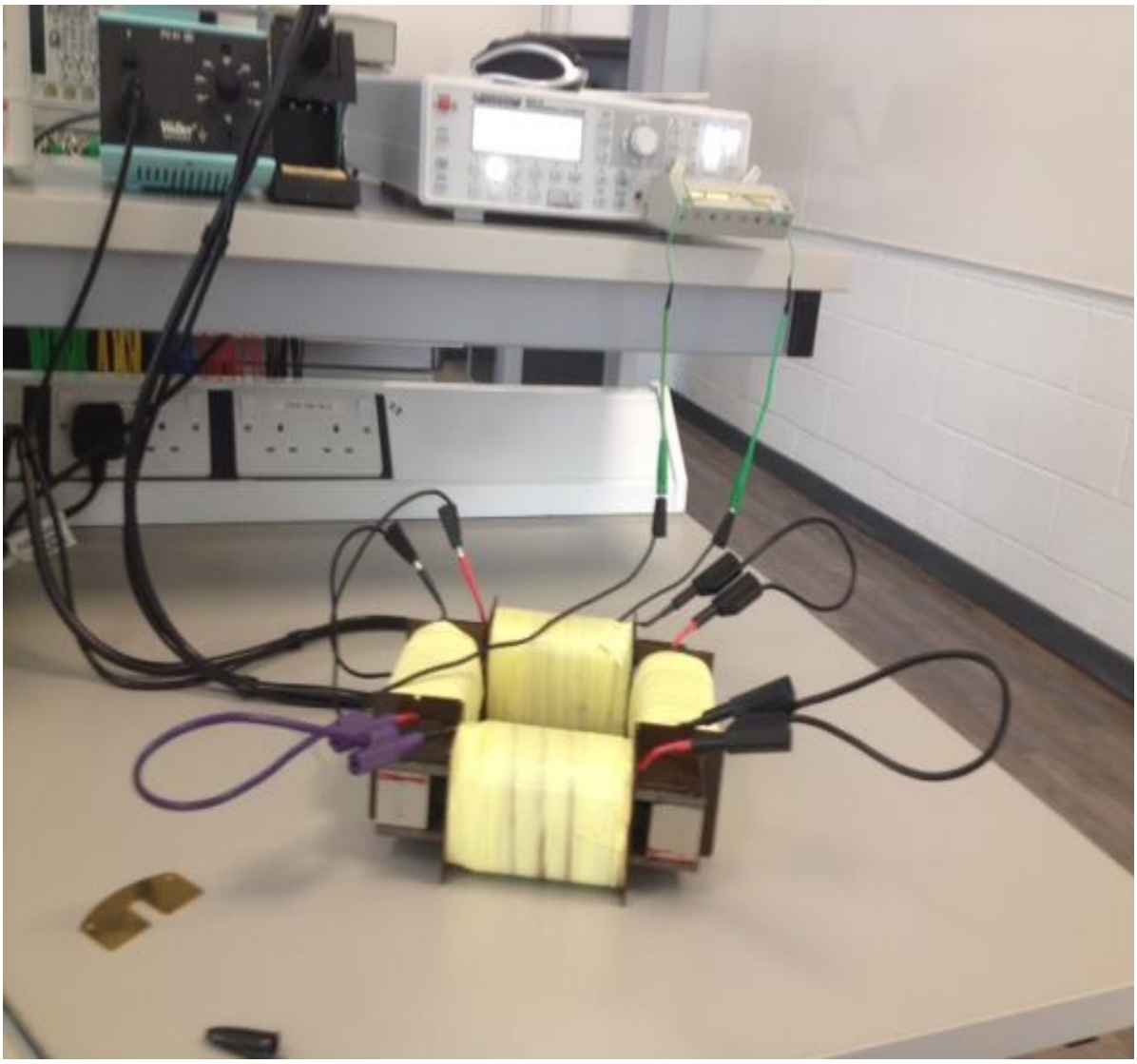

The device off power load measurements

The measurements as discussed in the thesis were taken prior to energizing the device.

The value of air-cored inductance and resistance

The data regarding the transient current test was captured by the oscilloscope.

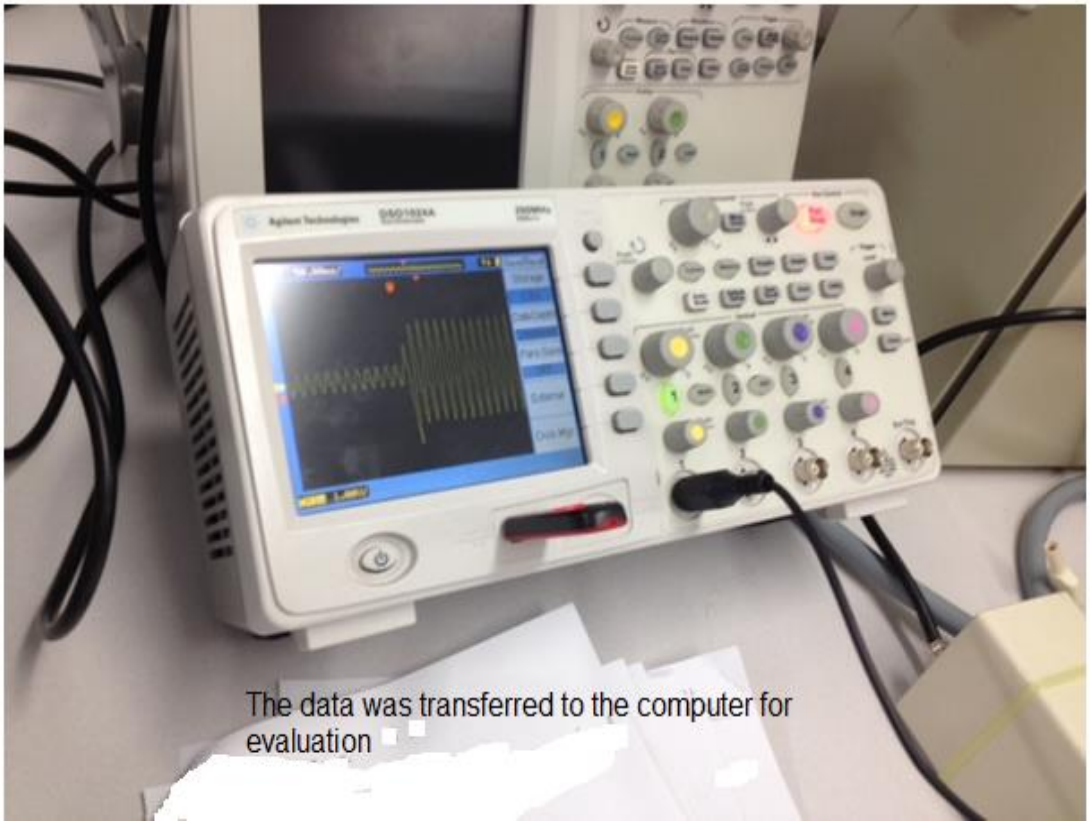

The current waveform before and after the fault

Appendix B

ANSI/IEEE Standard Device Numbers

Device Numbers (the more commonly used ones are in bold)

1 - Master Element

2 - Time Delay Starting or Closing Relay

3 - Checking or Interlocking Relay

4 - Master Contactor

5 - Stopping Device

6 - Starting Circuit Breaker

7 – Rate of Change Relay

8 - Control Power Disconnecting Device

9 - Reversing Device

10 - Unit Sequence Switch

11 – Multifunction Device

12 - Overspeed Device

13 - Synchronous-speed Device

14 - Underspeed Device

15 - Speed or Frequency-Matching Device

16 – Data Communications Device

20 - Elect. operated valve (solenoid valve)

21 - Distance Relay

23 - Temperature Control Device

24 – Volts per Hertz Relay

25 - Synchronizing or Synchronism-Check

Device

26 - Apparatus Thermal Device

27 - Undervoltage Relay

30 - Annunciator Relay

32 - Directional Power Relay

36 - Polarity or Polarizing Voltage Devices

37 - Undercurrent or Underpower Relay

38 - Bearing Protective Device

39 - Mechanical Conduction Monitor

40 –Field (over/under excitation) Relay

41 - Field Circuit Breaker

42 - Running Circuit Breaker

43 - Manual Transfer or Selector Device

46 – Rev. phase or Phase-Bal. Current Relay

47 - Phase-Seq. or Phase-Bal. Voltage Relay

48 - Incomplete-Sequence Relay

49 - Machine or Transformer Thermal Relay

50 - Instantaneous Overcurrent

51 - AC Time Overcurrent Relay

52 - AC Circuit Breaker

53 – Field Excitation Relay

55 - Power Factor Relay

56 - Field Application Relay

59 - Overvoltage Relay

60 - Voltage or Current Balance Relay

62 - Time-Delay Stopping or Opening Relay

63 - Pressure Switch

64 - Ground Detector Relay

65 - Governor

66 – Notching or jogging device

67 - AC Directional Overcurrent Relay

68 - Blocking or "out of step" Relay

69 - Permissive Control Device

74 - Alarm Relay

75 - Position Changing Mechanism

76 - DC Overcurrent Relay

78 - Phase-Angle Measuring Relay

79 - AC-Reclosing Relay

81 - Frequency Relay

83 - Automatic Selective Control or Transfer Relay

84 - Operating Mechanism

85 – Pliot Communications, Carrier or Pilot-

Wire Relay

86 - Lockout Relay

87 - Differential Protective Relay

89 - Line Switch

90 - Regulating Device

91 - Voltage Directional Relay

92 - Voltage and Power Directional Relay

94 - Tripping or Trip-Free Relay